FINAL REPORT

Contract Nas 5- 21666

LASER RADAR STUDIES

A STUDY OF THE FEASIBILITY OF REMOTE MEASUREMENT OF ATMOSPHERIC DENSITY AND TURBIDITY BY MEANS OF ROTATIONAL RAMAN SCATTERING OF LASER LIGHT

by

Nathan Reiss

and

Richard M. Schotland

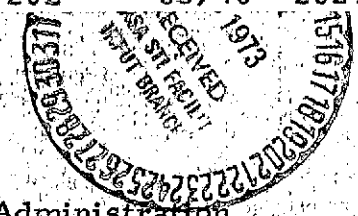

Submitted to: National Aeronautics and Space Administration
Goddard Space Flight Center

Department of Meteorology and Oceanography
New York University
School of Engineering and Science
University Heights, New York, N.Y. 10453

Research Division

July 1973

Table of Contents

List of Figures

ACKNOWLEDGMENTS

I wish to thank Professor R. M. Schotland for his invaluable advice and encouragement during the preparation of this work.

Special thanks are due my colleagues for their constant consultation, particularly to Mr. R. Leifer and Dr. H. Mark. I should also like to thank Mr. A. Pace and Mr. L. Amelio of the Meteorology Department for their advice and assistance in construction of experimental equipment, Mr. D. Ziff of the Chemistry Department for his outstanding glasswork and Professor R. A. Wohl of the Chemistry Department of Rutgers University for making available and instructing me in the use of the Raman spectrophotometer.

I am especially grateful to my wife, who gave me continuous assistance and encouragement.

Finally, I would like to thank Mrs. G. Fisher for drafting the figures. This work was supported by the National Aeronautics and Space Administration under Contract No. NAS 5 21666.

ABSTRACT

A remote sensing technique is described which utilizes elastic scattering and rotational Raman scattering of laser light in the atmosphere to obtain soundings of turbidity, transmissivity and density.

When irradiated by monochromatic light, both molecular and particulate components of the atmosphere scatter light at the incident frequency. In addition, the gaseous component produces a temperature-dependent pure rotational Raman spectrum which extends about 200 cm^{-1} above and below the incident frequency. It is shown that particulate scattering, as well as that from the minor atmospheric constituents, is negligibly small in this interval, in comparison to that from N_2 and O_2.

A scheme is devised whereby, through selective weighting of the rotational Raman lines, the effect of atmospheric temperature structure may be eliminated.

The close spectral proximity of the elastic and Raman-scattered signals, combined with the fact that the Raman scattering is quite weak, produces special requirements for the spectroscopic and light-gathering components of a rotational Raman laser radar system. These requirements are investigated, with a view toward the design of

a practical system.

A computation of typical signal-to-noise ratios is made. It is shown that daytime signal-to-noise ratios greater than 10 db are to be expected for observation heights of 5 km and below. For nighttime work, 10 db signal-to-noise ratios are achievable to altitudes as high as 15 km.

Chapter I.

INTRODUCTION

Several investigators have utilized optical probing to obtain remote density and turbidity profiles of the atmosphere. Their studies depend on the fact that some photons, in passing through the atmosphere, undergo elastic collisions with gas molecules and particulates, and are thereby scattered away from their original paths. Some of these photons are scattered toward the receiver and constitute the observed return signal. All of these studies have in common the problem of separating the return due to collisions with molecules from that due to collisions with particulates. Furthermore, since knowledge of the number of photons returned in a given direction in an atmosphere containing particulates does not uniquely determine the amount of signal attenuation or the amount of scattering, some assumptions must be made in this respect. As a result of the latter problem, most work in this area has focussed on stratospheric probing, where particulate effects are relatively small or confined to discrete layers, and where signal attenuation is nearly constant with height.

Elterman (1966) assumed a molecular number density

distribution and confined his study to determining profiles of attenuation due to particulates. He further assumed that particulate attenuation was zero at 35 km, except when that assumption led to negative particle attenuation values at lower altitudes, in which case the attenuation at 35 km was adjusted to the smallest value that would give values greater than zero at all lower altitudes. Since Elterman employed a searchlight system and determined his observation heights through triangulation, his observations for different heights were made at varying scattering angles, and thus it was necessary for him to assume a phase function, or directional distribution pattern, for the particle scattering. Had he used a laser radar system and monitored only backscattered radiation, it would not have been necessary for him to concern himself with the details of a phase function, but instead to assume some relationship between the number of photons scattered toward the receiver and the total number scattered out of the beam.

Fiocco and Smullin (1963), Fiocco and Grams (1964), Clemesha, et.al. (1966), Collis and Ligda (1966), Kent, et.al. (1967), Schuster (1970) and others have directed their analyses toward finding discrete aerosol layers in the stratosphere. In each of these studies, the observed

stratospheric profile is fitted to a model of the expected profile for a molecular atmosphere, and the small regions of deviation are ascribed to the presence of aerosol layers.

Kent, et.al. (1971), on the other hand, fit their soundings to a standard atmosphere at the 30 km level, and assume that all deviations above that level are due to density variations, particulate scattering being assumed as negligible.

Barrett and Ben-Dov (1967) obtained soundings extending to less than 1 km, and assumed in some cases that attenuation was negligible, and in others that the ratio of the particle backscatter cross section to the attenuation cross section was a known constant, obtained from a model. Furthermore, they assumed a molecular number density profile.

With recent advances in laser technology and in the production of photomultipliers and optical filters, it has become possible to examine the spectral composition of the light returned in a laser radar system, and thereby to obtain additional information needed to dispense with some of the assumptions discussed above.

The high monochromaticity of the laser source, used in

conjunction with an optical filter with a sharp frequency response, enables the investigator to monitor regions of the spectrum extremely close to the frequency of the transmitted light, with minimal interference from that light. The high photon densities obtainable through use of lasers, together with the high quantum efficiencies afforded by modern photomultiplier tubes, allow the observation of secondary scattering phenomena that were hitherto unobservable outside of the laboratory. This secondary, or Raman scattering, comes about as a result of the exchange of energy between the incident photons and the matter composing the atmosphere, and appears as light scattered at frequencies different from that of the incident light (Herzberg, 1939). The character of this exchange is uniquely dependent upon the molecular characteristics of the particular substance and, as such, can be used as a means of detecting the presence of that substance.

Leonard (1967) was the first to demonstrate that Raman scattering could be employed for atmospheric observations when he monitored returns from atmospheric nitrogen and oxygen. These returns were the result of vibrational quantum transitions (vibrational Raman scattering), and represented frequency shifts of 2328 cm^{-1} and 1551 cm^{-1}

due to N_2 and O_2 respectively.

Nitrogen and oxygen also produce a rich spectrum of scattering frequencies due to rotational quantum transitions (rotational Raman scattering). These frequencies lie in a region extending from about 10 cm^{-1} to 200 cm^{-1} to either side of the incident frequency. Salzman, et.al. (1971) are presently attempting to exploit the strong temperature sensitivity of the lines in the vicinity of 200 cm^{-1} to obtain remote temperature profiles.

In liquids and solids, where intermolecular forces are greater than in gases, molecular rotation is inhibited or absent entirely. In its place, however, there may exist molecular librations (in liquids) or lattice vibrations (in solids) which act to produce scattering in the same range of frequencies as molecular rotation.

If it can be shown that the off-frequency component of light scattered by liquid and solid constituents of the atmosphere is negligibly small compared to that scattered by the gaseous components, and if a relationship can be found between the intensity of off-frequency scattering and molecular number density, then we should be able to remove at least part of the arbitrariness which now exists in the interpretation of density and turbidity profiles.

Schotland (1969) discussed this possibility in general terms.

It will be shown here that the off-frequency component of light scattered by liquid and solid constituents of the atmosphere is, indeed, negligible compared to that from gaseous components. It will be shown that, through selective weighting of the received off-frequency components, a relationship may be established between these components and molecular number density. An investigation is conducted into the feasibility of developing a practical laser radar system which employs these principles to obtain density and turbidity profiles.

Chapter II.

METHOD

List of Symbols

K_e System constant for elastic channel (W-cm).

K_r System constant for Raman channel (W-cm).

n Molecular number density of air (cm^{-3}).

P_e Power received in elastic channel (W).

P_r Power received in Raman channel (W).

$\mathcal{T}_m$ Atmospheric transmission - molecular component.

$\mathcal{T}_{me}$ Atmospheric transmission at frequency of elastic scattering - molecular component.

$\mathcal{T}_{mr}$ Atmospheric transmission at frequency of Raman scattering - molecular component.

$\mathcal{T}_p$ Atmospheric transmission - particulate component.

$\mathcal{T}_{pe}$ Atmospheric transmission at frequency of elastic scattering - particulate component.

$\mathcal{T}_{pr}$ Atmospheric transmission at frequency of Raman scattering - particulate component.

z Height (cm).

α_m Molecular absorption coefficient (cm^{-1}).

β_m Attenuation coefficient - molecular component (cm^{-1}).

β_p Attenuation coefficient - particulate component (cm^{-1}).

η_e Particulate elastic backscatter coefficient of air (cm^{-1}).

η_r Particulate Raman backscatter coefficient of air (cm^{-1}).

σ_e Molecular elastic backscatter cross section of air (cm^2-$ster^{-1}$).

σ_r Raman backscatter cross section of air (cm^2-$ster^{-1}$).

τ Atmospheric turbidity.

A. General.

Consider a pulsed, monostatic laser radar system, with a receiver which simultaneously monitors the frequency of elastic scattering (i.e., the transmitted frequency), ν_e, and a frequency ν_r, at which rotational Raman scattering occurs. As shown by Schotland (1969), the applicable radar transfer equations are

$$P_e = K_e \left[\sigma_e n + \eta_e\right] \cdot \left[\mathcal{T}_{me}\, \mathcal{T}_{pe}\right]^2 \qquad (1)$$

and

$$P_r = K_r \left[\sigma_r n + \eta_r\right] \cdot \left[\mathcal{T}_{me}\, \mathcal{T}_{pe}\, \mathcal{T}_{mr}\, \mathcal{T}_{pr}\right] \qquad (2)$$

Elterman (1968) tabulated atmospheric attenuation profiles for the entire visible spectral region, using a large body of observed data, together with an attenuation model. Some figures derived from his results are presented in Table 1. The references to visibility are estimated following the discussion of meteorological visual range given by Middleton (1951). The table shows that, for visibilities greater than about seven miles, the variation of transmittance with frequency is generally below one percent per 100 cm^{-1}. For the very turbid atmosphere in Table 1.c., the variation is still less than two percent

Table 1.

a. Variation with frequency of total one-way atmospheric transmission between the surface and selected altitudes (percent change per 100 cm^{-1}) for an atmosphere with attenuation coefficients equal to those given by Elterman (1968). For this atmosphere, the horizontal visibility at the surface is approximately 14 miles.

Wavelength Interval (μ)	0.40-0.45	0.45-0.50	0.50-0.55	0.55-0.60	0.60-0.65	0.65-0.70	0.70-0.80	0.80-0.90	0.90-1.06
z (km)									
2	0.19	0.14	0.11	0.09	0.10	0.09	0.07	0.07	0.09
5	0.33	0.24	0.18	0.15	0.16	0.14	0.10	0.09	0.11
10	0.47	0.34	0.30	0.21	0.21	0.18	0.13	0.12	0.13
20	0.51	0.41	0.26	0.23	0.31	0.26	0.16	0.15	0.15
∞	0.61	0.40	0.23	0.19	0.44	0.34	0.18	0.17	0.15

b. Same as a., but with Elterman's attenuation coefficients multiplied by uniform factor of two (Surface visibility approximately 7 miles).

2	0.38	0.27	0.22	0.19	0.21	0.22	0.23	0.27	0.35
5	0.74	0.49	0.38	0.30	0.33	0.33	0.34	0.39	0.45
10	1.09	0.73	0.50	0.44	0.36	0.38	0.40	0.46	0.55
20	1.39	0.91	0.55	0.57	0.54	0.55	0.56	0.62	0.68
∞	1.50	1.15	0.75	0.73	0.70	0.69	0.75	0.68	0.86

c. Same as a., but with Elterman's attenuation coefficients multiplied by uniform factor of five (Surface visibility approximately 2.8 miles).

2	0.82	0.73	0.71	0.48	0.53	0.55	0.57	0.69	0.88
5	2.12	1.34	0.95	0.82	0.81	0.79	0.87	0.99	1.18
10	3.30	2.08	1.40	1.15	1.05	1.01	1.16	1.19	1.43
20	4.57	2.63	1.58	1.51	1.45	1.48	1.53	1.55	1.65
∞	5.54	2.94	2.19	2.00	1.93	1.87	1.91	1.75	1.70

for wavelengths longer than 0.60μ, and less than three percent per 100 cm^{-1} for wavelengths longer than 0.45μ. It is evident that, given the range of altitudes and turbidities in which one wishes to operate, a range of wavelengths can be found for which:

$$\left[\mathcal{T}_{me}\mathcal{T}_{pe}\right]^2 = \mathcal{T}_{me}\mathcal{T}_{pe}\mathcal{T}_{mr}\mathcal{T}_{pr} = \left[\mathcal{T}_m\mathcal{T}_p\right]^2 \qquad (3)$$

We shall assume for the present, and show in Chapter III.H.3, that

$$\eta_r \ll \sigma_r n \qquad (4)$$

That is, the off-frequency component of scattering due to particulates is, at all altitudes, negligible in comparison to that due to molecules.

B. Measurement of particulate backscatter.

By combining (1) through (4) in such a manner as to eliminate $(\mathcal{T}_m\mathcal{T}_p)^2$, we obtain

$$\frac{\eta_e}{\sigma_r n} = \frac{K_r}{K_e}\frac{P_e}{P_r} = \frac{\sigma_e}{\sigma_r} \qquad (5)$$

the ratio K_r/K_e is a system constant obtained through laboratory measurements. P_e and P_r are the quantities measured by the laser radar system. The constant $\eta_e/\sigma_r n$

is determined in Chapter III.G. and is an invariant quantity for a given gas, as long as resonance scattering conditions do not exist.

Equation (5) is the expression which allows the determination of one of the quantities of interest here, $\eta_e / \sigma_r n$, which represents the ratio of light backscattered by particulates to that backscattered by molecules, and is a measure of atmospheric turbidity.

There is no standard definition of turbidity. For example, Elterman (1968) uses

$$\tau(z) = \frac{\beta_p}{\beta_m} \tag{6}$$

where

$$\beta_p = -\frac{1}{\mathcal{J}_p} \frac{d\mathcal{J}_p}{dz} \tag{7}$$

and

$$\beta_m = -\frac{1}{\mathcal{J}_m} \frac{d\mathcal{J}_m}{dz} \tag{8}$$

This definition includes absorbing properties of the constituents as well as oblique scattering, while the quantity $\eta_e / \sigma_r n$ does not. A definition similar to that of Elterman (1968) is that of DeBary, et.al. (1965), who used

$$\tau\Big|_0^z = 1 + \frac{\ln \tilde{\jmath}_p}{\ln \tilde{\jmath}_m} = 1 + \frac{\int_0^z \beta_p dz}{\int_0^z \beta_m dz} \qquad (9)$$

The relationship between $\sigma_r n$ and β_m is simply

$$\beta_m = \frac{8\pi}{3}\frac{\sigma_e}{\sigma_r}\sigma_r n + \alpha_m \qquad (10)$$

via Rayleigh's phase function for small scatterers (Chandrasekhar, 1960). In fact, there are many spectral regions accessible to laser radar for which

$$\alpha_m \ll \frac{8\pi}{3}\frac{\sigma_e}{\sigma_r}\sigma_r n \qquad (11)$$

making (10) even simpler. Unfortunately the relationship between η_e and β_p is not as clear, depending as it does upon the particulate phase function and absorption coefficient, which are as highly variable as the size distribution, shape and composition of the particles suspended in the atmosphere (Deirmendjian, 1969). Thus, there can be no simple conversion between the ratio, $\eta_e / \sigma_r n$, to be measured here, and the various other definitions of turbidity.

The primary requirement for a definition of turbidity to be useful from an operational standpoint is that the quantity can be measured reproducibly at different times and places. The ratio $\eta_e / \sigma_r n$ satisfies this requirement.

C. Measurement of tropospheric transmission and particle attenuation.

In equation (5) it was required only that we know the ratios K_r/K_e and σ_e/σ_r. Suppose that we are able to obtain K_r and σ_r explicitly. Then, for each altitude z, using (2) through (4), we may solve the off-frequency transfer equation for the transmission:

$$\mathcal{T}_m \mathcal{T}_p = \left[\frac{P_r}{K_r \sigma_r n}\right]^{\frac{1}{2}} \qquad (12)$$

Molecular number density, n, is the only unknown quantity on the right side of (12).. At tropospheric altitudes, it may be estimated to a fair degree of accuracy from statistical information or from recent synoptic data. Thus, using the off-frequency transfer equation together with an estimate of the molecular number density at a given height, we can compute the transmission from the surface to that height. It should be noted that any error in the estimate of n results in an error in the computed transmission that is only half as great.

In a spectral region where molecular absorption is negligible, an estimate of n implies an estimate of β_m and $\mathcal{T}_m$, as may be ascertained from equations (8) and (10).

Without any further assumptions then, we compute $\mathcal{T}_p$ from equation (12) and, consequently, β_p, using equation (7).

D. Measurement of upper atmospheric number densities.

Several studies, such as those by Smith (1964), Nee (1964) and that in the Handbook of Physics and Space Environments (1965) have shown that there exists near a height of 7 km, an "isopycnic level" in the atmosphere, where density has a minimum variation in time and horizontal space. Smith's (1964) study shows, for instance, that at Buffalo, N. Y., 99% of all density observations at 7 km lie within ± 3.6 percent of the annual mean (e.g., a RMS deviation of ± 1.2 percent) for that station. This value is typical of those given by smith for other stations in temperate and polar regions. While no similar studies could be found for tropical regions, it is expected that densities there could be even more closely estimated from climatology, since sharp air mass contrasts do not exist there.

Elterman (1968) shows that, at a wavelength of 0.7μ, $(\mathcal{T}_m \mathcal{T}_p)^2$ decreases by only about 11% between 7 km and the top of the atmosphere. About 60% of this quantity, or 6.6 percent of the total decrease is due to aerosols.

Writing (12) as

$$n = \frac{P_r}{K_r \sigma_r (\mathcal{T}_m \mathcal{T}_p)^2} \tag{13}$$

we see that, if $(\mathcal{T}_m \mathcal{T}_p)^2$ at 7 km is determined by the method of the previous section, using the annual mean value of n for the location in question, then we may determine n from 7 km to the top of the atmosphere to a fair degree of accuracy, even if the contribution to $\mathcal{T}_p$ above that altitude is neglected altogether. We can improve the accuracy of our determination of n considerably by employing some model for $\mathcal{T}_p$, such as an extrapolation of $\mathcal{T}_p$(7 km) according to Elterman's (1968) aerosol extinction profile. Elterman's aerosol transmission factors for 0.45μ and 0.70μ are presented as fractions of the aerosol transmission factor at 7 km in Table 2.

Table 2. Two-way aerosol transmission factors (0 - z) relative to the value at 7 km $\left[\mathcal{T}_p(z)/\mathcal{T}_p(7\text{ km})\right]$. After Elterman (1968).

z (km)	$\mathcal{T}_p(z)/\mathcal{T}_p(7\text{ km})$ (0.45μ)	$\mathcal{T}_p(z)/\mathcal{T}_p(7\text{ km})$ (0.70μ)
7	1.000	1.000
8	0.992	0.994
9	0.984	0.990
10	0.978	0.984
11	0.970	0.978
12	0.965	0.974
13	0.957	0.969
14	0.951	0.965
15	0.946	0.959
16	0.940	0.955
17	0.934	0.951
18	0.929	0.947
19	0.925	0.944
20	0.921	0.940
21	0.918	0.938
22	0.916	0.938
23	0.916	0.936
24	0.914	0.936

Chapter III.

CHARACTER OF THE ROTATIONAL RAMAN SPECTRUM OF AIR

List of Symbols

A	Cross sectional area of sample cell (cm^2).
$\mathcal{A}$	Avogadro's number ($mole^{-1}$).
a	Radial distance of atom from molecular axis of symmetry (cm).
B_i	Molecular rotational constant at vibrational quantum number, i (cm^{-1}).
$b^j_{j'}$	Probability of occurrence of transitions between quantum state j and j'.
c	Speed of light ($cm\text{-}sec^{-1}$).
D_i	Molecular rotational constant at vibrational quantum number, i (cm^{-1}).
d	Diameter of tubing (cm).
e	Partial pressure of H_2O in the atmosphere ($dyne\text{-}cm^{-2}$).
g	Gravity ($cm\text{-}sec^{-2}$).
g_j	Statistical weight of rotational quantum state, j.
H	Scale height (cm).
h	Planck's constant (erg-sec).
I	Relative intensity of scattered light.
$I_{e_\parallel}$	Relative intensity of parallel polarized component of elastic scattering.
$I_{e_\perp}$	Relative intensity of perpendicular polarized component of elastic scattering.

$I_{e_{\parallel+\perp}}$ Relative intensity of elastic scattering of both polarizations.

$I_{r_{\parallel}}$ Relative intensity of parallel polarized component of Raman scattering (O- and S-branches).

$I_{r_{\perp}}$ Relative intensity of perpendicular polarized component of Raman scattering (O- and S-branches).

$I_{r_{\parallel+\perp}}$ Relative intensity of Raman scattering of both polarizations (O- and S-branches).

$\mathcal{I}$ Molecular moment of inertia (gm-cm^2).

i Vibrational quantum number of initial state.

j Rotational quantum number of initial state.

j' Rotational quantum number of final state.

K Constant.

k Boltzmann constant (erg-^{o}K).

L Horizontal length of tubing (cm).

M Atomic mass (gm).

m Refractive index.

m_{part} Mass concentration of particulate matter in the atmosphere (gm-cm^{-3}).

N Particulate number density (cm^{-3}).

N_o Particulate number density at z = 0 (cm^{-3}).

$\mathcal{N}$ Average number of particles viewed by spectrometer during integrating time interval.

n Molecular number density (cm^{-3}).

n_j Number density of molecules in rotational quantum state, j (cm^{-3}).

n_W Number density of molecules with energy W (cm^{-3}).

p Atmospheric pressure (dyne-cm^{-2}).

Q Volume flow rate of air through spectrometer sample cell (cm^3-sec^{-1}).

Re Reynolds number.

r Particle radius (cm).

r_{max} Maximum radius considered in particulate number density computation (cm).

r_{min} Minimum radius considered in particulate number density computation (cm).

T Temperature (^oK).

v Maximum speed of particle motion through sample cell ($cm\text{-}sec^{-1}$).

$\bar{v}$ Mean speed of particle motion through spectrometer sample cell ($cm\text{-}sec^{-1}$).

W(J) Amount of energy in a rotational or vibrational state of quantum number J (ergs).

$W_R(j)$ Amount of energy in a rotational state of quantum number j (ergs).

$W_V(i)$ Amount of energy in a vibrational state of quantum number i (ergs).

w Settling velocity of particles ($cm\text{-}sec^{-1}$).

z Height (cm).

α Mean molecular polarizability (cm^3).

γ Anisotropy of molecular polarizability (cm^3).

Δ Depolarization ratio.

$\Delta\nu$ Frequency of Raman line relative to frequency of

elastic scattering (cm^{-1}).

Δt Spectrometer integrating time interval (sec).

$\delta\nu$ Spectral slit width of the spectrometer system (cm^{-1}).

η Dynamic viscosity of air (cm^2-sec^{-1}).

$\mathcal{M}$ Molecular mass of matter composing particulates (gm-$mole^{-1}$).

ν Frequency (cm^{-1}).

ρ_{Air} Mass density of air (gm-cm^{-3}).

ρ_{Part} Mass density of particulate matter (gm-cm^{-3}).

$\sigma(\mathcal{N})$ Standard deviation of the mean, $\mathcal{N}$, as viewed by the spectrometer.

σ_{Ram} Raman backscatter cross section, including O- and S-branches and both parallel and perpendicular polarizations (cm^2-$ster^{-1}$).

σ_{Ray} Rayleigh backscatter cross section, including Q-branch Raman scatter and both parallel and perpendicular polarizations (cm^2-$ster^{-1}$).

A. General.

In attempting to explain the scattering properties of a molecule, it is helpful to consider it as an asymmetric aggregate of electrons which act to deflect passing photons. The asymmetry of the electronic aggregate is a result of the asymmetry of bonding forces and the nuclear mass distribution.

The molecular parameter usually used to represent this physical picture is the molecular polarizability, a tensor. For rotating molecules whose axes are randomly oriented with respect to the observer, it is convenient to refer to the polarizability in terms of its statistical properties:

1. Mean polarizability, α — The portion of the polarizability that remains constant as the molecule rotates.

2. Mean polarizability anisotropy, γ — The portion of the polarizability associated with molecular asymmetries.

The deflection (or scattering) of photons due to the mean polarizability is thus independent of the shape of the molecule and is often known as Rayleigh scattering. We shall point out later, however, that the common operational definition of Rayleigh scattering also includes some portions of the scattering due to the polarizability anisotropy. Scattering due to the polarizability anisotropy

depends upon the asymmetries in the distribution of electrons. A molecule with perfect spherical symmetry has $\gamma = 0$. The intensity of rotational Raman scattering (that is, the scattering associated with molecular rotation) thus depends entirely upon the magnitude of γ.

In the sections which follow, we shall first discuss the characteristics of rotational Raman scattering, and then show more specifically how rotational Raman scattering and Rayleigh scattering are interrelated.

The subject of rotational Raman spectra is one that is often fraught with many complexities. We are indeed fortunate that the major components of the earth's atmosphere, nitrogen and oxygen, exist overwhelmingly as homonuclear, diatomic, electronically unexcited molecules. Simple theoretical models of molecules such as these were among the early results of the development of quantum theory [see, for instance, Placzek and Teller (1933)]. Numerous subsequent studies [e.g. Stoicheff (1959)] showed that the simple models gave results that were compatible with actual observations.

In recent years, with the increasing availability of sophisticated laser Raman spectrophotometers, second order Raman effects, not explained by the simple model have been

observed [e.g. Abe and Shimanouchi (1969)] . These effects constitute an extremely small fraction of the total Raman energy and have been observable only in conjunction with the rotational Raman lines that are very close to the exciting line. As we shall see later, these first few Raman lines are of only peripheral importance to our study, and second order effects superimposed upon these lines are of no concern to us.

The theoretical development that follows will utilize the simple "dumbbell" model for diatomic molecules. An extensive discussion of rotational Raman scattering in general, and this model in particular, is given by Herzberg (1939).

B. Population of molecular energy levels.

At any given temperature, molecules of gases take on distributions of discrete rotational, vibrational and electronic states. Since we are concerned here only with neutral gases and relatively low temperatures ($200^{\circ}K$-$320^{\circ}K$), we shall consider only the "ground" electronic state.

The number of molecules in any rotational or vibrational state depends upon the following factors:

1. Boltzmann factor. If W(J) is the amount of energy

in a rotational or vibrational state of quantum number, J, then according to the Boltzmann energy distribution law (Herzberg, 1939), the number of molecules, dn_W, that have a rotational or vibrational energy between W and W+dW is proportional to $e^{-W(J)/kT}dW$. We see that, as temperature is increased, more molecules are found in higher energy states, relative to the number found in lower states.

2. Degeneracy. Molecular motions are "space quantized." That is, only certain modes of motion are permitted, with each mode having an equal likelihood of occurrence. It can be shown (Herzberg, 1939) that 2J+1 times as many modes are permitted for a molecule in the J^{th} state of vibration or rotation as in the zeroth state.

3. Statistical weight, g_j. Due to the influence of nuclear spin within molecules upon the selection rules for the occurrence of the various rotational quantum states, a regular alternation in the relative number of molecules in each state takes place (Herzberg, 1939). In homonuclear, diatomic molecules such as oxygen, in which the nuclei have no spin, the ratio of the number of molecules in even-numbered states to that in odd-numbered states is 0:1. That is, even-numbered states are completely unpopulated. In the case of nitrogen, where nuclei have a spin, the

ratio is 2:1. The even-numbered rotational states of nitrogen have twice the population of odd-numbered states.

Combining the above factors, we may state that the ratio of the number of molecules in the i^{th} vibrational state and j^{th} rotational state, $n_{i,j}$, to the total number of molecules, n, is:

$$\frac{n_{i,j}}{n} = \frac{\left[(2i + 1)\ e^{-W_V/kT}\right]\cdot\left[g_j\ (2j + 1)\ e^{-W_R/kT}\right]}{\sum_{i,j=0}^{\infty}\left\{\left[(2i + 1)\ e^{-W_V/kT}\right]\cdot\left[g_j\ (2j + 1)\ e^{-W_R/kT}\right]\right\}} \qquad (14)$$

The sum in the denominator of (14) represents summation over all possible vibrational and rotational states. Herzberg (1939) showed that we may write, to a good approximation,

$$W_R = hc\left[B_i\ j(j + 1) - D_i\ j^2(j + 1)^2\right] \qquad (15)$$

where B_i and D_i are molecular rotational constants which depend somewhat on the vibrational state, i, of the molecule. Since the discussion here will concern itself only with the pure rotational Raman spectrum (i = 0), we shall concern ourselves only with

$$W_R = hc\left[B_o\ j(j + 1) - D_o\ j^2(j + 1)^2\right] \qquad (16)$$

The magnitude of W_R is such that, at atmospheric temperatures, rotational states in the range, $0 \leqslant j \leqslant 30$, are significantly populated. Values of B_o and D_o for N_2 and O_2 have been computed from laboratory observations by Stoicheff (1959) and are known to sufficient accuracy for the present application.

Concerning the character of W_V, we shall state only that it is much larger than W_R, so that at atmospheric temperatures, the ratio of the number of molecules in the first to that in the zeroth vibrational state is about 1.40×10^{-5} for N_2 and 5.74×10^{-4} for O_2, as observed by Herzberg (1939). That is, virtually all atmospheric N_2 and O_2 molecules are in the zeroth vibrational state. Thus, (14) can be simplified to read

$$n_j = n \frac{g_j (2j + 1) e^{-W_R/kT}}{\sum_{j=0}^{\infty} \left[g_j (2j + 1) e^{-W_R/kT} \right]} , \quad i = 0 \qquad (17)$$

in the atmospheric range of temperatures.

C. Rotational Raman transitions.

The rotational Raman effect is the result of transitions of the type,

$$j' - j = 0, \pm 2$$

where j is the quantum number of the initial state and j' that of the final state.

When the collision between a photon and a gas molecule is elastic, then a transition of the type, $j' - j = 0$, occurs. The Raman-scattered radiation is thus at the same frequency as the incident light. The lines of scattered energy (one for each j-value) resulting from this type of transition are superimposed at the frequency of the incident light and are known as the "Q-branch". They are sometimes described as that portion of the Rayleigh scattering due to the anisotropy of the polarizability tensor.

When a collision is accompanied by a net transfer of energy to the molecule, then a transition of the type,

$$j' - j = +2$$

occurs, and the Raman-scattered radiation is lower in frequency than the incident light. The lines in which energy is scattered at frequencies lower than that of the incident light are known as "Stokes" or "S-branch" lines.

For the case where there is a net loss of energy by the molecule, we have,

$$j' - j = -2$$

and the Raman scattering occurs at frequencies higher than

that of the incident light. These lines are known as "anti-Stokes" or "O-branch" lines.

The frequency separation between successive lines can be closely determined by considering the molecule as a "rigid rotator"; that is, by assuming that the centers of mass composing the molecule remain fixed relative to each other as the molecule rotates. When this assumption is made, the lines are found to be separated from the frequency of the incident light by an amount

$$\Delta\nu = \pm 4B_o (j + 3/2) \tag{18}$$

as shown by Herzberg (1939). For large values of j (large rotation rates), the "rigid rotator" assumption becomes less accurate, and a correction term must be added to (18) to account for the effect of centrifugal distortion. The expression then usually takes the form,

$$\Delta\nu = \pm \left[(4B_o - 6D_o)(j + 3/2) - 8D_o (j + 3/2)^3\right] \tag{19}$$

Neglect of the correction term in (19) results in less than a one percent error in $\Delta\nu$ at j=30, for both nitrogen and oxygen.

The intensity of the j^{th} rotational Raman line is shown by Herzberg (1939) to be proportional to the Boltzmann fac-

tor and the statistical weight of the initial level,

$$g_j \, e^{-W_R(j)/kT}$$

and the degeneracy of the lower of the two levels,

$$\underset{\text{Stokes}}{(2j + 1)} \qquad \text{or} \qquad \underset{\text{anti-Stokes}}{(2j' + 1)}$$

as well as the transition probability, $b^j_{j'}$, and the square of the anisotropy of the molecular polarizability, γ^2. That is,

$$I_j \propto \frac{(2j + 1)\, g_j\, b^j_{j'}\, e^{-W_R(j)/kT}}{\sum_{O,Q,S} \sum_{j=0}^{\infty} \left[(2j + 1)\, g_j\, b^j_{j'}\, e^{-W_R(j)/kT}\right]} n\gamma^2 \qquad (20)$$

Stokes

and

$$I_j \propto \frac{(2j' + 1)\, g_j\, b^j_{j'}\, e^{-W_R(j)/kT}}{\sum_{O,Q,S} \sum_{j=0}^{\infty} \left[(2j' + 1)\, g_j\, b^j_{j'}\, e^{-W_R(j)/kT}\right]} n\gamma^2 \qquad (21)$$

anti-Stokes

Transition probabilities, $b^j_{j'}$, have been derived by Placzek and Teller (1933). The expressions corresponding to pure rotational Raman scattering are:

$$b^{j}_{j'} = \frac{3(j+1)(j+2)}{2(2j+1)(2j+3)} \qquad (22)$$

(S- and O-branches)

and

$$b^{j}_{j'} = \frac{j(j+1)}{(2j-1)(2j+3)} \qquad (23)$$

(Q-branch)

Values of γ for many substances have been determined in the laboratory, primarily through measurements of depolarization ratios. Such measurements were made by Bridge and Buckingham (1966) for N_2 and O_2. Their results were checked by this author through comparison of their figures with measurements of the rotational Raman spectrum of air made by Miller, et.al. (1968). If the ratio of molecular number densities of N_2 and O_2 is known, then the ratio $\gamma^2_{N_2}/\gamma^2_{O_2}$ can be extracted from the observed spectrum of air through comparison of the intensity of N_2 lines relative to the O_2 lines. This was done, and the ratio $\gamma^2_{N_2}/\gamma^2_{O_2}$, so determined, differed from that obtained by Bridge and Buckingham by only a fraction of a percent.

If we neglect, for the time being, the ν^4 dependence inherent in all the intensities (Goody, 1964), then sever-

al statements may be made about the distribution of energy scattered in the pure rotational Raman spectrum:

1. At atmospheric temperatures, where vibrational transitions are insignificant, the total energy scattered in the O-, Q- and S-branches ramains constant with changes in temperature. This may be verified by computing $\sum_{j=0}^{\infty} I_j$ for the O-, Q- and S-branches, using Equations (20) through (23).

2. In a like manner, we find that the fraction of the energy scattered in the Q-branch remains constant at one fourth of the total. Thus, the total energy scattered in the O- and S-branches must be independent of temperature. When temperature is increased, scattered energy shifts from lower to higher j-values, and from the S-branch to the O-branch.

3. The S-branch is always more intense than the O-branch, since scattering intensity is proportional to the number of molecules in the initial state, and there are always more molecules in the lower-lying qauantum states than in the higher ones (see Section III.B.1.). From computations to be made later in this chapter, we shall see that for air, the average S/O intensity ranges from about 1.50:1 at 200°K to 1.39:1 at 300°K.

D. Raman scattering in relation to Rayleigh scattering.

Having determined the intensities of the various rotational Raman lines relative to each other, we wish to examine the rotational Raman scattering in relation to Rayleigh scattering. This relationship is best approached from a classical point of view, although it must always be recognized that classical mechanics does not fully explain the Raman scattering phenomenon. The classical derivation, for instance, predicts a continuum of scattered energy, rather than a series of discrete lines. Furthermore, it predicts that the O- and S-branches will contain equal amounts of energy. Nevertheless, this technique does predict the total energy in the O- and S-branches relative to that found in the Q-branch, and that found in the portion of the Rayleigh line due to the isotropic part of the polarizability tensor.

Stuart (1934) performed the computations in detail. For 90-degree scattering, in the plane perpendicular to the plane of oscillation of the electric vector of the incident field, the relative intensities, per unit solid angle, are:

$$I_{e_{\parallel}} \propto \left[\alpha^2 + \gamma^2/45\right] \qquad (24a)$$

$$I_{e_{\parallel+\perp}} \propto \left[\alpha^2 + 7\gamma^2/180\right] \qquad (24)$$

$$I_{e_{\perp}} \propto \gamma^2/60 \qquad (24b)$$

$$I_{r_{O+S_{\parallel}}} \propto \gamma^2/15 \qquad (25a)$$

$$I_{r_{O+S_{\parallel+\perp}}} \propto 7\gamma^2/60 \qquad (25)$$

$$I_{r_{O+S_{\perp}}} \propto \gamma^2/20 \qquad (25b)$$

It can be shown that the same results hold for 180-degree scattering in that plane. For a direction making an angle, θ, with the parallel direction, the intensity is simply given by

$$I_{\theta} = I_{\parallel} \cos^2\theta + I_{\perp} \sin^2\theta$$

as is shown by Chandrasekhar (1960). We thus have a complete picture of the relative intensity and angular dependence of rotational Raman and Rayleigh scattering. This is shown pictorially in Figure 1.

Since we know the distribution of energy within the O- and S-branches from earlier calculations, we are now in a position to compute the intensity of any individual rota-

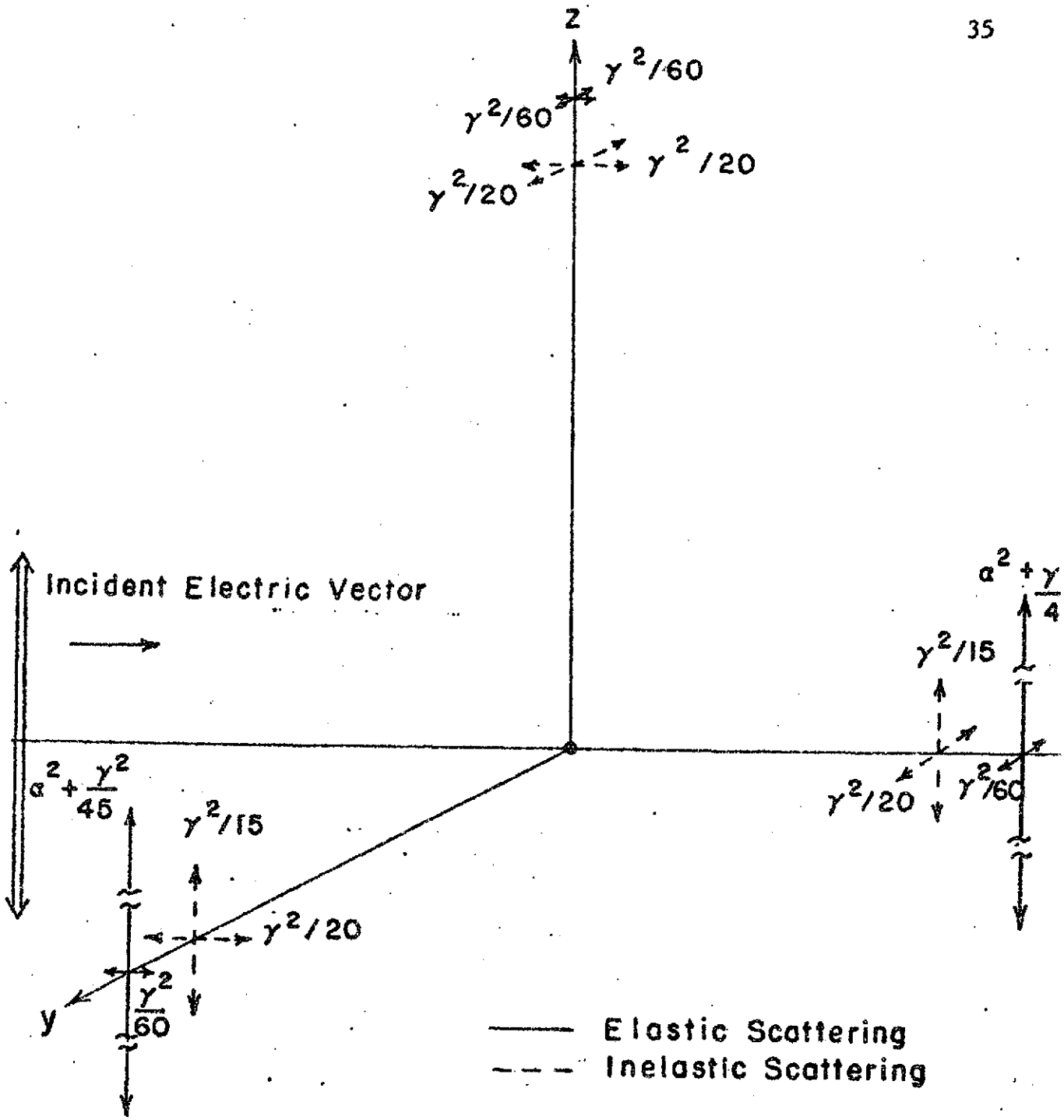

Figure 1. Angular dependence of rotational Raman and Rayleigh scattering.

tional Raman line relative to that of the Rayleigh line, for any scattering angle.

Further, we may compute the total scatter cross section for any line (that is, the cross section integrated over all solid angles).

E. Rotational constants and computations for nitrogen.

Stoicheff (1959) computed the rotational constants for N_2 from observations of rotational Raman line spacing. His values are:

$$B_o = 1.9897 \pm 0.0003 \text{ cm}^{-1}$$

$$D_o = (6.1 \pm 0.5) \times 10^{-6} \text{ cm}^{-1}$$

He points out that these values are in excellent agreement with values computed from the electronic spectrum by Wilkinson (1957), namely

$$B_o = 1.9898 \pm 0.0005 \text{ cm}^{-1}$$

$$D_o = 6.4 \times 10^{-6} \text{ cm}^{-1}$$

Stoicheff's values are used in the present calculations. Relative line locations and intensities within the O-, Q- and S-branches of the nitrogen spectrum computed using equations (19) through (23) are presented in Figure 2.

The relative intensities calculated here are compared to those observed by Miller, et.al. (1968) in Figure 3.

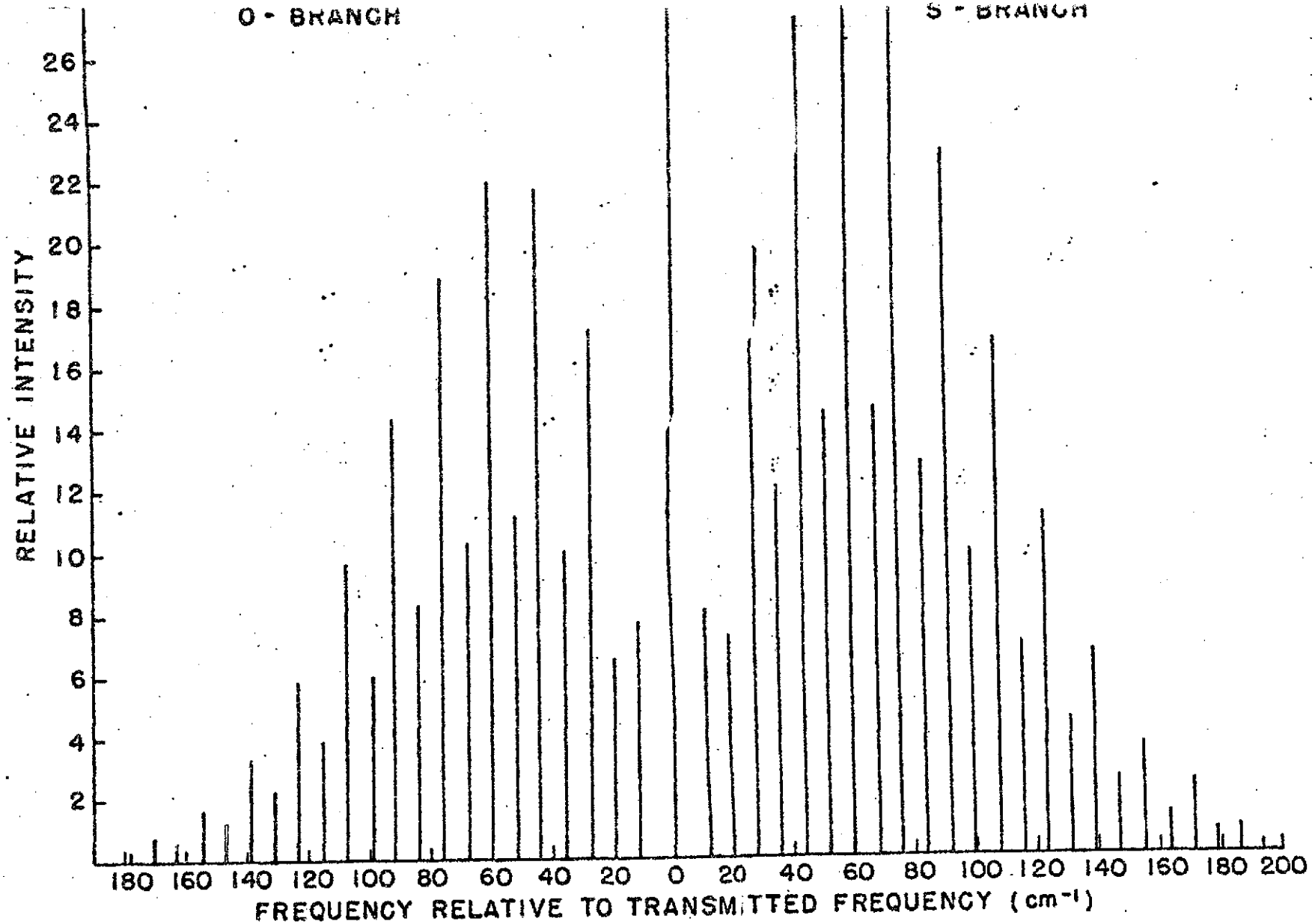

Figure 2. Computed rotational Raman line locations and intensities for nitrogen.

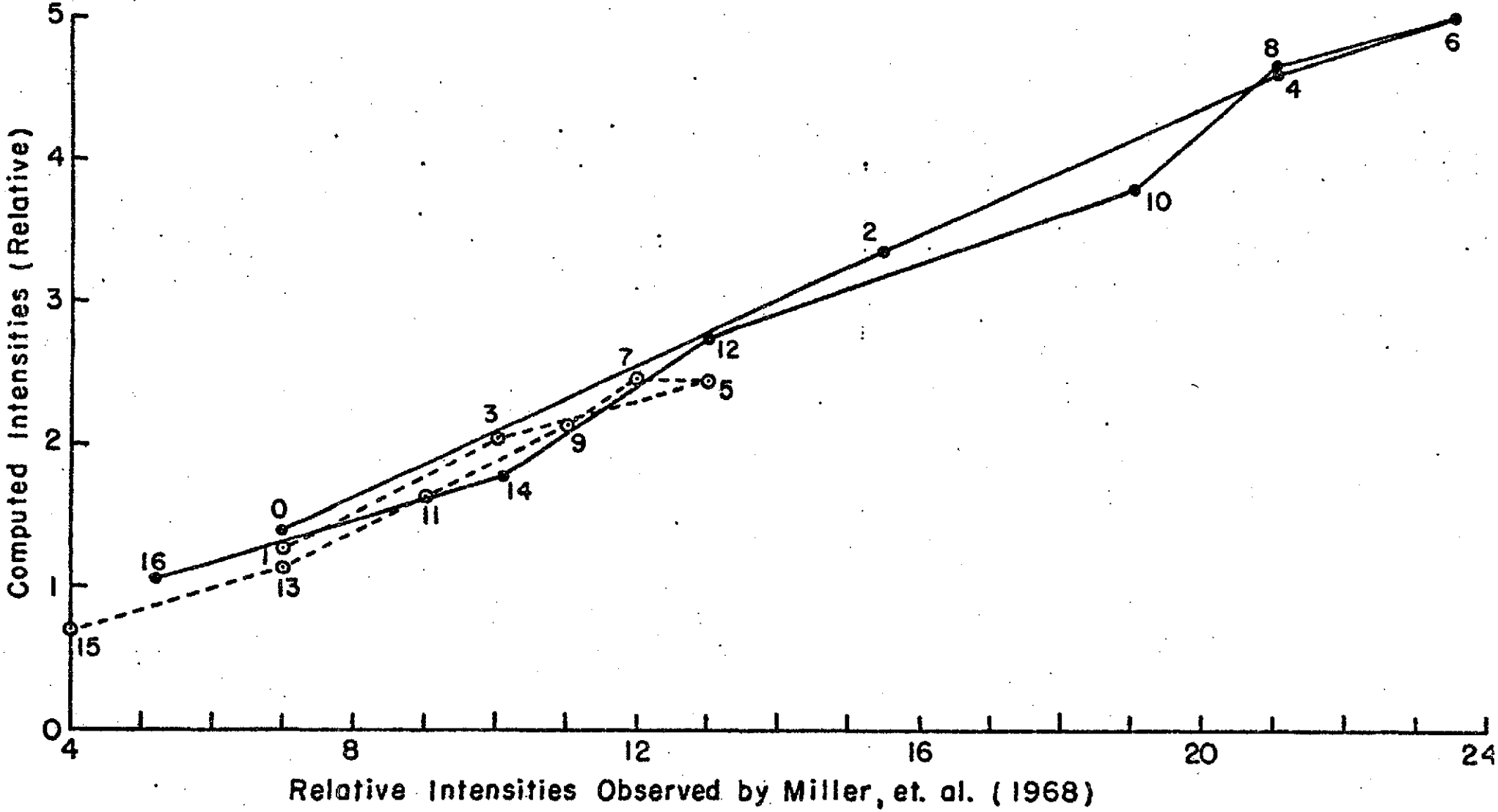

Figure 3. Computed relative intensities for nitrogen compared to those

Miller, et.al., in their observations, made no attempt to determine the gas temperature. Thus, in order to compare the present computations with their observations, it was first necessary to estimate the temperature at which the measurements were made. To accomplish this, line intensities were computed at a number of temperatures, and the results for each line plotted against observed values extracted from chart records given by Miller, et.al. For incorrect temperatures, the result was a graph similar to Figure 3, but with the points representing high- and low-numbered lines scattered to opposite sides of the best fit straight line. The temperature value inserted into the computations was adjusted until the selective scatter of points was minimized. The final result, shown in Figure 3, is a series of points falling close to a straight line distribution. A straight line relationship between the two sets of intensities shows that the observed and computed intensities differ from each other by a constant factor (that is, the shape of the two distributions is the same).

F. Rotational constants and computations for oxygen.

Table 3 gives rotational Raman line spacings observed in O_2 by Stoicheff (1959). Through use of the graphical

Table 3. Rotational line spacings in O_2 determined by Stoicheff (1959).

j	$\Delta\nu$ (cm^{-1})
1	14.31
3	25.85
5	37.37
7	48.84
9	60.33
11	71.80
13	83.26
15	94.72
17	106.16
19	117.57

technique described by him, the applicable rotational constants were determined by this author. They are:

$$B_o = 1.439 \text{ cm}^{-1}$$

$$D_o = 4.05 \times 10^{-6} \text{ cm}^{-1}$$

For purposes of comparison, B_o was also calculated using independently computed constants: the radial distance of the oxygen atoms from the molecular axis of symmetry,

$$a = 6.037 \times 10^{-9} \text{ cm}$$

which is given by Wacker, et.al. (1964), and the mass of an oxygen atom,

$$M = 2.656 \times 10^{-23} \text{ gm}$$

This allows us to compute the molecular moment of inertia,

$$\mathcal{I} = 2Ma^2 = 1.936 \times 10^{-39} \text{ gm cm}^2 \qquad (26)$$

From classical mechanics, we have the expression for the rotational constant,

$$B_o = \frac{h}{8\pi^2 c \mathcal{I}} \qquad (27)$$

Inserting our computed value of $\mathcal{I}$, we obtain

$$B_o = 1.445 \text{ cm}^{-1}$$

which differs from the value computed from Stoicheff's (1959) data by about 0.4 percent.

The values of B_o and D_o computed from Stoicheff's data are used here. Relative line intensities computed using (19) through (23) and line locations within the O-, Q- and S-branches of the oxygen spectrum are presented in Figure 4. The relative intensities calculated here are compared to those observed by Miller, et.al. (1968) in Figure 5. A detailed explanation as to how this comparison was carried out is given in the previous section, in the discussion of Figure 3.

G. The rotational Raman backscatter cross section of air (N_2 and O_2).

Through use of the expression derived by Chandrasekhar (1960) for the Rayleigh backscatter cross section, together with the results of Stuart (1934) described in Chapter III.C, for the ratio of Raman to Rayleigh intensities, we determine that the rotational Raman backscatter cross section of air is given by

$$\sigma_{\substack{\text{Ram} \\ \parallel+\perp \\ o+s}}(\text{Air}) = \left(\frac{2\pi}{\lambda}\right)^4 \left[\frac{7}{60}\gamma^2(\text{Air})\right] \qquad (28)$$

The effective polarizability anisotropy of air, squared, $\gamma^2(\text{Air})$, is merely an average of squares of the anisotropies for N_2 and O_2, weighted by number density:

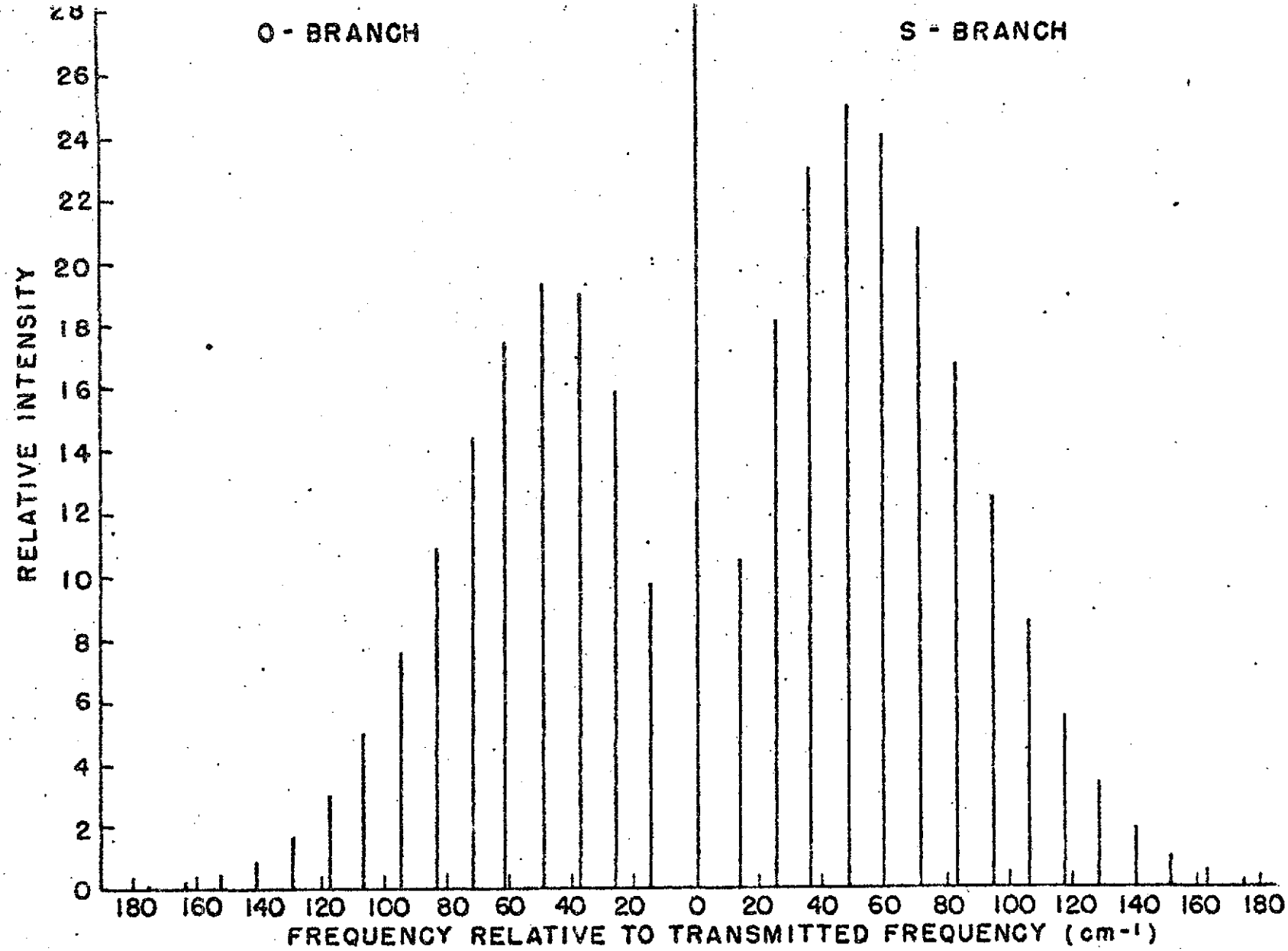

Figure 4. Computed rotational Raman line locations and intensities for oxygen. . .

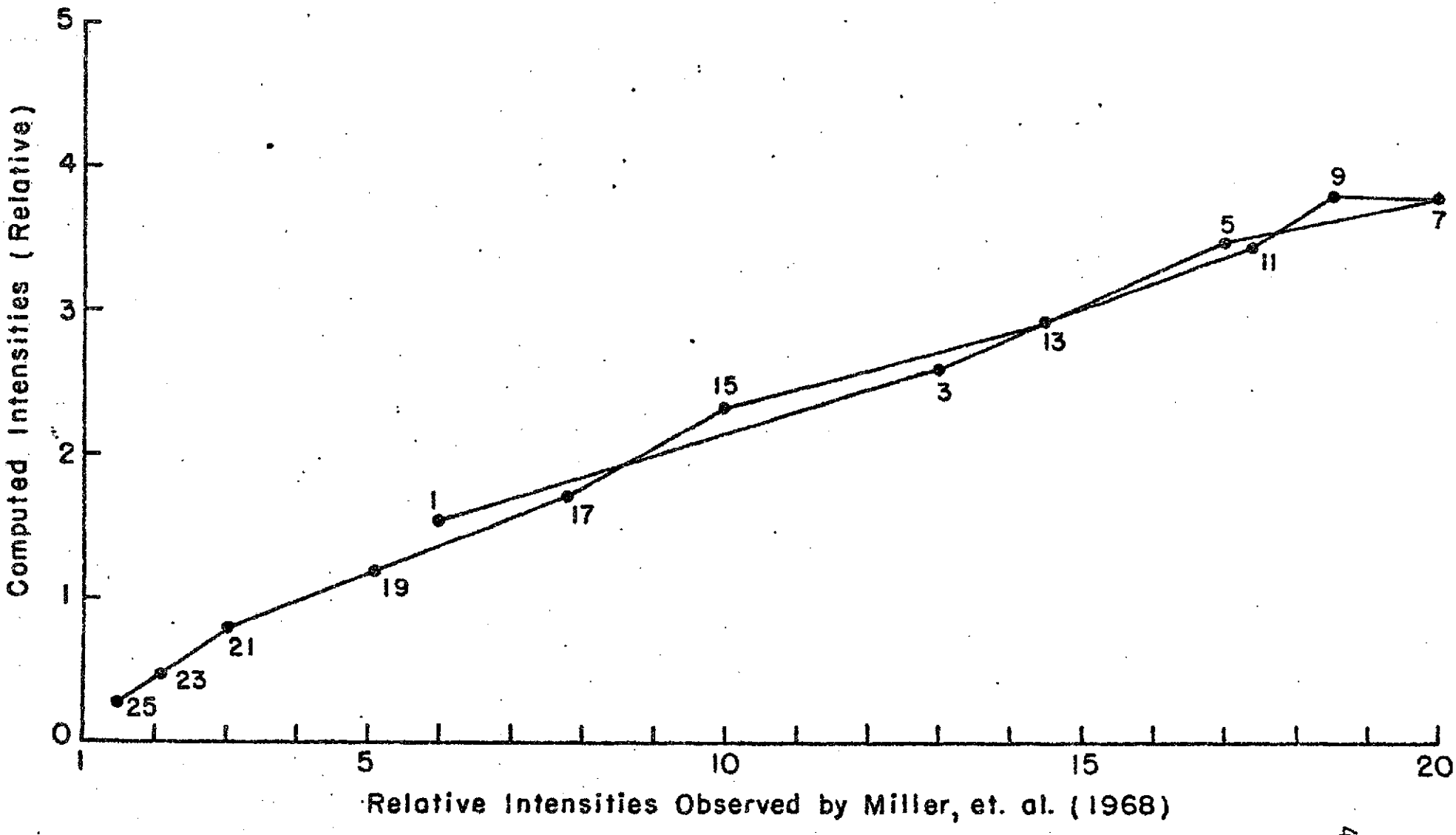
Computed Intensities (Relative)
Relative Intensities Observed by Miller, et. al. (1968)
0
1
2
3
4
5
1
5
10
15
20
25
23
21
19
17
15
13
11
9
7
3
1

$$\gamma^2(\text{Air}) = \gamma^2(N_2)\left[\frac{\frac{\gamma^2(O_2)}{\gamma^2(N_2)} + \frac{n(N_2)}{n(O_2)}}{1 + \frac{n(N_2)}{n(O_2)}}\right] \qquad (29)$$

The number density ratio in the atmosphere is considered in the U. S. Standard Atmosphere, 1962 to be constant with height between the surface and 90 km. The number density ratio is given as

$$\frac{n(N_2)}{n(O_2)} = \frac{78.084}{20.946} = 3.728 \quad (0 \leqslant z \leqslant 90 \text{ km})$$

Values for the polarizability anisotropies in N_2 and O_2 were obtained by Bridge and Buckingham (1966) from measurements of depolarization ratios. Their values, which were obtained from measurements made at 6328 Å, are

$$\gamma(N_2) = 0.69 \text{ Å}^3$$
$$\gamma(O_2) = 1.09 \text{ Å}^3$$

These figures give a ratio,

$$\frac{\gamma^2(N_2)}{\gamma^2(O_2)} = 0.401$$

The Landolt-Börnstein Tables (1951), citing observations made in 1928, give values of

$$\gamma(N_2) = 0.93 \text{ Å}^3$$
$$\gamma(O_2) = 1.14 \text{ Å}^3$$

which result in the ratio,

$$\frac{\gamma^2(N_2)}{\gamma^2(O_2)} = 0.665$$

Ory and Yura (1965) computed γ for N_2 from theoretical considerations and obtained a value of 1.02 Å^3.

There are obviously considerable differences among the various determinations of polarizability anisotropies. Although the determination of quantitative turbidity soundings depends upon knowledge of the absolute values of these anisotropies, the design considerations which follow depend only upon the ratio $\gamma^2(N_2)/\gamma^2(O_2)$.

Miller, et.al. (1968) observed the composite rotational Raman spectrum of air directly. Through the use of the relative strengths of N_2 and O_2 lines in their results, together with the precisely known ratio, $n(N_2)/n(O_2)$, the ratio $\gamma^2(N_2)/\gamma^2(O_2)$ was computed here for comparison with the above figures.

The observations by Miller, et.al. (1968) were found to agree closely with those of Bridge and Buckingham (1966) (See Appendix 1.), and thus their figures are used in the

present study. We therefore find that

$$\gamma^2(\text{Air}) = 1.317\ \gamma^2(N_2)$$

and, for Bridge and Buckingham's value of $\gamma(N_2)$,

$$\gamma^2(\text{Air}) = 0.627\ \text{Å}^6$$

This gives the rotational Raman backscatter cross section of air as

$$\sigma_{\substack{\text{Ram} \\ \parallel+\perp \\ o+s}}(\text{Air}) = 4.91 \times 10^{-30}\ \text{cm}^2\text{-ster}^{-1} \quad (\lambda = 6943\text{Å})$$

At 300°K, the distribution of scattering between the S- and O-branches is in the ratio 1.39:1, or

$$\sigma_{\substack{\text{Ram} \\ \parallel+\perp \\ s}}(\text{Air}) = 2.85 \times 10^{-30}\ \text{cm}^2\text{-ster}^{-1}$$

and

$$\sigma_{\substack{\text{Ram} \\ \parallel+\perp \\ o}}(\text{Air}) = 2.06 \times 10^{-30}\ \text{cm}^2\text{-ster}^{-1}$$

Figure 6 shows the composite rotational Raman spectrum of air.

H. The Rayleigh backscatter cross section of air (N_2 and O_2).

The Rayleigh backscatter cross section of air has been variously defined to include all of the rotational Raman lines, to include some of the rotational Raman lines, to include only scattered radiation polarized parallel to the

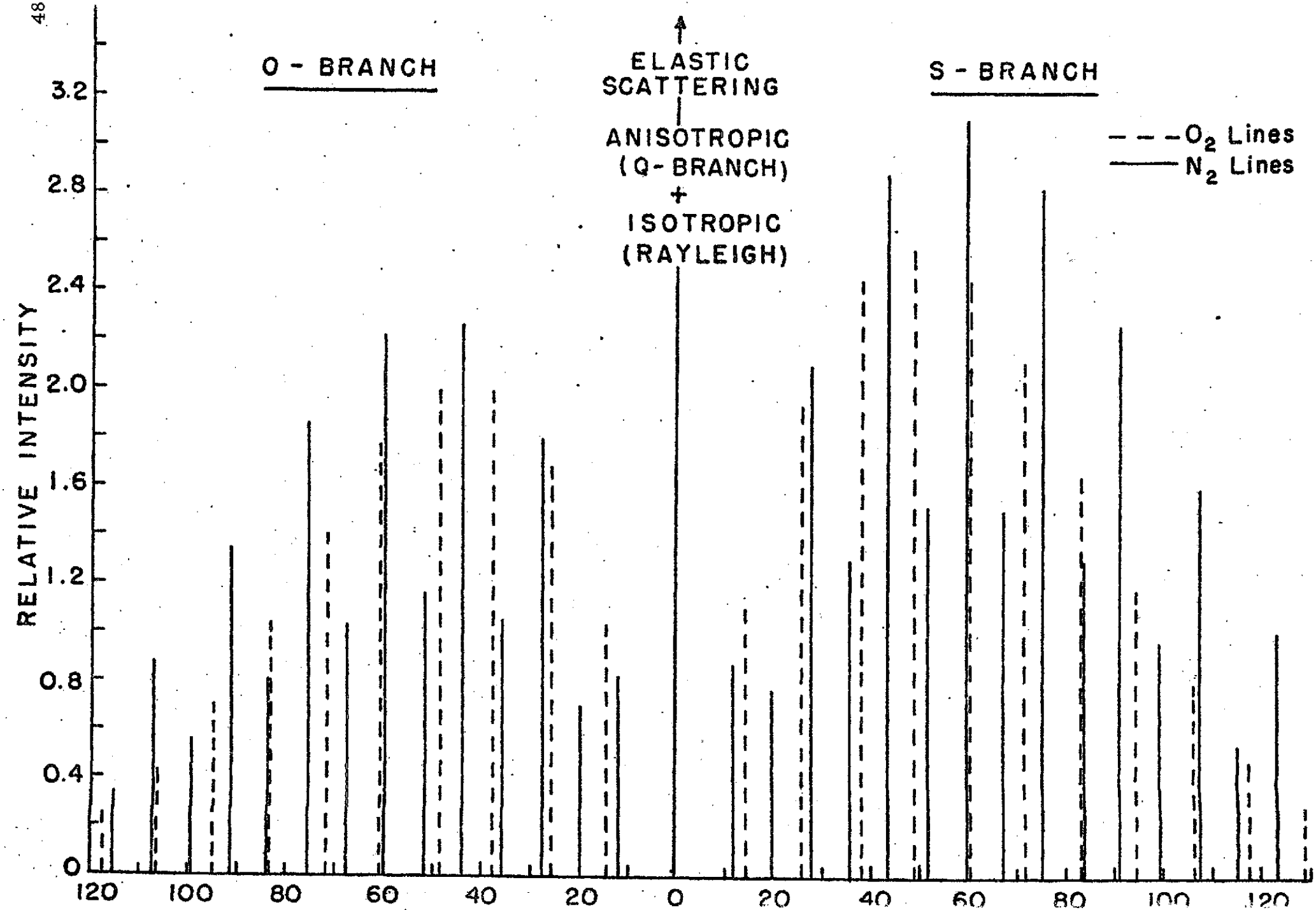
O - BRANCH
ELASTIC SCATTERING
ANISOTROPIC (Q-BRANCH) + ISOTROPIC (RAYLEIGH)
S - BRANCH
O_2 Lines
N_2 Lines
RELATIVE INTENSITY
3.2
2.8
2.4
2.0
1.6
1.2
0.8
0.4
0
120
100
80
60
40
20
0
20
40
60
80
100
120

incident light, or to include both parallel and perpendicularly polarized radiation.

Each of the above definitions has merit and has enjoyed some popularity in the literature, and it is of course necessary to keep these various definitions in mind when comparing the results of different investigators. The definition of the Rayleigh backscatter cross section to be used here includes only light returned at the wavelength of the incident light, without regard to polarization. As such, through use of the expression derived by Chandrasekhar (1960) together with the results of Stuart (1934), we find the Rayleigh backscatter cross section to be

$$\sigma_{\substack{\text{Ray} \\ \parallel+\perp}}(\text{Air}) = \left(\frac{2\pi}{\lambda}\right)^4 \left[\alpha^2(\text{Air}) + \frac{7}{180}\gamma^2(\text{Air})\right] \quad (30)$$

In a manner analogous to that of the previous section, we obtain

$$\alpha^2(\text{Air}) = \alpha^2(N_2)\left[\frac{\dfrac{\alpha^2(O_2)}{\alpha^2(N_2)} + \dfrac{n(N_2)}{n(O_2)}}{1 + \dfrac{n(N_2)}{n(O_2)}}\right] \quad (31)$$

The polarizability of air may be determined from measurements of the refractive index and total molecular

number density by means of the Lorentz - Lorenz formula (Born and Wolf, 1959),

$$\alpha = \frac{3}{4\pi n} \left| \frac{m^2 - 1}{m^2 + 2} \right| \qquad (32)$$

Elterman (1968), using an expression determined by Edlen (1953), gives the refractive index of air at 6943 Å, for standard temperature and pressure (1013 mb and 15°C) as

$$m = 1.00027584$$

The U. S. Standard Atmosphere, 1962 gives the number density at that temperature and pressure as

$$n = 2.5471 \times 10^{19} \text{ cm}^{-3}$$

Thus, we obtain

$$\alpha^2(\text{Air}) = 2.97 \text{ Å}^6$$

from considerations of refractive index.

The Landolt Börnstein Tables (1951) give

$$\alpha(N_2) = 1.76 \text{ Å}^3$$

$$\alpha(O_2) = 1.60 \text{ Å}^3$$

from spectroscopic measurements. These figures result in

$$\alpha^2(\text{Air}) = 2.99 \text{ Å}^6$$

Stansbury, Crawford and Welsh (1953) computed $\alpha(N_2)$ and $\alpha(O_2)$ using refractive indices given in the International Critical Tables for 4358 Å. They give

$$\alpha(N_2) = 1.79 \text{ Å}^3$$

$$\alpha(O_2) = 1.63 \text{ Å}^3$$

or

$$\alpha^2(\text{Air}) = 3.10 \text{ Å}^6$$

Ory and Yura (1965) derived $\alpha(N_2)$ from molecular orbital considerations. Their theoretical approach yielded

$$\alpha(N_2) = 1.41 \text{ Å}^3$$

Kolker and Karplus (1963), who also employed a theoretical approach, found that

$$\alpha(N_2) = 2.40 \text{ Å}^3$$

In this study, we adopt a value for $\alpha^2(\text{Air})$ intermediate between that computed from refractive index considerations (2.97 Å^6) and that computed from spectroscopic data (2.99 Å^6), or

$$\alpha^2(\text{Air}) = 2.98 \text{ Å}^6$$

It is felt that this value is representative of our present knowledge of $\alpha^2(\text{Air})$.

Using this value of $\alpha^2(\text{Air})$, together with the value of $\gamma^2(\text{Air})$ found in the previous section, we obtain

$$\sigma_{\substack{\text{Ray} \\ \parallel+\perp}}(\text{Air}) = 2.01 \times 10^{-28} \text{ cm}^2\text{-ster}^{-1}$$

for a wavelength of 6943 Å. This value is 40.9 times as

large as the Raman backscatter cross section of air.

I. Off-frequency components of scattering from minor constituents of the atmosphere.

1. Gases.

a. Permanent constituents.

Table 4 shows the relative abundance of gaseous atmospheric constituents with molecular number densities greater than 10^{-6} of the total. The monatomic gases, A, Ne, He and Kr, by virtue of their inherent molecular symmetry, have no rotational Raman spectrum (Herzberg, 1945). Methane, CH_4, while not monatomic, also has no rotational Raman spectrum, since it is a "spherical top" molecule, and therefore has no polarizability anisotropy (Herzberg, 1945).

Thus, the only permanent gaseous atmospheric constituent other than N_2 and O_2 which could produce rotational Raman lines is CO_2, a linear triatomic molecule which is highly anisotropic. Bridge and Buckingham (1966) give the polarizability anisotropy of CO_2 as $2.10\ \text{Å}^3$.

We may write the ratio of the intensity of Raman scattering from CO_2 to that from N_2 and O_2 as

$$\frac{I(CO_2)}{I(N_2+O_2)} = \frac{n(CO_2)\,\gamma^2(CO_2)}{n(N_2)\,\gamma^2(N_2) + n(O_2)\,\gamma^2(O_2)} \qquad (33)$$

Table 4. Relative abundance of permanent gaseous constituents of the atmosphere with molecular number densities greater than 10^{-6} of the total. (After Goody, 1964)

Molecule	Fraction of Total Number Density
N_2	7.8084×10^{-1}
O_2	2.0946×10^{-1}
A	9.34×10^{-3}
CO_2	3.3×10^{-4}
Ne	1.818×10^{-5}
He	5.24×10^{-6}
CH_4	1.6×10^{-6}
Kr	1.14×10^{-6}

When we insert the appropriate anisotropies and number densities into (33), we arrive at an intensity ratio of 0.23 %. Thus, for the purposes of this study, we may neglect the effect of rotational Raman scattering from CO_2, as well as that from the other permanent constituents of air other than N_2 and O_2.

b. Water vapor.

(1) Rotational Raman backscatter cross section.

H_2O is a planar asymmetric top molecule and, as such, has a very complex rotational Raman spectrum (Herzberg, 1945). We shall not concern ourselves here with individual spectral lines, but only with the ratio of the total water vapor Raman cross section to that of air. However, it should be noted here that Eisenberg and Kauzmann (1969) state that, at room temperature, the rotation band is most intense near $\Delta\nu = 200\ cm^{-1}$.

In Chapter III.F., we determined the polarizability anisotropy, γ, of air, and noted that rotational Raman scatter cross sections are proportional to γ^2, independent of the nature of the spectral distribution of the lines or molecular geometry. We thus limit our task to finding γ^2 for H_2O, in order that we may compare it to γ^2 for air.

The optical properties of water vapor are not well known. As a simplification, Dorsey (1940) assumed that two of the axes of the polarizability ellipsoid are equal. By employing this approximation, he was able to treat the H_2O molecule as though it had an axis of symmetry (that is, that the polarizability ellipsoid was an ellipsoid of revolution). For such a molecule, the polarizability anisotropy is given by Stuart (1934) as

$$\gamma^2 = \alpha^2\left[\frac{45\,\Delta}{6 - 7\Delta}\right] \tag{34}$$

Dorsey (1940) gives α as 1.59 Å^3 and Fabelinskii (1968) gives Δ as 0.020. Thus, we find that

$$\gamma^2(H_2O) = 0.39\ \text{Å}^6$$

In Chapter III.G., it was shown that γ^2(Air) is 0.629 Å^6. Then the ratio of the squares of the polarizability anisotropies for H_2O and for air is 0.62.

(2) Number density in the atmosphere.

In order to place limits on the water vapor number densities which might be encountered in the atmosphere, we recognize that atmospheric water vapor content decreases much more rapidly with height than does the number density of air. As such, we expect to find the worst case at or

near the surface. Consider a very moist atmosphere with p = 1013 mb, T = 30°C and RH = 100%. Then, using the table given by Hess (1959), we obtain

$$\frac{n(H_2O)}{n(Air)} = \frac{e}{p} = \frac{4.243 \times 10^4}{1.013 \times 10^6} = 3.99 \times 10^{-2} \qquad (35)$$

or 3.99 percent.

(3) Raman scattering from water vapor relative to that from air.

The ratio of scattered light intensity from H_2O, relative to that from air is given by

$$\frac{I(H_2O)}{I(Air)} = \frac{n(H_2O)\,\gamma^2(H_2O)}{n(Air)\,\gamma^2(Air)} \qquad (36)$$

Using the results of Sections (1) and (2) above, we find that

$$\frac{I(H_2O)}{I(Air)} = 2.47 \times 10^{-2}$$

or 2.47 percent, under the pessimistic circumstances cited above.

2. Liquids.

a. General.

When a gaseous substance condenses into liquid form, intermolecular forces become much greater and, as a result, molecular rotation is hindered or absent entirely. Herzberg (1945) discusses the nature of Raman scattering in liquids. He shows that, instead of a series of lines, the off-frequency component consists of a continuum of energy extending to either side of the undisplaced line, and decreasing monotonically with $\Delta\nu$. Superimposed on this continuum may be broad lines resulting from transitions between hindered rotational or translational states and intermolecular bending and stretching modes.

The only liquid present to any appreciable extent in the atmosphere is water, and the remainder of this discussion will be confined to this substance.

b. Raman spectrum of liquid water.

The Raman spectrum of liquid water has been studied by several investigators [e.g., Cross, et.al. (1937), Narayanaswamy (1948), Walrafen (1964, 1967) and Senior and Thompson (1965)]. It is generally agreed that, in addition to the continuum mentioned in Part a. above, broad

lines exist near $\Delta\nu = 60\ cm^{-1}$ and $\Delta\nu = 165\ cm^{-1}$, as well as at other frequencies outside out region of interest. Unfortunately, none of the above studies deals with the intensities of these lines relative to the elastic scattering. The study by Walrafen (1964) shows that both lines decrease in intensity by about a factor of three as temperature is increased from 0°C to 40°C.

To place an upper limit on the Raman scatter cross section per molecule of liquid water, we recall that such scattering is merely a hindered form of the scattering that occurs in water vapor and, as such must be lower in intensity. Thus, we may write, as an upper limit, that

$$\sigma_{\substack{Ram \\ H_2O\ Liquid}} = \sigma_{\substack{Ram \\ H_2O\ Vapor}} \tag{37}$$

Since we found previously that

$$\sigma_{\substack{Ram \\ H_2O\ Vapor}} = 0.62\ \sigma_r \tag{38}$$

we may write

$$\sigma_{\substack{Ram \\ H_2O\ Liquid}} \leq 0.62\ \sigma_r \tag{39}$$

c. Molecular number density of liquid water in the atmosphere.

Typical clouds have water contents of the order of 3×10^{-7} gm-cm^{-3}, or about 1×10^{16} molecules-cm^{-3}. Air density ranges from about 2.5×10^{19} molecules at the surface to 8.6×10^{18} molecules-cm^{-3} at 10 km. Thus, a conservative upper limit for the ratio of liquid water molecules to air molecules ranges from 4×10^{-4} at the surface to 1.2×10^{-3} at 10 km. Above 10 km, water clouds should be of no significance.

Thus, for a relatively dense cloud at 10 km, under these pessimistic assumptions, the scattered intensity ratio would be

$$\frac{I_{Cloud}}{I_{Air}} = \frac{\tilde{\sigma}_{Ram\ H_2O\ Liquid}}{\sigma_r} \cdot \frac{n_{H_2O\ Liquid}}{n(Air)} \qquad (40)$$

$$= (0.62)(1.2 \times 10^{-3}) = 0.074\ \%$$

3. Solids.

a. General.

When a substance assumes a solid state, molecules are bound tightly together into a relatively fixed lattice. Molecular rotation is not possible, but low frequency lat-

tice vibrations occur which cause off-frequency scattering components in the same region as rotational Raman scattering. For a given substance, the character (frequency and intensity) of the lattice vibrations and, therefore, of the scattering, vary with lattice defects and impurities. As in the case of liquids, these lines are generally quite broad. Mitra (1969) presents an extensive discussion of Raman scattering in solids.

b. Particulates in the atmosphere.

Consider a highly turbid urban atmosphere in which the particle number density distribution varies with height according to

$$N\ (\text{particles-cm}^{-3}) = N_o\, e^{-\frac{z}{H}} \qquad (41)$$

where N_o, the particle number density near the surface, is about 5×10^5 particles-cm^{-3} and the scale height, H, is 1.67 km. This is similar to several distributions shown by Junge (1963). We also assume that the size distribution is of the form,

$$\frac{dN}{d \log r} = Kr^{-3} \qquad (42)$$

which is given by Junge (1963). In alternative form, this

may be written as

$$\frac{dN}{dr} = \frac{3Nr^{-4}}{r_{min}^{-3} - r_{max}^{-3}} \tag{43}$$

If we assume that the particles are spherical, then the number of molecules per increment of radius is

$$\frac{dn_{Part}}{dr} = \frac{\frac{4}{3}\pi r^3 \rho_{Part} a}{\mu} \frac{dN}{dr} \tag{44}$$

Combining (43) and (44) and integrating, we obtain the number of molecules found in particulates in the finite interval of radii, $r_{min} \leqslant r \leqslant r_{max}$,

$$n_{Part} = \frac{4\pi \rho_{Part} a N}{\mu (r_{min}^{-3} - r_{max}^{-3})} \ln \frac{r_{max}}{r_{min}} \tag{45}$$

Let $r_{min} = 10^{-6}$ cm and $r_{max} = 10^{-4}$ cm, $\mu = 100$ gm-mole^{-1} and $\rho_{Part} = 1$ gm-cm^{-3}. Then,

$$n_{Part} = 3.5 \times 10^5 N$$

At $z = 0$, where $N = 5 \times 10^5$ particles-cm^{-3},

$$n_{Part} = 1.73 \times 10^{11} \text{ molecules-cm}^{-3}$$

The mass loading associated with a particulate distribu-

tion of this sort is

$$m_{Part} = \frac{\mu n_{Part}}{a} = 28.8\ \mu g\text{-}m^{-3} \qquad (46)$$

The distribution of mass loading with particle radius interval is shown in Figure 7. These quantities are of the same magnitudes as those found in urban areas.

Distribution of particulate concentration with radius interval is shown in Figure 8. Particulate concentrations computed in this manner for the region $r > 0.3\mu$ will be shown in Chapter III.H.3.c.(2)(a) to agree with observed concentrations.

The molecular number density of air at $z = 0$ is typically 2.5×10^{19} molecules-cm^{-3}, as was mentioned earlier. Thus, for off-frequency scattering from particulates to be even one percent of that from air molecules, the scatter cross section per molecule would have to be 1.5×10^{6} times the rotational Raman cross section of air. Were this the case, Raman scattering from large crystals would be an easily observable phenomenon, which it is not. Mitra (1969), in fact, states that Raman scattering from crystals is a second order process.

By virtue of the molecular number densities involved, and the fact that Raman scattering from crystals is a

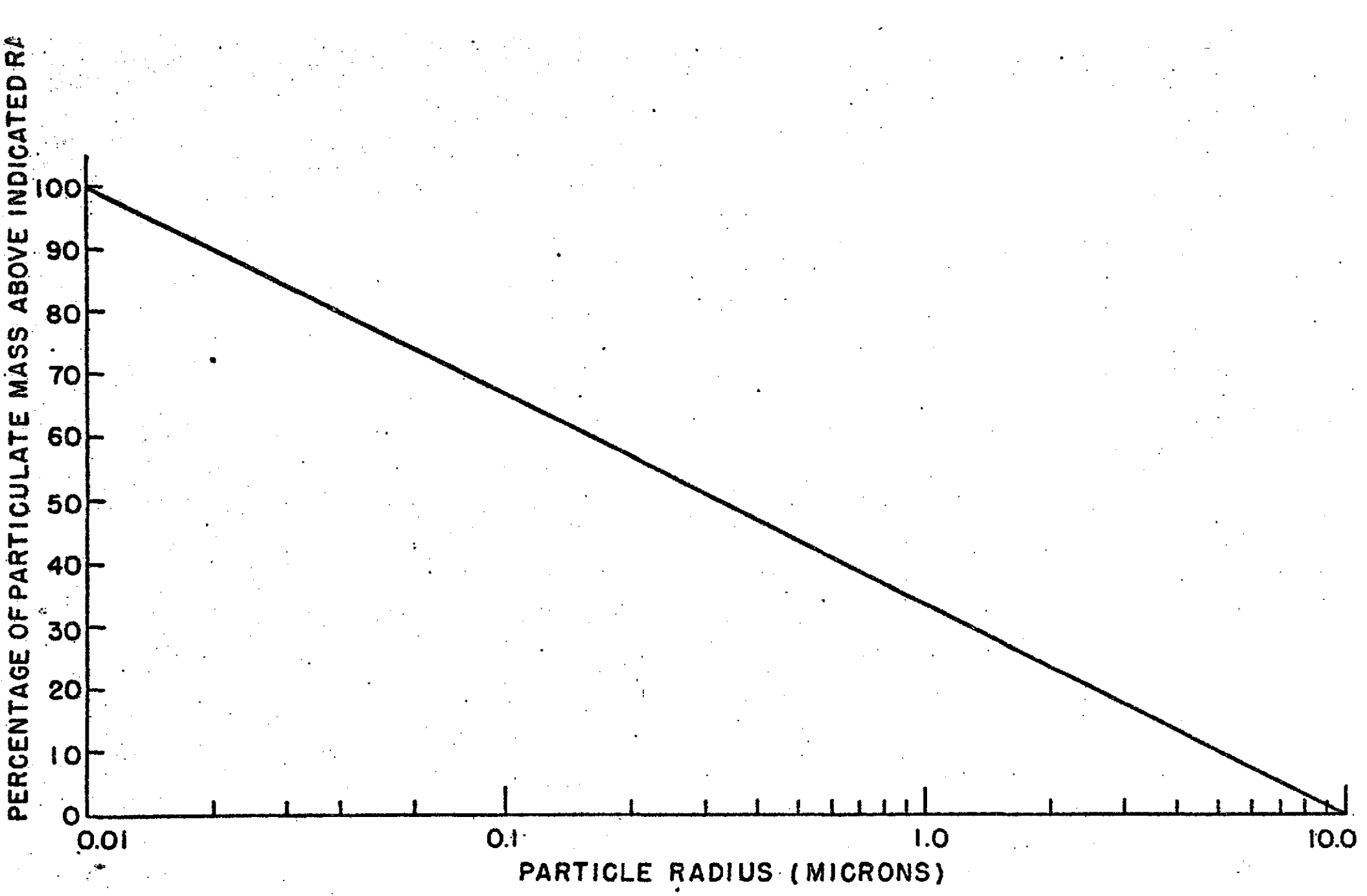

Figure 7. Distribution of particulate mass loading with particle radius interval, as given by model discussed in text.

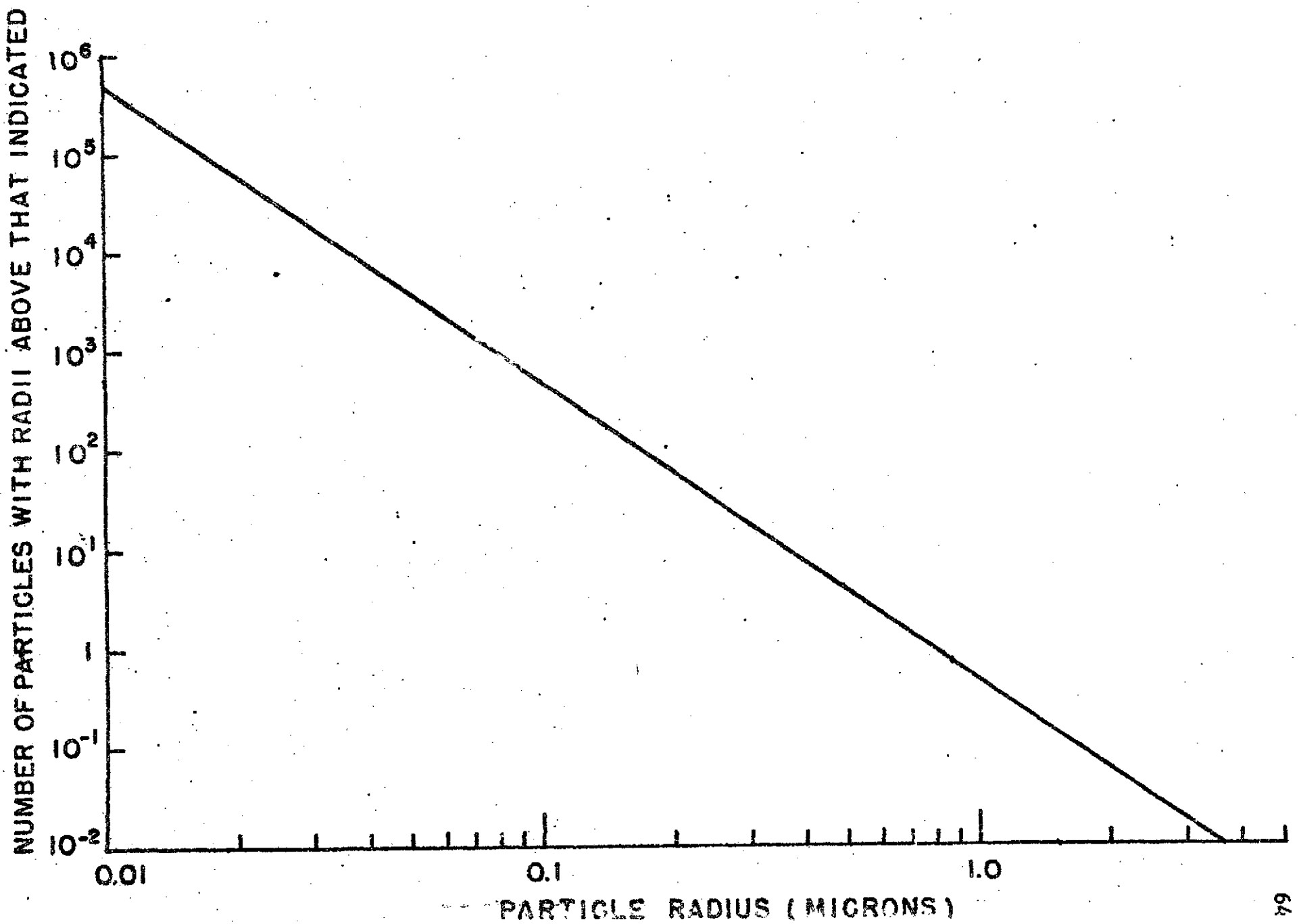
NUMBER OF PARTICLES WITH RADII ABOVE THAT INDICATED
10^6
10^5
10^4
10^3
10^2
10^1
1
10^{-1}
10^{-2}
0.01
0.1
1.0
PARTICLE RADIUS (MICRONS)

second order process, we expect to be justified in assuming that the off-frequency component of scattering from atmospheric particulates is negligible in comparison to that from air. In the next section, an experiment will be described which shows that this is indeed the case.

c. Verification in the laboratory that the contribution of off-frequency particulate scatter to the Raman spectrum of air is insignificant compared to that of molecular scatter.

(1) Design of the experiment.

We wish to duplicate in the laboratory, using a Cary* Model 82 Raman Spectrophotometer, the ratio of off-frequency particulate to molecular scattering observed in the atmosphere by a laser radar system. According to Haber (1972), the sample volume of the Model 82 may be considered as a cube, 50μ on a side (i.e., a volume of $1.25 \times 10^{-7} cm^3$). If we assume that a typical urban atmosphere may contain as little as 10^4 particles per cubic centimeter, then, at any given time, there will be an average of only 0.00125 particles in the sample volume. Thus, we cannot rely on spatial averaging of particle number density to give us a

*Cary Instruments, 2724 S. Peck Rd., Monrovia, CA 91016.

statistically significant result. We must instead rely upon time averaging as a means of obtaining statistical stability.

Suppose that particles are forced through the bottom boundary of the sample volume with velocity $\bar{v}$. Then the average rate at which particles pass through that boundary is

$$\frac{d\bar{n}}{dt} = NA\bar{v} \tag{47}$$

where N is the average particulate number density, and A is the area of the bottom of the sample volume.

The average number of particles seen by the spectrophotometer in the integrating time interval is

$$\bar{n} = \frac{d\bar{n}}{dt}\,\delta t = NA\bar{v}\,\delta t \tag{48}$$

If we assume Poisson statistics, then the standard deviation of this number is

$$\sigma(\bar{n}) = \bar{n}^{\frac{1}{2}} = \left[NA\bar{v}\,\delta t\right]^{\frac{1}{2}} \tag{49}$$

and

$$\frac{\sigma(\bar{n})}{\bar{n}} = \left[NA\bar{v}\,\delta t\right]^{-\frac{1}{2}} \tag{50}$$

The integrating time, δt, is related to the spectral slit

width, $\delta\nu$, by

$$\delta t = \frac{\delta\nu}{d\nu/dt} \tag{51}$$

where $d\nu/dt$ is the spectral scan rate of the instrument (constant). Thus,

$$\frac{\sigma(\bar{n})}{\bar{n}} = \left[\frac{d\nu/dt}{NA\bar{v}\,\delta\nu}\right]^{\frac{1}{2}} \tag{52}$$

Let $\delta\nu = 2\ cm^{-1}$, $d\nu/dt = 0.4\ cm^{-1}\text{-}sec^{-1}$, and $A = 2.5 \times 10^{-5}\ cm^2$. Then

$$\frac{\sigma(\bar{n})}{\bar{n}} = \left[\frac{8 \times 10^4}{N\bar{v}}\right]^{\frac{1}{2}} \tag{53}$$

or

$$\bar{v} = \frac{8 \times 10^4}{N\left[\sigma(\bar{n})/\bar{n}\right]^2} \tag{54}$$

If $N = 10^4$ particles-cm^{-3}, and

$$\frac{\sigma(\bar{n})}{\bar{n}} = 0.1$$

Then

$$\bar{v} = 800\ cm\text{-}sec^{-1}$$

If the sample cell through which this flow takes place has a cross sectional area of $0.5\ cm^2$, as is the case for the Cary Model 82 Raman Spectrophotometer, then the required air flow rate is 24 liters-min^{-1}.

Suppose that we wish to use ambient outside air as our sample source, drawing it through the spectrophotometer by means of a vacuum pump as shown in Figure 9. We desire to minimize impaction of particles on the walls of the tubing leading to the spectrophotometer. We examine first the range of tubing diameters required if the flow through the tubing is to be laminar.

The flow rate through the tube is related to the diameter of the tube and flow velocity via

$$Q = \tfrac{1}{4}\pi d^2 \bar{v} \tag{55}$$

We require that the Reynolds number for the flow be less than the critical value above which the laminar flow regime gives way to turbulence. According to Haltiner and Martin (1957), the Reynolds number is given by

$$Re = \frac{v_{max} d}{\eta} \tag{56}$$

Combining our two requirements, we find that

$$d = \frac{4Q}{\pi \eta Re} \frac{v_{max}}{\bar{v}} \tag{57}$$

For air at a pressure of one atmosphere, in the atmospheric range of temperatures,

$$\eta \doteq 0.14 \text{ cm}^2\text{-sec}^{-1}$$

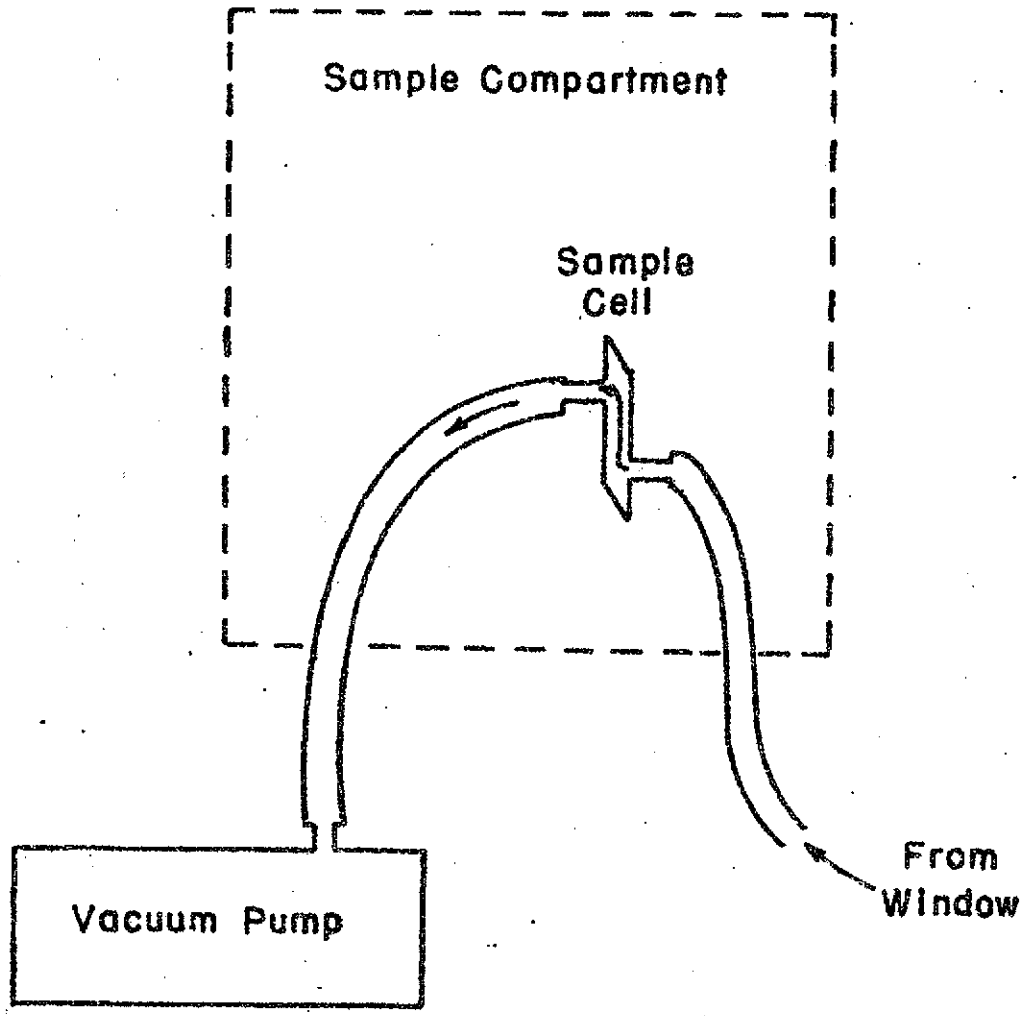

Figure 9. Arrangement of pumping system for drawing particulate matter through spectrophotometer sample cell.

Haltiner and Martin give the critical value of Re as 24,000. If we make the conservative assumption that

$$\frac{v_{max}}{\bar{v}} = 2$$

then

$$d_{crit} = 7.6 \times 10^{-4} Q$$

If we take Q as 1000 $cm^3 \cdot sec^{-1}$, considerably greater than the minimum value determined above, we find that

$$d_{crit} = 0.76 \text{ cm}$$

While considerations of wall effects limit the minimum tubing diameter, the maximum diameter is limited by the sedimentation rate of the particles; that is, if the velocity of the particles through the tube is too small, they will sediment out of the air stream before passing through the entire length of the tube.

If we assume that both the horizontal and vertical components of the particle motion are constant, we may write

$$d = 2 \frac{w}{v} L \qquad (58)$$

as the minimum allowable diameter for a given tubing length, for a particle entering along the center line of

the tube. If we assume that the particles are spheres and that their terminal velocities are given by Stokes' Law (Fleagle and Businger, 1963), then

$$w = \frac{2}{9} \frac{r^2 \rho_{Part}}{\eta \rho_{Air}} g \qquad (59)$$

The relationship,

$$Q = \tfrac{1}{4} \pi v d^2 \qquad (60)$$

must be satisfied, as before. So,

$$d = \frac{9Q\eta \rho_{Air}}{\pi r^2 \rho_{Part} gL} \qquad (61)$$

Assuming values for Q and η as before, and $r = 10^{-4}$ cm, $\rho_{Air} = 1.2 \times 10^{-3}$ gm-cm^{-3}, $\rho_{Part} = 2$ gm-cm^{-3} and $g = 980$ cm-sec^{-2}, we obtain

$$d = \frac{4.91 \times 10^4}{L}$$

For a 35 foot (1067 cm) length of tubing, the maximum permissible diameter is thus

$$d = 46 \text{ cm}$$

Since, for a given flow rate, gas velocity increases as $1/d^2$ and fall path increases as d, then tubing of diameter smaller than the value given above should be satisfactory from the standpoint of sedimentation.

It thus appears that any tube size with

$$0.76 \text{ cm} < d < 46 \text{ cm}$$

is compatible with our flow requirements. The only remaining consideration concerns the impaction of particles due to bends in the tubing. Some bends are necessary, but every attempt must be made to minimize their effect.

(2) Execution of the experiment.

The experimental arrangement employed here consisted of components essentially identical to those described above, including teflon tubing with a diameter of 1.9 cm.

A schematic diagram of the area surrounding the spectrophotometer is shown in Figure 10.

(a) Particle counter.

In order to ascertain the extent to which the tubing affected the observed particle counts in the sample cell, a Bausch & Lomb* Model 40-1 Dust Counter was employed to measure particle concentrations at both ends of the tubing. The instrument is capable of counting only particles with radii greater than about 0.3μ. It was felt, however, that if the tubing could efficiently transport particles of this

*Bausch & Lomb, Inc., Rochester, New York.

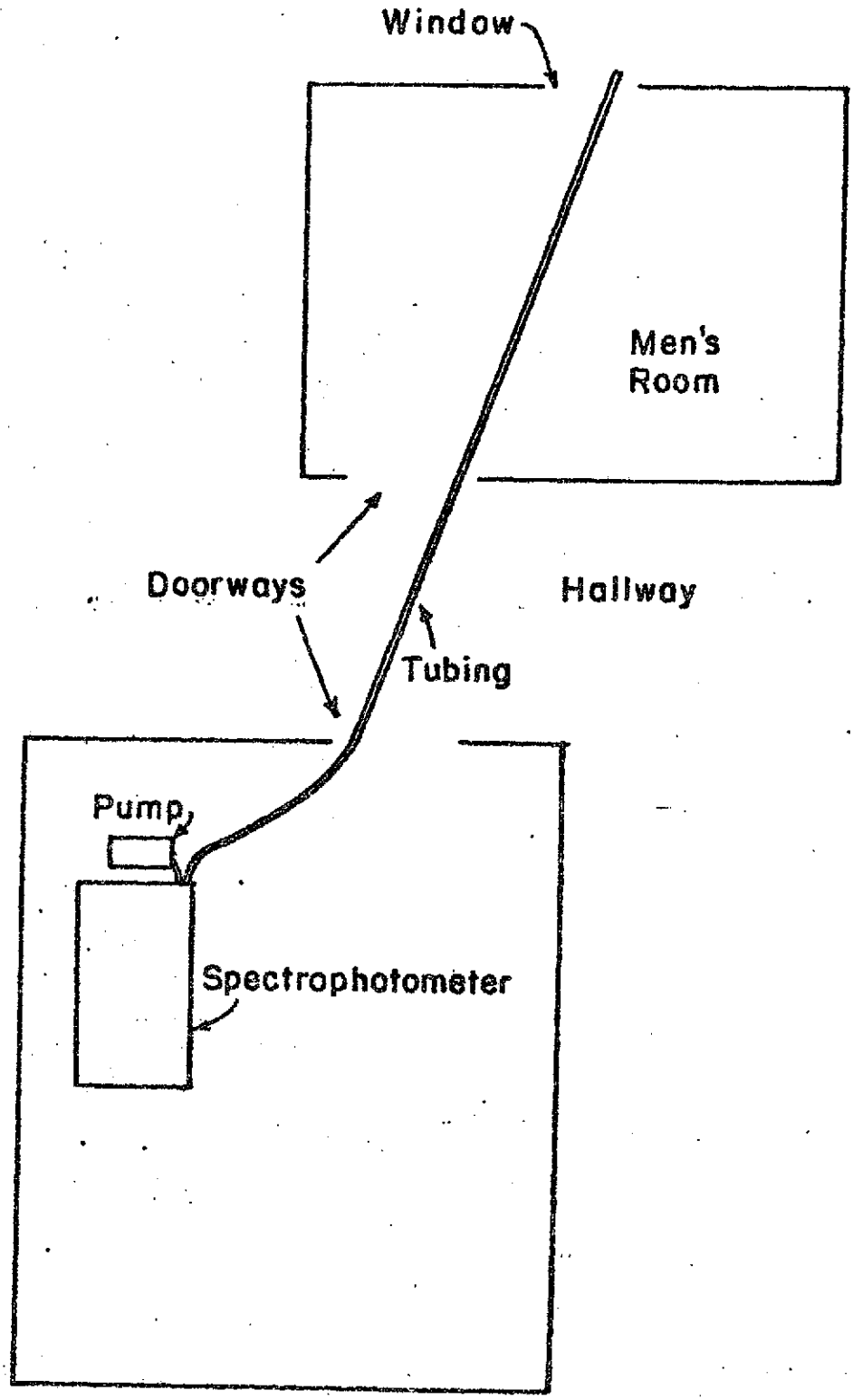

Figure 10. Scale diagram of area surrounding the spectrophotometer, showing the manner in which outside air was drawn in.

size, it would also transport smaller particles.

The counter utilized a small pump to divert a small sample of the air flow through an optical particle counting apparatus. In attempting to use the counter, however, it was found that the pump was not sufficiently powerful to counteract the pressure drop produced when the air was pulled through the tubing. This pressure drop was found to amount to about 35 mm Hg while, upon further investigation, it was found that the counter could not be operated at pressures differing by more than 0.22 mm Hg from the ambient pressure of the instrument.

In order to circumvent this requirement, the entire instrument was enclosed in an airtight plexiglas box which was maintained at the pressure of the air inside the tubing (see Figure 11).

Testing of the complete system, composed of tubing, sample cell, spectrophotometer, pump and dust counter, was conducted at the Wright Chemistry Laboratory of Rutgers University, the location of the spectrophotometer. At the time of the experiment, July 10, 1972, between 2:30 and 3:30 PM EDST, the counter indicated the following values:

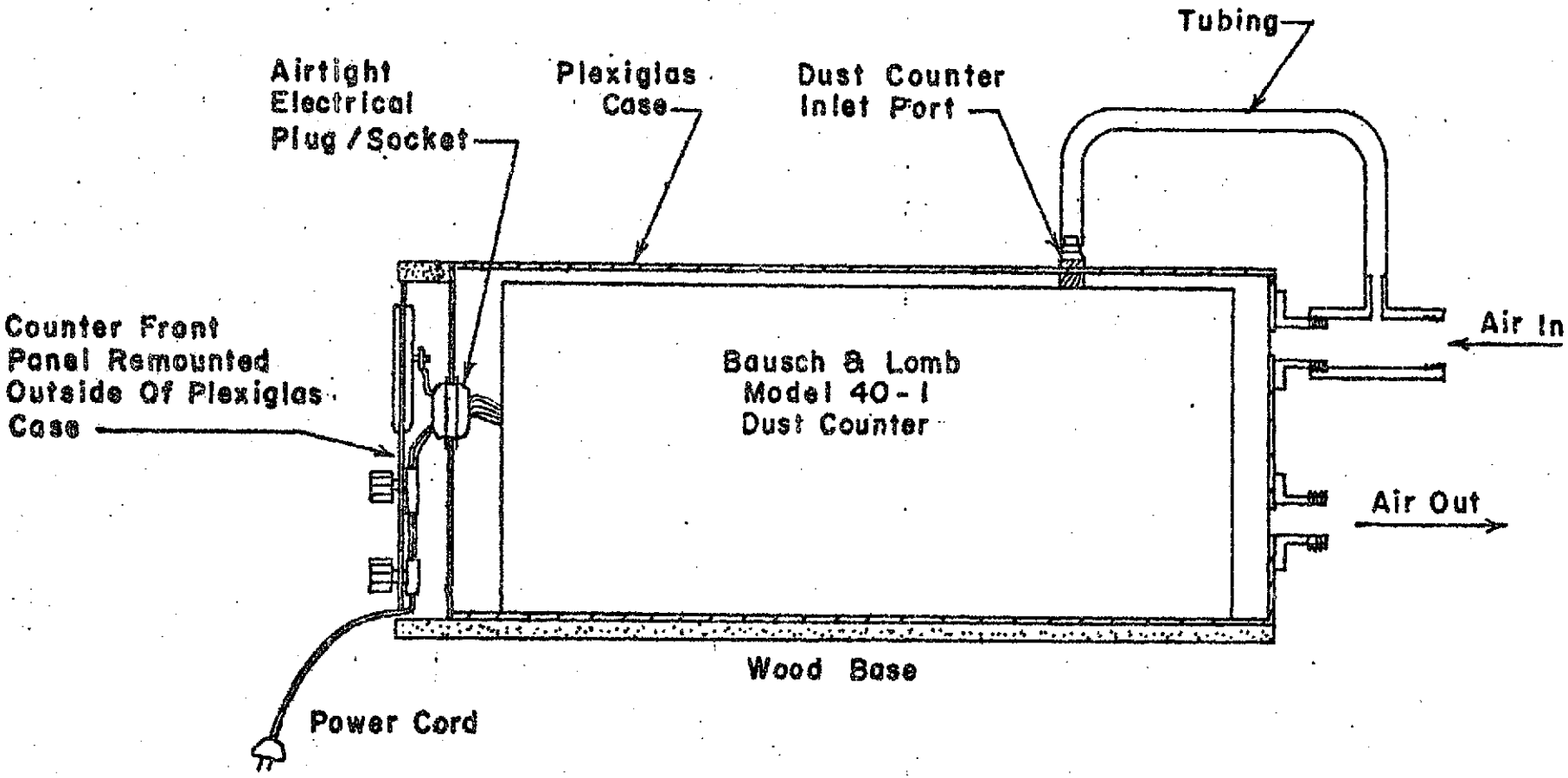

Figure 11. Diagram of enclosure that was constructed to maintain particle counter at pressure of air at the entrance to the spectrophotometer sample cell.

Size Range	Number Density (particles-cm^{-3})		
	Before Tubing	After Tubing	Model used in Computations
$>0.3\mu$	30	30	19
$>0.5\mu$	4	4	4
$>1.0\mu$	0.8	0.3	0.5
$>2.0\mu$	0.0	0.0	0.04

These observations are consistent with the model introduced in Chapter III.H.3.b. In this and in another trial run conducted at New York University, it was apparent that, at least for particles with radii less than one micron, the tubing did not introduce severe losses.

On the above date, observing stations of the New Jersey Environmental Protection Department at Perth Amboy and at Somerville recorded particulate loadings of 45 $\mu g\text{-}m^{-3}$ and 123 $\mu g\text{-}m^{-3}$ respectively, values that are representative of urban areas (Junge, 1963).

(b) Sample cell.

The Cary Model 82 Raman Spectrophotometer comes equipped with a roughly cylindrical multipass gas sample cell with Brewster angle windows at each end, and a single stopcock-equipped opening for filling. Since, for the purposes of this experiment, a continuously flowing sample was

required, a sample cell was purchased from Cary and modified to add a second opening and to replace the existing opening with one that did not contain a constriction. Figure 12 shows, schematically, the original and modified gas cells. The cell, as modified, was found to introduce a pressure drop of approximately 115 mm Hg into the flow.

(c) Vacuum pump.

A pump was desired which could give a flow rate of at least 1000 cm^3-sec^{-1} (2.1 cfm) at a pressure drop of 150 mm Hg (35 mm in the tubing plus 115 mm in the sample cell). The pump selected was the Gast* 0822-V103-G271X, which is rated at 5.6 cfm under the above conditions.

(d) Spectrophotometer.

With all of the other equipment in place, experimentation with the spectrophotometer controls indicated that the best possible spectra could be obtained with a spectral slit width of about 2 cm^{-1} and a scan rate of 0.4 cm^{-1}-sec^{-1}. These parameters are somewhat less favorable than those used in demonstration air spectra shown in the manufacturer's advertisements. The difference is attributable, first, to

---

*Gast Mfg. Corp., P. O. Box 97, Benton Harbor, Mich 49022.

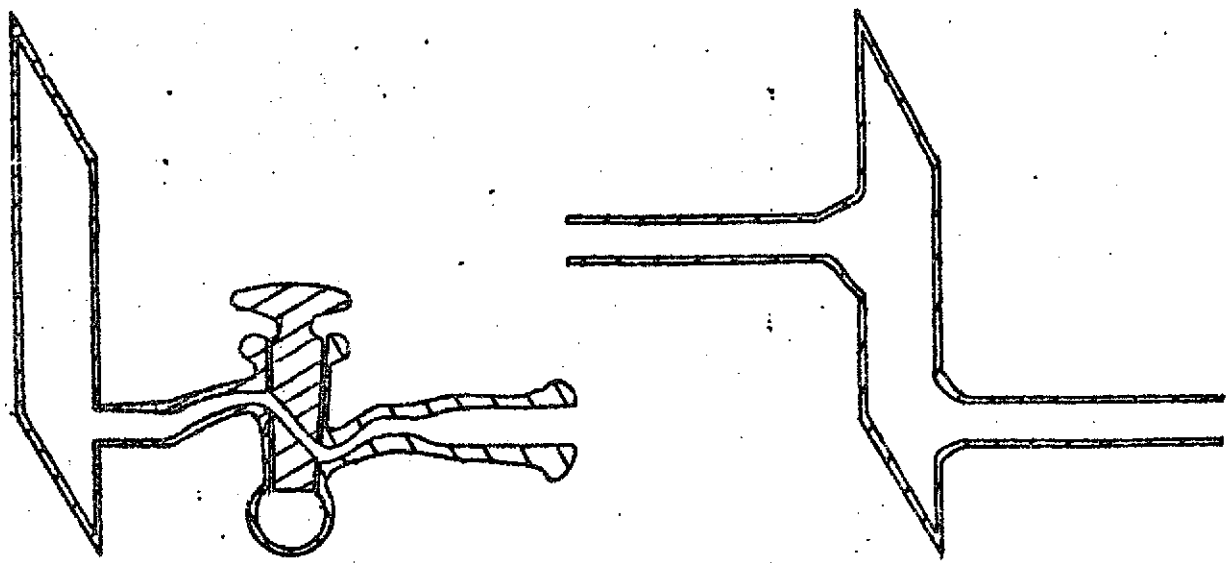

Figure 12. Scale drawing of the original and modified multipass gas sample cell.

the fact that the optical properties of the sample cell were, of necessity, damaged when the modifications were made. After modification, there was evidence of distortion of the Brewster angle windows which form the ends of the cell. In addition, the side walls of the cell, through which the Raman-scattered radiation passes, were slightly distorted. The second source of degradation of the Raman spectra was the fact that attachment of the tubing to the sample cell caused some slight dislocation of the cell, as well as backlash in the adjustments, for which no compensation could be made.

(3) Results.

Several spectra were taken with aged, air conditioned, room air in the sample cell. One of these spectra is shown in Figure 13. The spectra were all identical, showing no peaks beyond those attributable to N_2 and O_2. Similarly, spectra taken with the sample cell removed entirely (un-aged, air conditioned room air containing suspended particulate matter) were identical.

Two spectra were taken with the pump in operation, drawing outside air through the sample cell (see Figure 14). These spectra also contained no peaks beyond those found in clean air.

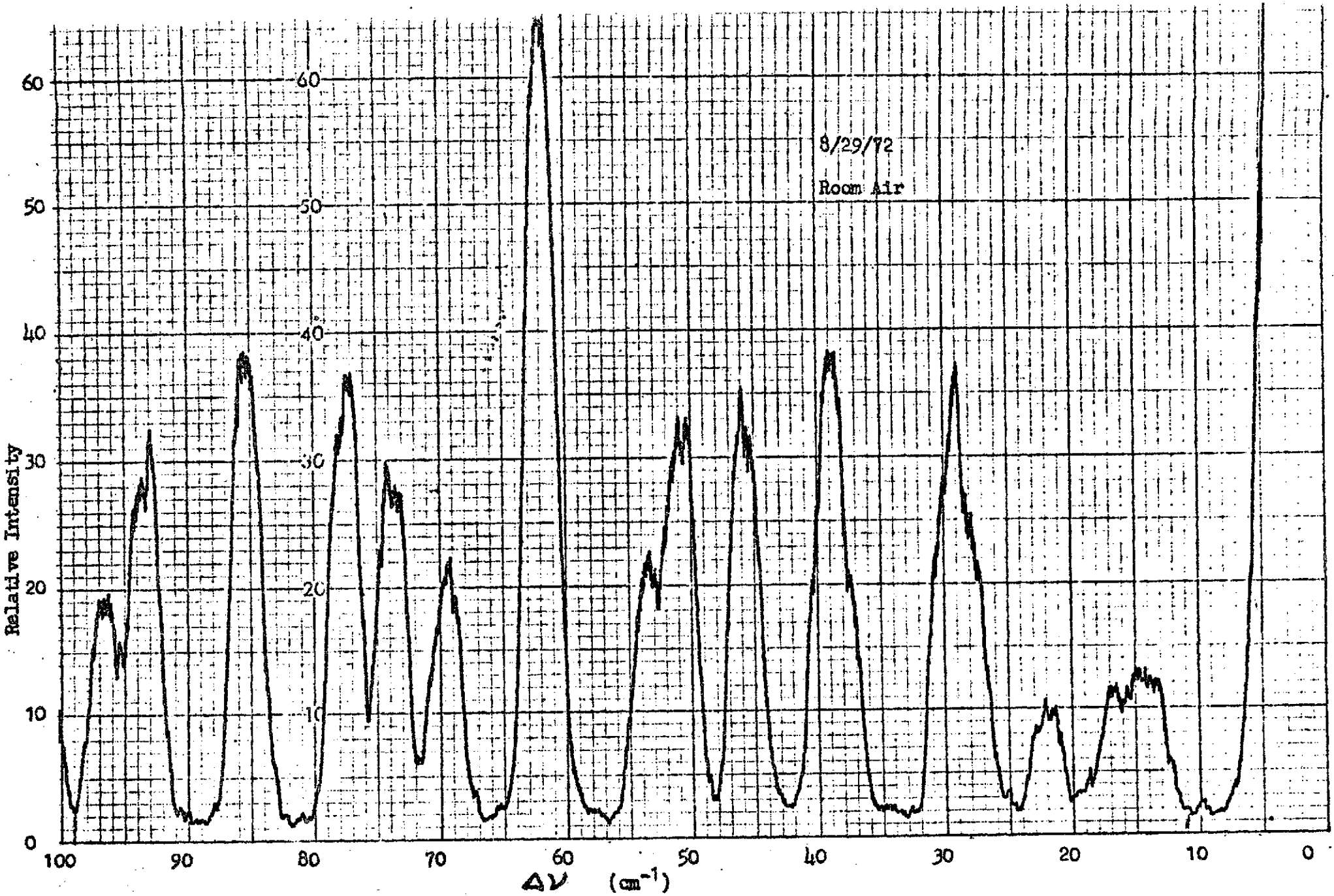

Figure 13. Typical spectrum taken using aged, air conditioned room air.

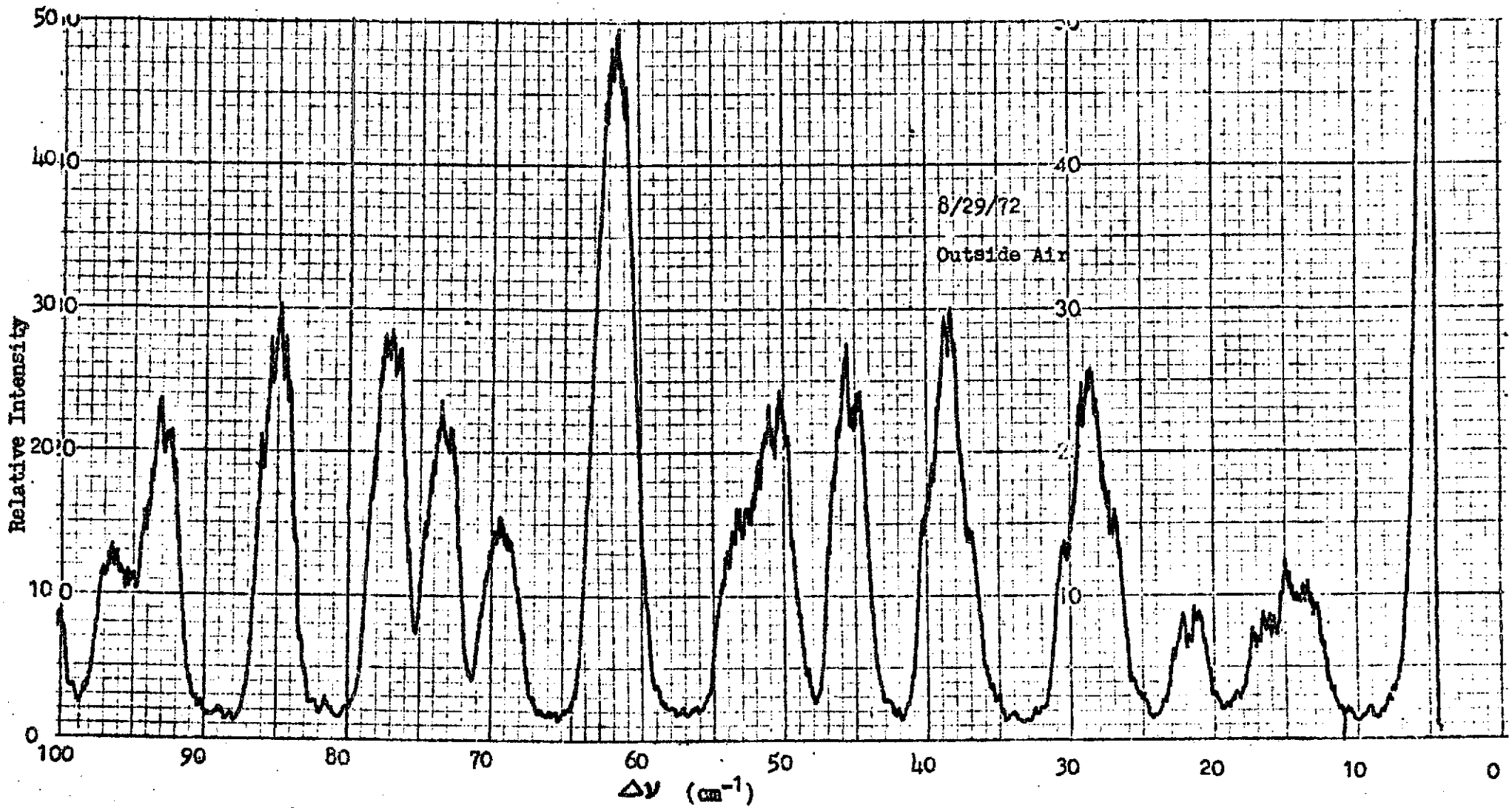

Figure 14. Typical spectrum taken using fresh outside air containing particulate matter.

A set of experiments was conducted to determine whether, perhaps, the return from particulate-laden air might contain a continuum of intensity across the Raman band that was not evident from observations of the individual line locations. Several pairs of observations were made, in each case without disturbing the adjustment of the spectrophotometer between observations. The first observation of each pair was of aged, air conditioned room air, while the second observation was of outside air, with the vacuum pump operating as described earlier. The object of the experiment was to show that there is no correlation between weather conditions and the rotational Raman backscatter cross section of air.

Since the indoor and outdoor temperatures did not differ greatly, and since our attention is focussed on the least temperature-sensitive portion of the Raman spectrum, the assumption could be made that the ratios between corresponding individual lines in the two spectra were the same for any one case; that is, if the line intensities in the "outside air" spectrum were multiplied by a uniform factor, the resulting intensities would equal those obtained in the "room air" spectrum. To obtain the best estimate of this factor, about fourteen prominent peaks in the frequency interval, 11 $cm^{-1} \leqslant \Delta\nu \leqslant$ 98 cm^{-1} were

identified in each of the spectra, and the least squares regression line between the "outside air" and "room air" spectrum was computed. One such regression line is shown in Figure 15. The slope of this line is the factor that we are seeking, and its y-intercept is the difference between the average background counts present in the two spectra. The computed background count values were integrated over the entire spectral interval, $11\ cm^{-1} \leqslant \Delta\nu \leqslant 98\ cm^{-1}$ and the resulting values normalized by the total (signal plus background) counts obtained over that same interval. The resulting value is the "best fit" differential background intensity over the interval, expressed as a fraction of the total intensity. These values are shown in Table 5. The values shown are, in some cases, several percent of the total intensity, and, in one case, almost twenty percent of the total. The computed differential background intensities take on both positive and negative values.

No definite explanation could be found for these fluctuations. There is a possibility that small amounts of room light may have been ducted into the sample chamber by means of the translucent tubing used to bring the sample air into the chamber. This light could have both temporal

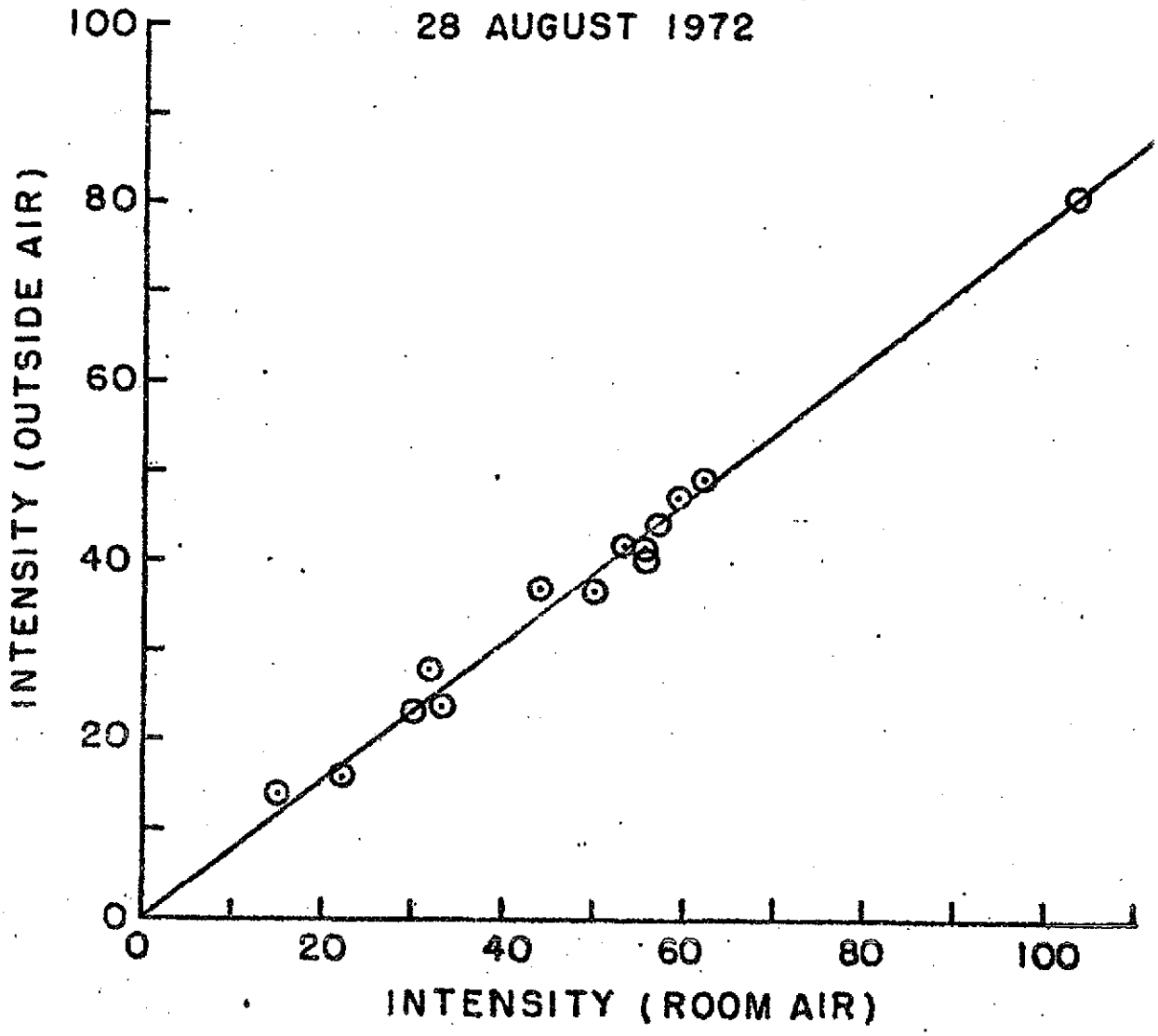

Figure 15. Typical example of the variation of the ratios of peak line intensities within a group of lines, about the line of best fit.

Table 5. Synopsis of measurements of meteorological parameters and concurrently observed Raman spectra.

Date	Time (EST)	Temperature * (°K)	Absolute Humidity * ($gm - m^{-3}$)	24 Hr Average Particulate Mass Loading * ($\mu g - m^{-3}$)	Spectral Slit Width (cm^{-1}) **	Average Count Rate at Line Center for Selected Lines (counts - sec^{-1})		Best Fit Regression Line		Integrated Intensity Outside Air (11 - 38 cm^{-1}) (in^2) ***	Background as fraction of integrated intensity - outside air
						Outside Air Spectrum	Room Air Spectrum	Slope (Ratio of peak line intensities outside/room air)	Intercept (Differential background level)		
8/ 8/72	1315	301.1	12.2	71.3	2.0	21.45	26.27	0.727	+2.358	10.42	+0.199
8/18/72	1030	294.4	15.1	72.0	2.0	45.58	54.58	0.838	-0.162	10.04	-0.014
8/28/72	1130	298.3	13.1	75.6	1.9	74.48	95.82	0.777	+0.012	15.17	+0.0007
8/29/72	0945	297.2	13.0	96.8	1.8	45.72	61.38	0.753	-0.524	9.59	-0.048
9/13/72	1000	290.5	13.6	172.	1.5	45.38	60.00	0.746	+0.614	9.00	+0.060
9/14/72	1000	297.7	16.4	104.	1.8	113.85	150.30	0.756	+0.290	8.70	+0.029
9/15/72	0900	291.6	9.60	113.	1.8	115.40	148.14	0.777	-0.429	9.46	-0.040
9/20/72	0930	287.2	8.47	75.9	1.8	114.85	146.68	0.783	-0.050	8.88	-0.005
9/22/72	1030	295.5	11.8	80.7	1.8	117.60	153.12	0.771	+0.369	9.02	+0.036
10/ 2/72	1045	291.1	10.3	89.9	1.8	113.55	148.63	0.765	+0.357	9.51	+0.033

* From hygrothermograph and high-volume sampler observations made at New Brunswick, N.J., about two miles from the location of the spectrophotometer.

** Signal levels and ratios indicated on the spectrophotometer were critically dependent on the slit width setting. This setting could not be reproduced accurately enough to be considered as constant from one run to the next. Consequently, the slit width was set to the smallest value for which reasonably noise-free signals could be obtained.

and spectral variability. Furthermore, there is the possibility of small fluctuations in the pumping rate.

The thrust of this examination, however, was to determine whether meteorological parameters influence the results. At the time of each set of observations, concurrent measurements of temperature, humidity and particulate mass loading were made, using a hygrothermograph and high volume sampler at the Rutgers University weather observation site, located about two miles from the spectrophotometer. A synopsis of the measurements is given in Table 5. Correlation coefficients were computed between the background values and the absolute humidity and the particulate mass loading. They are as follows:

Differential background vs. Absolute humidity: +0.279

Differential background vs. Particle mass loading: -0.157

According to the significance test for correlation coefficients given by Brooks and Carruthers (1953), neither of the above values is significantly different from zero.

Chapter IV.

TEMPERATURE DEPENDENCE OF ROTATIONAL RAMAN LINE INTENSITIES AND DESIGN OF FAMILIES OF FILTERS WHICH NEUTRALIZE TEMPERATUR DEPENDENCE OF SCATTERING FROM THE ROTATIONAL RAMAN LINES OF A

List of Symbols

b_D Doppler broadening (half) half width (cm^{-1}).

b_p Pressure broadening (half) half width (cm^{-1}).

C_1 Constant ($cm^{-1}-{}^oK^{-\frac{1}{2}}$).

C_2 Constant ($cm^{-1}-{}^oK^{-\frac{1}{2}}$).

c Speed of light ($cm-sec^{-1}$).

D Distance between interferometer and multipass reflection mirror (cm).

d Width of a diffraction grating groove (cm).

E(h) Fraction of available Raman energy used by a filter with (half) half width h.

e Vapor pressure of sodium in absorption cell ($dyne-cm^{-2}$

e_o Reference vapor pressure of sodium ($dyne-cm^{-2}$).

G Gaussian filter form factor.

H Size of spot of light on interferometer (cm).

h Filter (half) half width (cm^{-1}).

I_ν Relative intensity of Raman line at frequency ν.

i Number of temperature values used in determining

mean line intensity.

j Rotational quantum number of initial state.

K Order number of principal energy maximum in light diffracted by diffraction grating.

L Latent heat of vaporization of sodium ($erg\text{-}gm^{-1}$).

M Atomic mass of sodium ($gm\text{-}mol^{-1}$).

$\hat{m}$ Refractive index of interference filter.

N Total number of grooves on diffraction grating.

$\mathcal{N}$ f/Number in an optical system.

n Number density of sodium molecules in absorption cell (cm^{-3}).

$\hat{n}$ Number of passes of light beam through interferometer.

P_i Power incident on diffraction grating (W).

$P_{p.m.}$ Power received in primary maximum of grating spectrum (W).

$P_{p.m.}^{r}$ Value of $P_{p.m.}$ due to Raman scattering (W).

$P_{s.m.}$ Power received in interval $U'_{min} \ll U' \ll U'_{max}$ of secondary diffraction pattern of grating spectrum (W).

$P_{s_e m.}$ Value of $P_{s.m.}$ due to elastic scattering (W).

p Pressure (atm).

R Reflectance of interferometer mirror.

R^* Universal gas constant ($erg\text{-}mol^{-1}\text{-}{}^{o}K^{-1}$).

T Temperature (^{o}K).

T_c Transmission of filter at center of its transmission curve.

T_o Reference temperature (^oK).

T_λ Transmittance of absorption cell at wavelength λ.

$T_\nu(h,\nu_c)$ Transmission at frequency ν, of filter centered at ν_c, with (half) half width h.

U Diffraction grating parameter relative to m=0.

U' Diffraction grating parameter relative to arbitrary order number, m.

U'_{max} Value of grating parameter U' at θ_{max}.

U'_{min} Value of grating parameter U' at θ_{min}.

W Diffraction grating parameter.

w Width of interferometer surface (cm).

x_c Length of light path through absorption cell (cm).

$\overline{\Delta I_{RMS}}$ RMS fluctuation of $\sum_{\Delta\nu} I_\nu$ about $\overline{\sum_{\Delta\nu} I_\nu}$, expressed as a fraction of $\overline{\sum_{\Delta\nu} I_\nu}$.

ΔL Geometric distance of diffracted Raman energy from diffracted elastic energy (cm).

$\Delta\lambda$ Free spectral range (Å).

$\Delta\nu$ Frequency interval over which Raman line intensities are summed (cm^{-1}).

$\Delta\nu_c$ Deviation of ν_c caused by deviation of incident light from the perpendicular (cm^{-1}).

$\delta\nu$ Spectral distance of frequency for which $\theta=\theta_{max}$ from that where $\theta=\theta_e$ (cm^{-1}).

ϵ Distance between adjacent diffraction grating grooves (cm).

θ Maximum allowable angle of light incident on filtering device.

θ_e Diffraction angle of elastic scattering.

θ_{max} Maximum diffraction angle of interval in which Raman lines are observed.

θ_{min} Minimum diffraction angle of interval in which Raman lines are observed.

θ_o Angle of light incident on diffraction grating, relative to normal.

θ' Angle of light diffracted by grating, relative to normal.

λ Wavelength ($\mathring{A}$).

ν Frequency (cm^{-1}).

ν_c Frequency at which filter transmission curve is centered (cm^{-1}).

ν_e Frequency of elastic scattering (cm^{-1}).

ν_f Free spectral range (cm^{-1}).

ν_o Center of spectral interval $\nu_e+\delta\nu \leqslant \nu \leqslant 2\nu_o-\nu_e-\delta\nu$ or $\theta_{max} \leqslant \theta \leqslant \theta_{min}$.

ν_r Frequency of Raman line, or nominal frequency of a group of Raman lines (cm^{-1}).

ρ Object or image radius in an optical system (cm).

$\sum_{\Delta\nu} I_\nu$ Sum of all Raman line intensities at temperature T in frequency interval, $\Delta\nu$.

$\overline{\sum_{\Delta\nu} I_\nu}$ Average of $\sum_{\Delta\nu} I_\nu$ over i temperature values.

σ_λ Absorption cross section of sodium vapor at wavelength λ (cm^2).

τ_c Optical thickness of absorption cell walls.

θ Angle of tilt of interferometer relative to multipass reflection mirror.

A. General.

As was mentioned earlier, although the total energy scattered in the O- and S-branches is independent of temperature, individual line intensities do vary considerably. In accordance with (20) and (21), as temperature is increased, the lines closest to the incident frequency decrease in intensity, while those in the far wings increase. Table 6 shows some typical intensity variations to be expected in the range of atmospheric temperatures.

Obviously, depending upon which spectral interval of the Raman band the observer chooses to monitor, rotational line intensities could be used as sensitive temperature indicators or as temperature-independent parameters.

For the purposes of this study, it is desirable to locate the family of spectral intervals in which there is an insignificant net temperature dependence. Since the rotational Raman cross section, as defined in Chapter III.F. is independent of temperature, this family includes, but is not limited to the interval encompassing all lines (i.e., $-\infty < [\nu_r - \nu_e] < \infty$). However, we prefer not to use an extremely wide interval, since, as will be shown later in this chapter, background radiation would become a problem. Furthermore, for practical reasons, we desire to examine

Table 6. Temperature dependence of some representative lines in the rotational Raman spectra of nitrogen and oxygen.

	j	$\Delta\nu$ (cm^{-1})	Midrange intensity (rel.units)	Percent change of intensity per $+10^{\circ}K$ temperature change
N_2	0	11.94	9.276	- 4.8
	9	83.51	12.585	- 0.34
	23	194.3	0.256	+14.
O_2	1	14.39	11.918	- 3.6
	11	71.89	20.335	- 0.50
	33	197.3	0.049	+16.

intervals which lie only to one side of the elastic line.

In the atmospheric range of temperatures, decreases in line intensity with increasing temperature occur only in the frequency intervals, $0 < |\nu_r - \nu_e| \leqslant 70\ cm^{-1}$. Thus, any group of lines whose total intensity is to be independent of temperature must take in lines on both the high frequency side and the low frequency side of $|\nu_r - \nu_e| = 70\ cm^{-1}$

B. Ideal filters.

For the purpose of illustrating the nature of these intervals, it was initially assumed that an ideal filter could be applied to the receiving apparatus; that is, it was assumed that one could choose to receive all the energy from any interval of lines within the O- or S-branches, and exclude all energy from outside that interval. When this assumption is made, there can be only as many groups of lines with near-zero temperature dependence as there are lines in the region, $0 < |\nu_r - \nu_e| \leqslant 70\ cm^{-1}$. There are, in fact, about eleven or twelve such lines in each branch. Intervals for near-zero temperature dependence were computed, beginning with each of the first eleven lines in turn. The method of computation was as follows:

Suppose that we are examining the total Raman-scat-

tered intensity due to all of the lines lying in some frequency interval, $\Delta\nu$,

$$\sum_{\Delta\nu} I_\nu$$

The average intensity observed over some temperature range, $\Delta T = T_2 - T_1$ is given by

$$\overline{\sum_{\Delta\nu} I_\nu} = \frac{1}{\Delta T}\int_{T_1}^{T_2}\left(\sum_{\Delta\nu} I_\nu\right) dT$$

Since $\sum_{\Delta\nu} I_\nu$ is a slowly-varying function of T, we may approximate the above integral by an average of $\sum_{\Delta\nu} I_\nu$ over i uniformly spaced temperature values in the interval of interest. That is,

$$\overline{\sum_{\Delta\nu} I_\nu} = \frac{1}{\Delta T}\int_{T_1}^{T_2}\left(\sum_{\Delta\nu} I_\nu\right) dT \doteq \frac{1}{i}\sum_{k=1}^{i}\left(\sum_{\Delta\nu} I_\nu\right)_{T_k}$$

In our ideal filter we wish to minimize the temperature dependence of $\sum_{\Delta\nu} I_\nu$. For the purpose of our computations, the interval of "minimum temperature dependence" was defined as the spectral interval, $\Delta\nu$, in which the RMS deviation of $\sum_{\Delta\nu} I_\nu$ from $\overline{\sum_{\Delta\nu} I_\nu}$ is a minimum, for temperature variations over ΔT. That is, the interval, $\Delta\nu$, for

which

$$\overline{\Delta I_{RMS}} = \frac{\sqrt{\sum_{\Delta T}\left(\sum_{\Delta\nu} I_\nu - \overline{\sum_{\Delta\nu} I_\nu}\right)^2}}{i \sum_{\Delta\nu} I_\nu} = \text{minimum} \qquad (62)$$

Intensities were computed for each 20°K in the interval $200^\circ K \leqslant T \leqslant 320^\circ K$ and are shown in Tables 7 and 8. The results of the calculations, shown in Table 9, indicate that, with an ideal filter, it is theoretically possible to achieve less than one percent temperature dependence while utilizing nearly all of the energy present in the O- and S-branches.

C. Gaussian interference filters.

1. General.

While maintaining the same criterion for "minimum temperature dependence" as was discussed above, we now extend our calculations by choosing a filter whose transmission function is Gaussian in character, with a specified center frequency and (half) half width (spectral distance from center frequency to the frequency at which transmission falls off by a factor of 0.5). That is,

$$G\ (h, \nu_c) = e^{-1n2\left(\frac{\nu - \nu_c}{h}\right)^2} \qquad (63)$$

Table 7. Computed line locations and relative intensities in the O-branch of the rotational Raman spectrum of air for temperatures in the range $200^{\circ}K \leqslant T \leqslant 320^{\circ}K$.

		J	Relative Frequency (cm^{-1})	Relative Intensities 200°K	220°K	240°K	260°K	280°K	300°K	320°K
0	N	0	1.194+01	1.047-02	9.598-03	8.858-03	8.224-03	7.674-03	7.193-03	6.769
1	O	1	1.439+01	1.318-02	1.212-02	1.122-02	1.044-02	9.761-03	9.165-03	8.636
2	N	1	1.990+01	8.649-03	7.989-03	7.422-03	6.928-03	6.496-03	6.114-03	5.774
3	O	3	2.590+01	2.026-02	1.875-02	1.770-02	1.675-02	1.582-02	1.499-02	1.42
4	N	2	2.785+01	2.204-02	2.057-02	1.927-02	1.813-02	1.710-02	1.618-02	1.53
5	N	3	3.581+01	1.238-02	1.171-02	1.109-02	1.052-02	1.001-02	9.535-03	9.10
6	O	5	3.740+01	2.258-02	2.157-02	2.066-02	1.980-02	1.898-02	1.821-02	1.749
7	N	4	4.377+01	2.559-02	2.458-02	2.359-02	2.263-02	2.173-02	2.087-02	2.007
8	O	7	4.891+01	2.375-02	2.253-02	2.027-02	1.980-02	1.935-02	1.888-02	1.849
9	N	5	5.172+01	1.743-02	1.813-02	1.182-02	1.149-02	1.115-02	1.082-02	1.06
10	N	6	5.967+01	2.280-02	2.277-02	2.258-02	2.227-02	2.189-02	2.146-02	2.100
11	O	9	6.040+01	1.662-02	1.711-02	1.739-02	1.753-02	1.755-02	1.748-02	1.735
12	N	7	6.762+01	9.997-03	1.022-02	1.043-02	1.055-02	1.060-02	1.025-02	1.01
13	O	11	7.189+01	1.100-02	1.273-02	1.347-02	1.403-02	1.445-02	1.475-02	1.49
14	N	8	7.557+01	1.680-02	1.703-02	1.721-02	1.869-02	1.883-02	1.895-02	1.89
15	O	13	8.336+01	7.547-03	8.506-03	9.480-03	1.026-02	1.092-02	1.148-02	1.19
16	N	9	8.351+01	6.779-03	7.321-03	7.745-03	8.072-03	8.317-03	8.495-03	8.61
17	N	10	9.143+01	1.054-02	1.174-02	1.275-02	1.358-02	1.428-02	1.481-02	1.52
18	O	15	9.483+01	4.325-03	5.244-03	6.111-03	6.911-03	7.637-03	8.289-03	8.86
19	N	11	9.939+01	3.950-03	4.552-03	5.004-03	5.347-03	5.945-03	6.282-03	6.56
20	C	17	1.063+02	2.257-03	2.934-03	3.623-03	4.304-03	4.960-03	5.583-03	6.16
21	N	12	1.073+02	5.719-03	6.834-03	7.869-03	8.808-03	9.649-03	1.039-02	1.10
22	N	13	1.153+02	2.000-03	2.466-03	2.956-03	3.402-03	3.815-03	4.194-03	4.53
23	O	19	1.177+02	1.073-03	1.506-03	1.983-03	2.486-03	3.002-03	3.518-03	4.02
24	N	14	1.232+02	2.707-03	3.507-03	4.318-03	5.116-03	5.884-03	6.611-03	7.29
25	O	21	1.291+02	4.649-04	7.102-04	1.003-03	1.335-03	1.697-03	2.078-03	2.47
26	N	15	1.311+02	8.806-04	1.200-03	1.533-03	1.874-03	2.214-03	2.546-03	2.86
27	N	16	1.390+02	1.129-03	1.595-03	2.119-03	2.677-03	3.253-03	3.833-03	4.40
28	O	23	1.405+02	1.892-04	3.084-04	4.704-04	6.680-04	8.973-04	1.153-03	1.43
29	N	17	1.469+02	3.454-04	5.148-04	7.125-04	9.328-04	1.167-03	1.411-03	1.65
30	C	25	1.519+02	6.677-05	1.235-04	2.006-04	3.117-04	4.406-04	6.020-04	7.81
31	N	18	1.548+02	4.118-04	5.458-04	9.332-04	1.266-03	1.636-03	2.032-03	2.48
32	N	19	1.627+02	1.187-04	1.968-04	2.976-04	4.197-04	5.503-04	7.163-04	8.84
33	O	27	1.633+02	2.218-05	4.565-05	8.267-05	1.358-04	2.066-04	2.958-04	4.02
34	N	20	1.706+02	1.329-04	2.553-04	3.699-04	5.430-04	7.505-04	9.886-04	1.25
35	O	29	1.746+04	6.796-06	1.559-05	3.105-05	5.527-05	9.011-05	1.370-04	1.96
36	N	21	1.785+02	3.607-05	6.723-05	1.120-04	1.715-04	2.457-04	3.340-04	4.35
37	O	31	1.860+02	1.889-06	4.922-06	1.085-05	2.104-05	3.693-05	5.983-05	9.06
38	N	22	1.864+02	3.799-05	7.533-05	1.323-04	2.116-04	3.147-04	4.420-04	5.92
39	N	23	1.943+02	9.708-06	2.054-05	3.906-05	6.373-05	9.859-05	1.432-04	1.97
40	O	33	1.973+02	4.851-07	1.438-06	3.330-06	7.498-06	1.422-05	2.466-05	3.97
41	N	24	2.021+02	9.629-06	2.479-05	4.271-05	7.501-05	1.209-04	1.819-04	2.59
42	O	35	2.085+02	1.145-07	3.090-07	1.070-06	2.502-06	5.154-06	9.595-06	1.66
43	N	25	2.100+02	2.319-06	5.925-06	1.169-05	2.156-05	3.624-05	5.658-05	8.32
44	N	26	2.179+02	5.166-06	5.655-06	1.248-05	2.423-05	4.255-05	6.899-05	1.04
45	O	37	2.198+02	2.485-08	9.746-08	3.021-07	7.820-07	1.757-06	3.527-06	6.45
46	N	27	2.257+02	4.914-07	1.582-06	3.248-06	6.650-06	1.222-05	2.061-05	3.24
47	O	39	2.310+02	4.961-09	2.263-08	7.038-08	2.091-07	5.640-07	1.225-06	2.40
48	N	28	2.335+02	4.330-07	1.416-06	3.300-06	7.136-06	1.375-05	2.414-05	3.95
49	N	29	2.414+02	9.262-08	3.951-07	8.128-07	1.871-06	3.783-06	6.931-06	1.17
50	C	41	2.421+02	9.117-10	4.874-09	1.955-08	6.294-08	1.705-07	4.026-07	8.50
51	N	30	2.492+02	7.697-08	2.755-07	7.510-07	1.919-06	4.079-06	7.803-06	1.37
52	O	43	2.533+02	1.543-10	9.755-10	4.484-09	1.622-08	5.058-08	1.251-07	2.84
53	N	31	2.570+02	1.503-08	6.051-08	1.867-07	4.809-07	1.076-06	2.153-06	3.93

Table 8. Computed line locations and relative intensities in the S-branch of the rotational Raman spectrum of air for temperatures in the range $200^{\circ}K \leqslant T \leqslant 320^{\circ}K$.

			Relative Frequency	Relative Intensities						
		J	(cm^{-1})	200°K	220°K	240°K	260°K	280°K	300°K	32
0	N	0	1.194+01	1.141-02	1.038-02	9.515-03	8.786-03	8.160-03	7.617-03	7.14
1	O	1	1.439+01	1.462-02	1.332-02	1.223-02	1.130-02	1.051-02	9.820-03	9.21
2	N	1	1.990+01	9.980-03	9.100-03	8.362-03	7.735-03	7.205-03	6.726-03	6.31
3	O	3	2.590+01	2.441-02	2.244-02	2.077-02	1.933-02	1.808-02	1.697-02	1.60
4	N	2	2.785+01	2.693-02	2.460-02	2.278-02	2.115-02	1.973-02	1.850-02	1.74
5	N	3	3.581+01	1.602-02	1.479-02	1.374-02	1.283-02	1.203-02	1.132-02	1.06
6	O	5	3.740+01	2.945-02	2.755-02	2.586-02	2.435-02	2.300-02	2.179-02	2.07
7	N	4	4.377+01	3.506-02	3.272-02	3.066-02	2.884-02	2.721-02	2.575-02	2.44
8	O	7	4.891+01	2.950-02	2.827-02	2.709-02	2.595-02	2.488-02	2.388-02	2.29
9	N	5	5.172+01	1.800-02	1.702-02	1.612-02	1.530-02	1.455-02	1.386-02	1.32
10	N	6	5.967+01	3.503-02	3.364-02	3.229-02	3.098-02	2.974-02	2.857-02	2.74
11	O	9	6.040+01	2.566-02	2.539-02	2.499-02	2.449-02	2.393-02	2.335-02	2.27
12	N	7	6.762+01	1.626-02	1.591-02	1.550-02	1.506-02	1.462-02	1.418-02	1.37
13	O	11	7.189+01	1.979-02	2.038-02	2.072-02	2.088-02	2.090-02	2.082-02	2.06
14	N	8	7.557+01	2.893-02	2.809-02	2.865-02	2.825-02	2.777-02	2.723-02	2.66
15	O	13	8.336+01	1.369-02	1.478-02	1.563-02	1.628-02	1.677-02	1.712-02	1.73
16	N	9	8.351+01	1.236-02	1.264-02	1.278-02	1.281-02	1.277-02	1.268-02	1.25
17	N	10	9.145+01	2.035-02	2.136-02	2.206-02	2.253-02	2.282-02	2.296-02	2.29
18	O	15	9.483+01	8.556-03	9.750-03	1.079-02	1.168-02	1.243-02	1.306-02	1.35
19	N	11	9.939+01	8.076-03	8.721-03	9.227-03	9.616-03	9.908-03	1.012-02	1.02
20	O	17	1.063+02	4.850-03	5.881-03	6.853-03	7.750-03	8.565-03	9.295-03	9.94
21	N	12	1.073+02	1.238-02	1.379-02	1.497-02	1.595-02	1.675-02	1.739-02	1.79
22	N	13	1.153+02	4.584-03	5.283-03	5.900-03	6.438-03	6.899-03	7.290-03	7.61
23	O	19	1.177+02	2.502-03	3.252-03	4.016-03	4.778-03	5.497-03	6.187-03	6.83
24	N	14	1.232+02	6.568-03	7.850-03	9.037-03	1.012-02	1.108-02	1.194-02	1.26
25	O	21	1.291+02	1.177-03	1.653-03	2.176-03	2.729-03	3.295-03	3.861-03	4.41
26	N	15	1.311+02	2.277-03	2.829-03	3.365-03	3.872-03	4.343-03	4.774-03	5.16
27	N	16	1.390+02	3.057-03	3.960-03	4.876-03	5.778-03	6.645-03	7.466-03	8.23
28	O	23	1.405+02	5.063-04	7.734-04	1.093-03	1.454-03	1.848-03	2.263-03	2.69
29	N	17	1.469+02	9.942-04	1.546-03	1.719-03	2.102-03	2.483-03	2.855-03	3.21
30	O	25	1.519+02	1.992-04	3.336-04	5.088-04	7.226-04	9.706-04	1.248-03	1.54
31	N	18	1.548+02	1.253-03	1.770-03	2.361-03	2.983-03	3.625-03	4.271-03	4.91
32	N	19	1.627+02	3.828-04	5.706-04	7.897-04	1.033-03	1.293-03	1.564-03	1.83
33	O	27	1.633+02	7.181-05	1.520-04	2.201-04	3.352-04	4.762-04	6.474-04	8.40
34	N	20	1.706+02	4.536-04	7.121-04	1.029-03	1.396-03	1.804-03	2.291-03	2.69
35	O	29	1.746+02	2.374-05	4.885-05	8.848-05	1.453-04	2.211-04	3.166-04	4.31
36	N	21	1.785+02	1.303-04	2.160-04	3.267-04	4.607-04	6.150-04	7.863-04	9.70
37	O	31	1.860+02	7.200-06	1.661-05	3.309-05	5.890-05	9.603-05	1.460-04	2.09
38	N	22	1.864+02	1.853-04	2.550-04	4.044-04	5.936-04	8.203-04	1.081-03	1.37
39	N	23	1.943+02	3.928-05	7.318-05	1.220-04	1.868-04	2.676-04	3.637-04	4.73
40	O	33	1.973+02	2.005-06	5.225-06	1.152-05	2.234-05	3.920-05	6.351-05	9.64
41	N	24	2.021+02	4.123-05	8.175-05	1.435-04	2.296-04	3.416-04	4.796-04	6.42
42	O	35	2.065+02	5.132-07	1.521-06	3.735-06	7.933-06	1.505-05	2.609-05	4.20
43	N	25	2.100+02	1.050-05	2.222-05	4.117-05	6.899-05	1.066-04	1.549-04	2.13
44	N	26	2.179+02	1.039-05	2.350-05	4.607-05	8.089-05	1.304-04	1.962-04	2.79
45	O	37	2.198+02	1.208-07	4.103-07	1.128-06	2.639-06	5.436-06	1.012-05	1.73
46	N	27	2.257+02	2.493-06	6.050-06	1.257-05	2.319-05	3.808-05	6.085-05	8.94
47	O	39	2.310+02	2.614-08	1.025-07	3.178-07	8.226-07	1.848-06	3.711-06	6.79
48	N	28	2.335+02	2.324-06	6.064-06	1.338-05	2.599-05	4.564-05	7.401-05	1.12
49	N	29	2.414+02	5.259-07	1.479-06	3.476-06	7.117-06	1.308-05	2.206-05	3.47
50	O	41	2.421+02	5.206-09	2.375-08	8.351-08	2.404-07	5.917-07	1.286-06	2.52
51	N	30	2.492+02	4.623-07	1.406-06	3.524-06	7.620-06	1.468-05	2.578-05	4.20
52	O	43	2.533+02	9.546-10	5.103-09	2.047-08	6.591-08	1.786-07	4.215-07	8.90
53	N	31	2.570+02	9.870-08	3.251-07	8.714-07	1.994-06	4.032-06	7.386-06	1.24

Table 9. Characteristics of various ideal filters. Line numbers refer to consecutive numbers assigned to each line in Tables 7 and 8.

First Line		Last Line					
Line No.	Line Freq. (cm^{-1})	Line No.	Line Freq. (cm^{-1})	Center Freq. (cm^{-1})	(Half) Half Width (cm^{-1})	Fraction of Available Energy Used	Percent RMS Intensity Variation over $200^{\circ}K$-$320^{\circ}K$
				O - Branch			
1	14.39	24	123.2	68.79	54.4	0.9483	0.38
2	19.90	22	115.3	67.60	47.7	0.8609	0.54
3	25.90	21	107.3	66.60	40.7	0.8276	0.59
4	27.85	20	106.3	67.08	39.2	0.7453	0.69
5	35.81	18	94.83	65.32	29.5	0.6551	0.82
6	37.40	17	91.45	64.43	27.0	0.5995	0.85
7	43.77	15	83.36	63.57	19.8	0.4676	0.91
8	48.91	14	75.57	62.24	13.3	0.3622	0.98
9	51.72	13	71.89	61.81	10.1	0.2403	0.99
10	59.67	12	67.62	63.65	3.98	0.1594	1.20
11	60.40	11	60.40	60.40	0.0	0.0555	-
				S - Branch			
4	27.85	33	163.3	95.58	81.7	0.8979	0.23
5	35.81	28	140.5	88.16	52.4	0.8305	0.40
6	37.40	26	131.1	84.30	46.9	0.7833	0.51
7	43.77	24	123.2	83.49	39.7	0.7107	0.62
8	48.91	22	115.3	82.11	33.2	0.6086	0.78
9	51.72	20	106.3	79.01	27.3	0.4972	0.79
10	59.67	19	99.39	79.53	19.9	0.4435	0.89

Obviously, there will be an infinite number of combinations of center frequency and half width that will satisfy our requirement for a small temperature dependence. We recognize immediately, from an examination of Table 9, that for a filter of near zero half width, the desired center frequency will fall at about 60 cm^{-1} in the O-branch and 75 cm^{-1} in the S-branch. Furthermore, we know that as the half width is increased, the desired center frequency will move progressively outward into the wings of the O- and S-branches.

Calculations were made of the various parameters of interest for filters with half widths of 25, 37.5, 50 and 75 cm^{-1}. Plots of net temperature dependence for various center-frequency/half width combinations are shown in Figure 16, illustrating the characteristics discussed above.

From the results shown in Figure 16, it is a simple matter to interpolate the center frequency/half width combinations that result in minimum intensity variation. These combinations, together with limits for $<1\%$ temperature dependence, are shown in Figure 17. The fraction of available Raman energy used, E(h), is given by

$$E(h) = \frac{\int_0^{\pm\infty} T_\nu\,(h, \nu_c)\; I_\nu \, d\nu}{\int_0^{\pm\infty} I_\nu \, d\nu} \qquad (64)$$

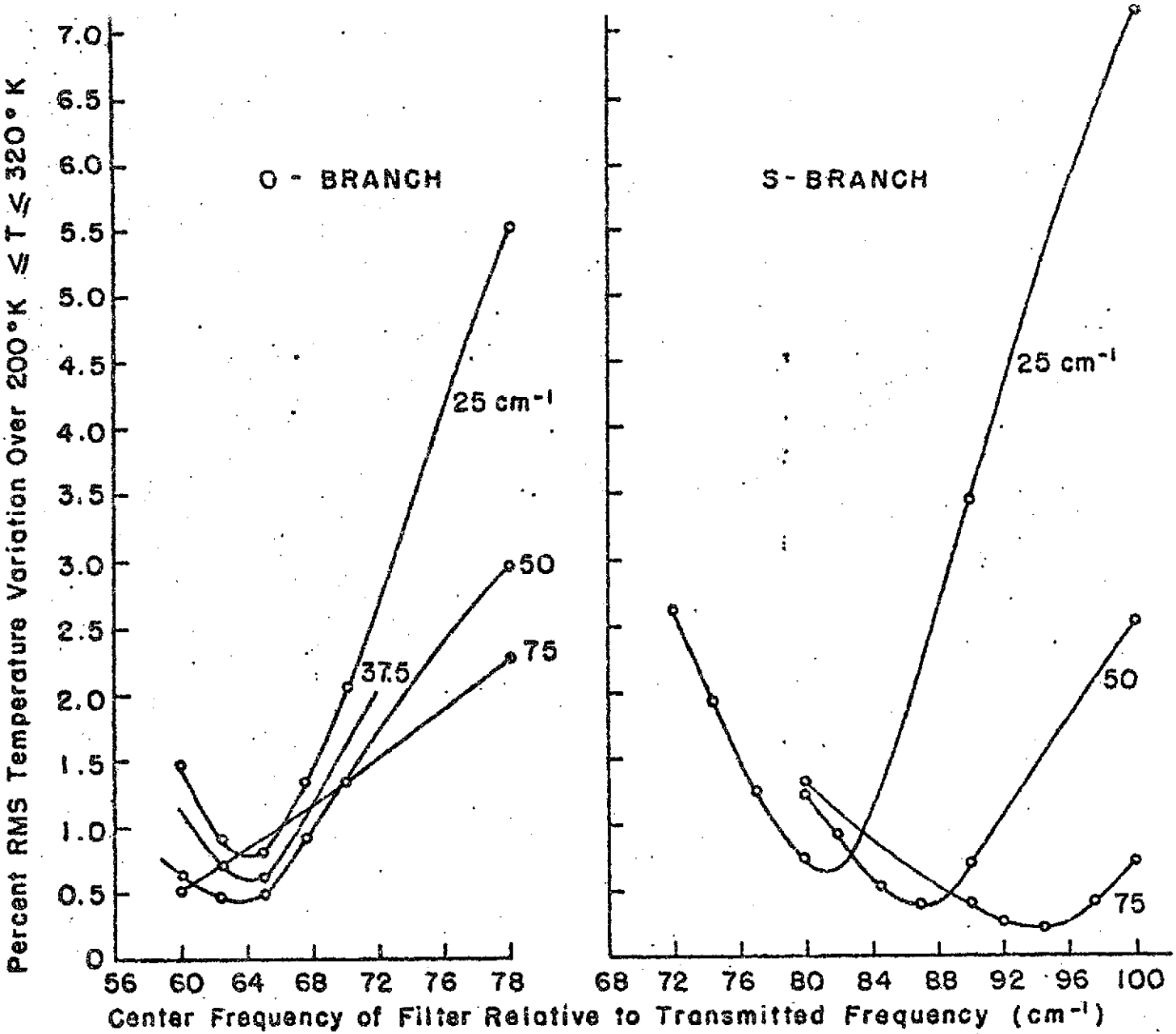

Figure 16. Net temperature dependence of energy transmitted through a Gaussian filter for various center frequency/half width combinations.

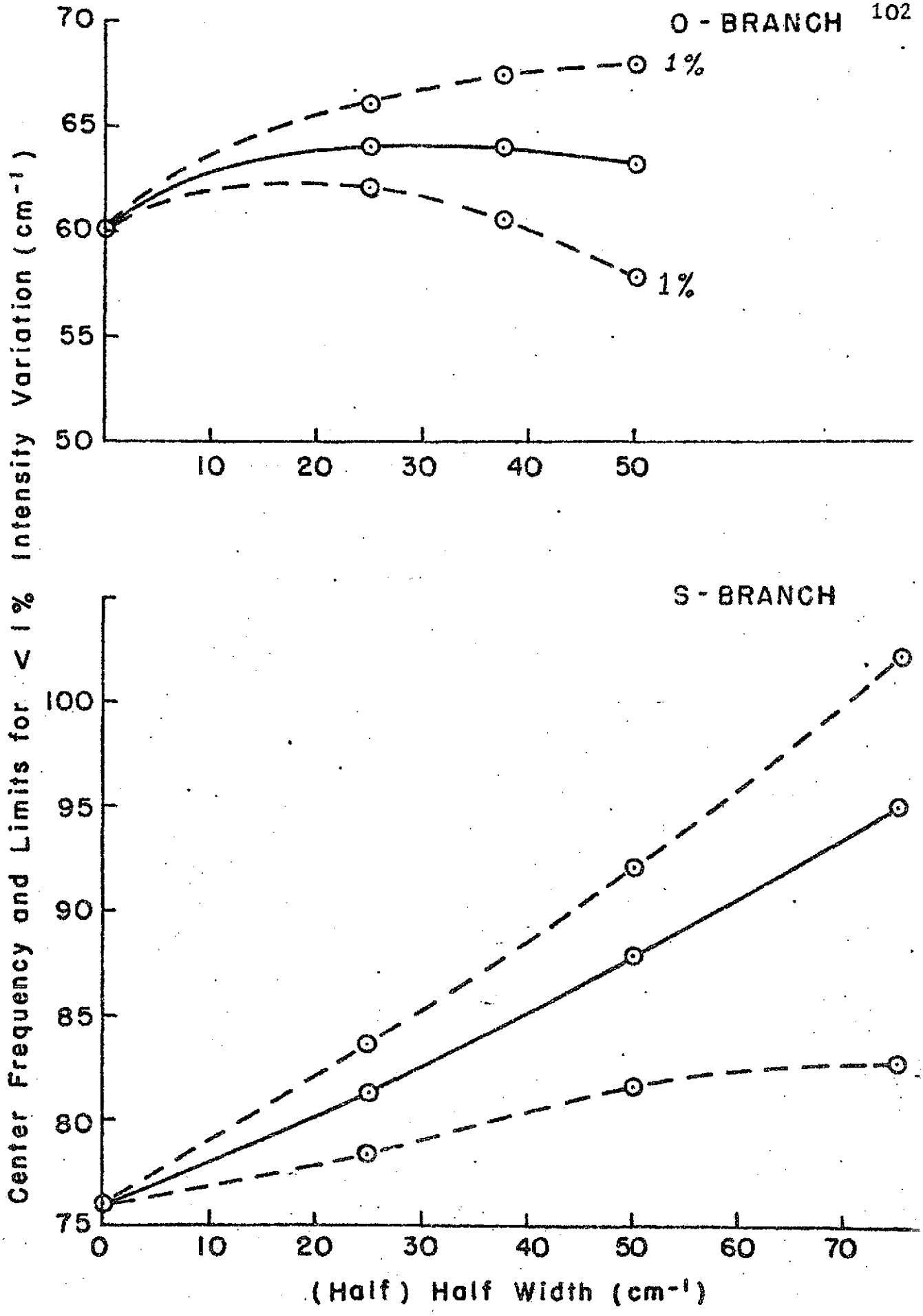

Figure 17. Temperature dependence field for energy transmitte

Here, h and ν_c are ordered pairs from Figure 17 which give minimum temperature dependence. A graph of E(h) versus h is shown in Figure 18.

Since we find that there are an infinite number of center frequency/half width combinations from which to choose, we shall investigate, in the following sections, some additional constraints which may be applied to the filter design. In the next section, we shall investigate the possibility of using the filter to suppress the signal due to elastic scattering from the Raman channel. In Chapter IV.A., we shall consider the possible selection of filter parameters to optimize the signal to noise ratio.

2. Collimation requirements.

When using interference filters, or any interferometric device for that matter, it is necessary to examine the requirements that the device imposes upon the collimation of the incident light. From the optical geometry of interference filters, it can be shown that the incidence angle, θ, and center frequency deviation, $\Delta\nu_o$, of a filter are related according to (Oriel Optics Corp., 1971):

$$\sin\theta = \hat{m}\left[2\left(\frac{\Delta\nu_o}{\nu_o}\right) - \left(\frac{\Delta\nu_o}{\nu_o}\right)^2\right]^{\frac{1}{2}} \qquad (65)$$

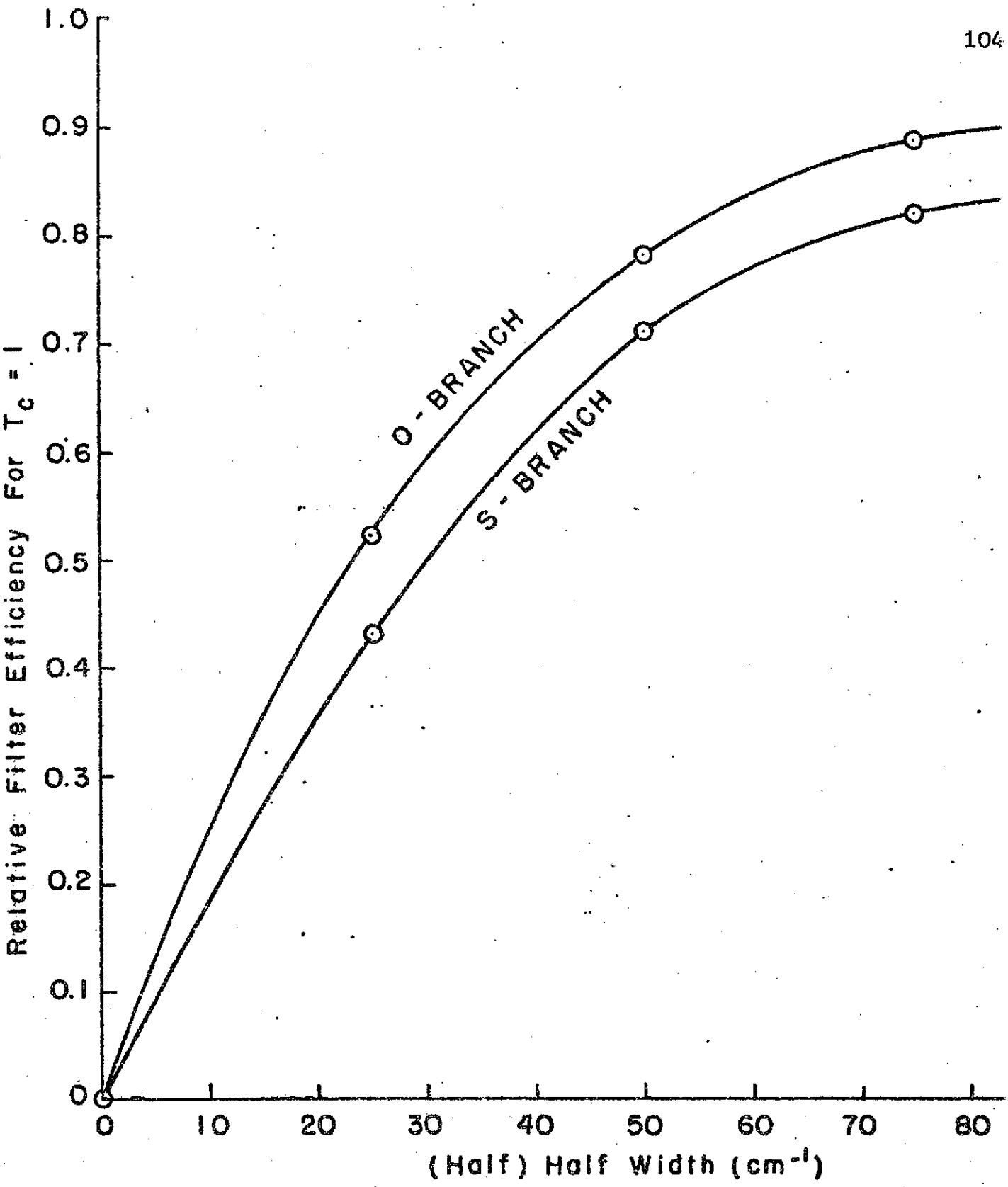

Figure 18. Fraction of available Raman energy transmitted by Gaussian filters of optimum center frequency and half width.

Typically $\hat{m}$, the refractive index of the filter, is about 1.7. For the types of filters discussed here, we shall require the center frequency to vary less than about 5 cm^{-1} with changing incidence angle. Then

$$\theta < 2.5^{o}$$

Figure 19 shows the interrelationship between f, $\mathcal{N}$ and θ in an optical system. In a system which introduces no losses or aberrations, it can be shown (Born and Wolf, 1959) that the quantity $f/\mathcal{N}$ is constant; that is, the optical properties of the system may be transformed along lines of constant $f/\mathcal{N}$. This is a convenient parameter for expressing our results, in that it allows the comparison of systems which require different blur radii and f/numbers.

A filter of radius 2 cm, with a maximum acceptance angle of 2.5^{o} falls at the location marked (A) in Figure 19. We see that, for an optical system to produce such a set of parameters, it is required that

$$f/\mathcal{N} \leq 0.17$$

A further discussion of the practical attainability of such a system will be presented in the following sections.

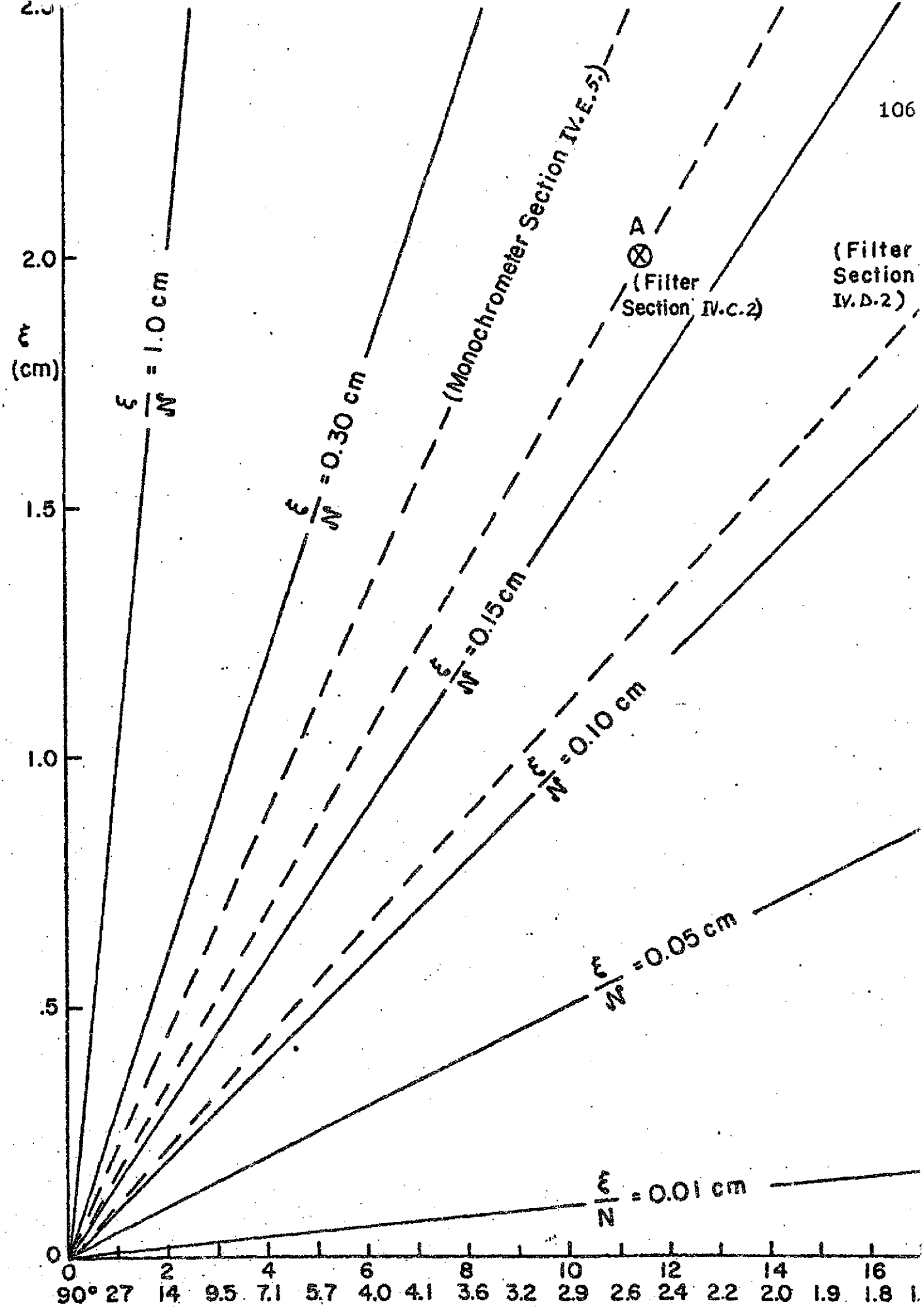

Figure 19. Interrelationship between $\mathcal{E}$, $\mathcal{N}$, and θ in an aberratic free system.

D. Interference filters which provide sufficient suppression of the elastic scattering in the Raman channel.

1. General.

It was shown in the previous section that, if in designing a filter system, we consider only neutralization of temperature dependence of the received signal, we have an infinite number of filter transmission functions from which to choose. With this fact in mind, we examine the possibility of additionally taking advantage of the filter's transmission function to suppress the elastically scattered light from the Raman channel.

In Chapter III.G. it was shown that S-branch Raman scattering is

$$\frac{2.85 \times 10^{-30}}{2.01 \times 10^{-28}} = 0.0142$$

times as intense as the elastic molecular scattering, and that the O-branch Raman scattering is 0.0102 times as intense.

We desire that the elastic scattering be suppressed to less than one percent of the Raman scattering, in the Raman channel. This implies a required transmission at the elastic frequency 1.42×10^{-4} times the effective Raman band transmission, $E(h)T_c$, and a factor of 1.02×10^{-4} for

the O-branch. When the effect of particulate elastic scattering is included, we find that the required rejection factor not only becomes larger, but also wavelength-dependent. In the spectral interval 0.35μ - 0.70μ, the intensity of molecular scattering varies by a factor of sixteen, while that of particulate scattering varies by a factor of less than two (Elterman, 1968). Thus, at 0.70μ, the rejection requirements for the filter are about ten times as stringent as at 0.35μ.

Elterman's tables, which give attenuation coefficients as a function of wavelength for an atmosphere with a visibility of approximately 14 miles, indicate that the ratio of particulate to molecular attenuation coefficients near the surface is about 30 at 0.70μ and 3 at 0.35μ. Deirmendjian's (1969) study of particulate phase functions indicates that the ratio of particulate to molecular backscatter cross sections should be of the same order of magnitude as that of the attenuation coefficients.

Under extremely hazy conditions, we might find these factors to be as much as five times as large (visibility less than three miles); that is, the ratio between particulate and molecular backscatter could be as high as 15 at 0.35μ, and 150 at 0.70μ under these extreme conditions

and the rejection characteristics of the interference filter must accordingly be specified 15-150 times as high as for a purely molecular atmosphere. The particulate contribution to the backscattering diminishes rapidly with height; the ratios of particulate to molecular backscattering are less by a factor of ten at 3 km, as compared to the ratios near the surface. Thus, for systems whose operation is confined to higher altitudes, the rejection requirements are not as stringent.

Thus, we see that, for an interference filter to provide the required suppression, the elastic frequency must fall far in the "wings" of the transmission function; that is, we require a relatively narrow filter whose transmission function drops steeply in the wings. In order to obtain design parameters for such a filter, Infrared Industries, Inc.*, a concern which manufactures interference filters was contacted. They supplied a set of typical transmission curves for filters that they produce. The filters are classified as one- through four-period filters, the term "period" referring to the number of sets of dielectric layers composing the filter. Four periods is

---

*P. O. Box 557, Waltham, Mass. 02154.

presently the maximum number commercially available. Through use of the curves, which are not Gaussian in character (See Figure 20), it was possible to find the widest filter of this type that would give a rejection of 10^{-4} or 10^{-5} at 6943 Å, and still give the desired non-temperature dependent Raman transmission. This was done, using the same computer program as was used in the calculations for ideal and Gaussian filters. The computed characteristics of such filters are shown in Figures 21 and 22, and in Table 10.

Table 10. Widest four period filters which give a rejection of 10^{-4} and 10^{-5} at 6943 Å, and still give the desired non-temperature dependent Raman transmission.

		Center Wavelength (Å)	(Half) Half Width (Å)	Fraction of Raman Branch Transmitted
10^{-5} Rejection	O-Branch	6212.9	8.1	0.361
	S-Branch	6980.6	10.0	0.384
10^{-4} Rejection	O-Branch	6912.3	11.7	0.500
	S-Branch	6981.3	14.6	0.523

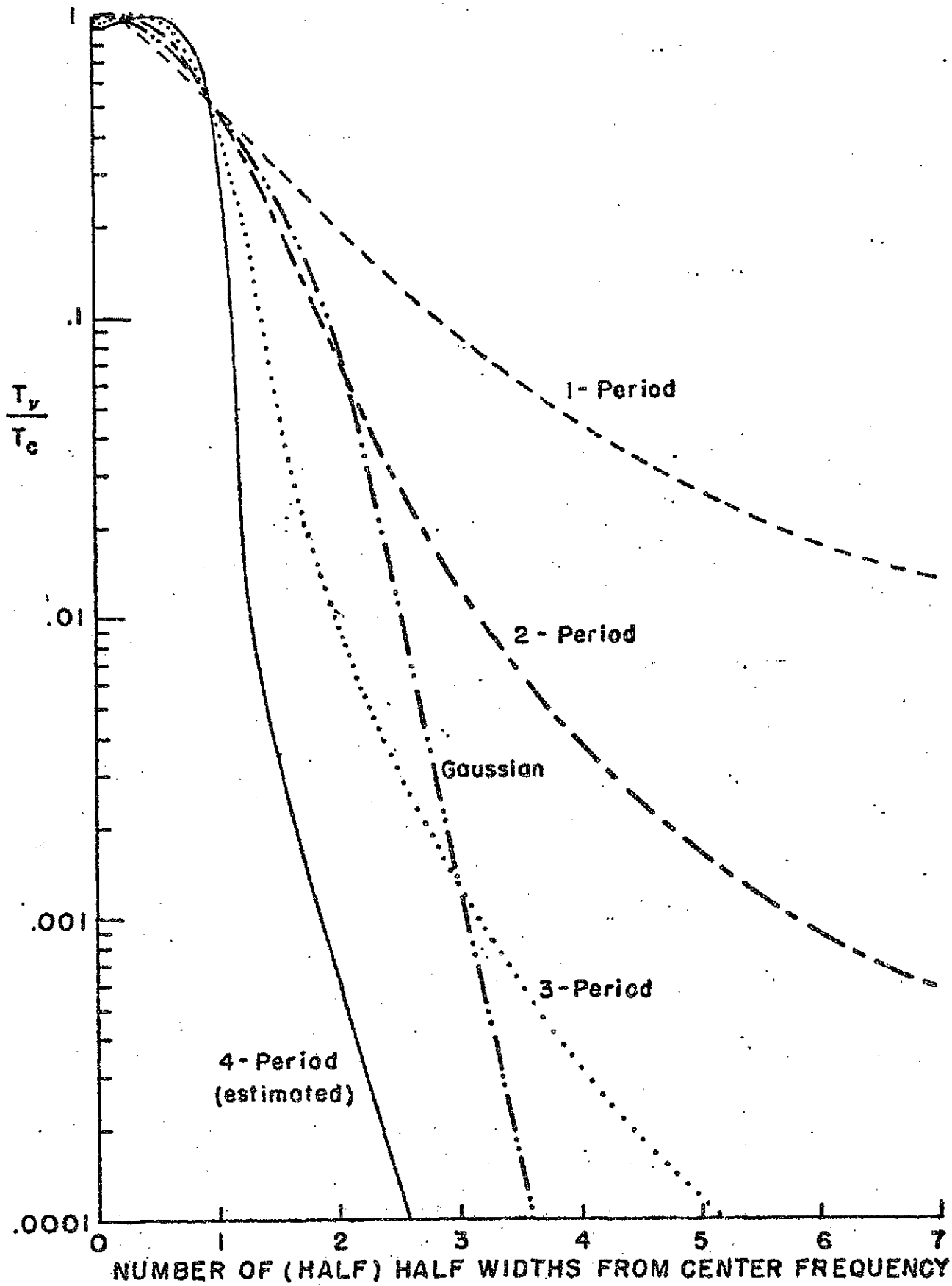

Figure 20. Transmission curves of typical single- and multi-period interference filters (after Infrared Industries data).

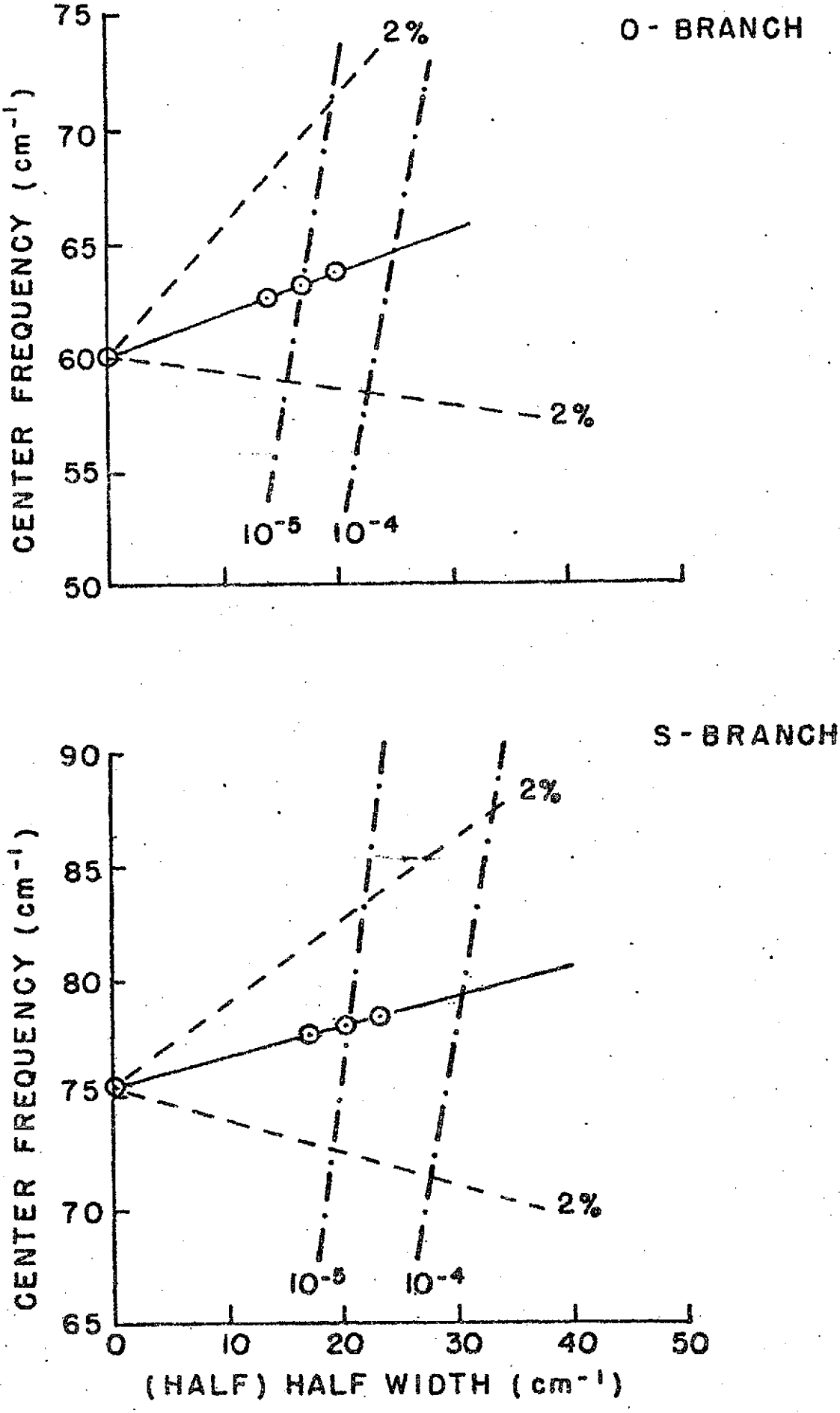

Figure 2D. Temperature dependence field for energy transmitted through four period filters of optimum center frequency and half width.

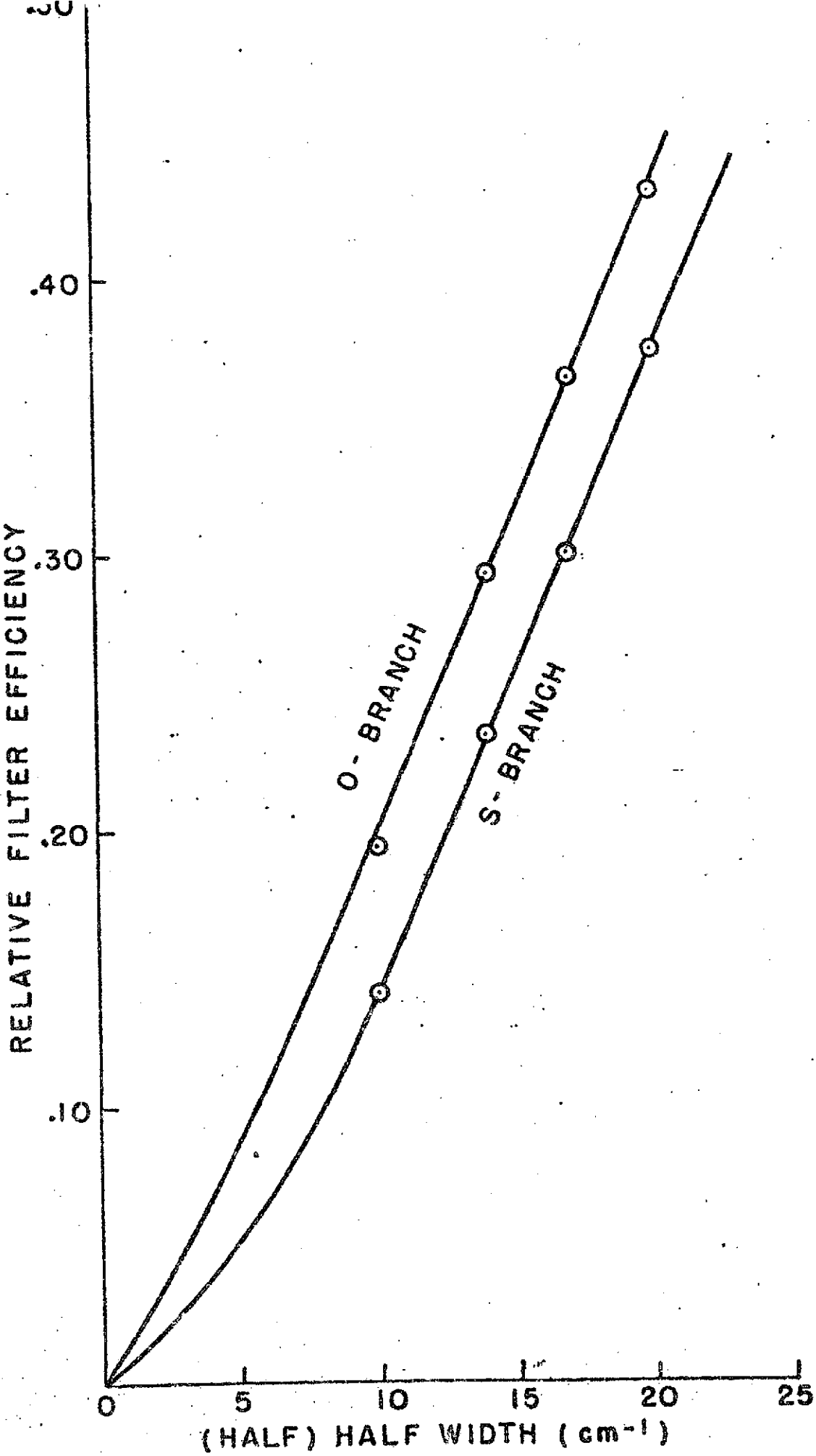

Figure 22. Fraction of available Raman energy used by four-peri filters of optimum center frequency and half width.

2. Collimation requirements.

Obviously, filters of this sort require a high degree of collimation. As a first approximation we can assume, with theoretical justification, that the entire transmission pattern of a filter is shifted in wavenumber space, without distortion, when the rays are incident at some small off-axis angle. Suppose we require that the off-axis rays may not change the center frequency (and, hence, that of the entire transmission pattern) by more than 2 cm^{-1}. For a filter centered at any of the wavelengths in Table 10, this amounts to a shift of less than 0.125 (half) half widths.

Such a shift has two effects that are of concern to us. First, there is an alteration in the degree to which the filter balances the temperature-induced fluctuations in the intensity of the Raman signal, and second, there is an alteration in the degree to which the elastically-scattered signal is rejected.

The magnitude of the first effect may be determined through examination of Figure 17, and is found to fall within the one percent limitation lines. The variation in the rejection of the elastically-scattered signal may be ascertained by inspection of Figure 20. At spectral dis-

tances beyond one (half) half width from the center frequency, the filter transmission variation induced by a frequency shift of 2 cm^{-1} is less than a factor of two.

The off-axis angle corresponding to a frequency shift of 2 cm^{-1} is, according to (65),

$$\theta < 1.6^{o}$$

Proceeding as in Chapter IV.C.2., we find that, for a filter of radius 2 cm, it is required that

$$F/\mathcal{N} < 0.11$$

which falls at the location marked (B) in Figure 19.

E. Filtering through use of a diffraction grating.

1. General.

The possibility of using a diffraction grating to separate spatially the elastic and Raman components of the received signal was considered.

While the necessary spectral and spatial resolutions are readily obtainable in commercially available gratings, the secondary diffraction pattern generated by the strong elastic signal is observed at the same angular position as the primary Raman lines, and can interfere. An investigation is made here into the magnitude of this problem, and into the design of a grating system which would minimize

it.

Consider a fully-illuminated grating with N grooves. The energy diffracted per unit angle is given by Ditchburn (1963) as

$$\frac{dP_i}{d\theta'} = P_i \frac{\sin^2 U}{U^2} \frac{\sin^2 NW}{\sin^2 W} \tag{66}$$

where

$$U = \frac{\pi \nu d}{c} (\sin\theta' - \sin\theta_o) \tag{67}$$

and

$$W = \frac{\pi \nu \epsilon}{c} (\sin\theta' - \sin\theta_o) \tag{68}$$

If $d = \epsilon$, as is approximately the case in modern gratings, then $U = W$, and

$$\frac{dP_i}{d\theta'} = P_i N^2 \frac{\sin^2 NU}{(NU)^2} \tag{69}$$

If the grating is blazed (Jenkins and White, 1957) such that the optimum order at ν_e is K, then (69) becomes

$$\frac{dP_i}{d\theta'} = P_i N^2 \frac{\sin^2 NU'}{(NU')^2} \quad , \quad (U' \equiv U - K\pi) \tag{70}$$

We define the "principal maximum" (p.m.) as the energy lying between the first energy minima to either side of $U = K\pi$ ($U' = 0$), the center of the pattern. These minima occur at $U' = \pm \pi/N$ (see Figure 23), and thus the energy in the principal maximum is

$$P_{p.m.} = \int_{-\frac{\pi}{N}}^{\frac{\pi}{N}} \frac{dP_i}{d\theta'} d\theta' = \int_{-\frac{\pi}{N}}^{\frac{\pi}{N}} \frac{dP_i}{d\theta'} \frac{d\theta'}{dU'} dU'$$

$$= \frac{2cP_iN}{\pi \nu_e d \cos\theta'} \int_0^{\pi} \frac{\sin^2 NU'}{(NU')^2} d(NU') \qquad (71)$$

and the energy in some interval, $\frac{\pi}{N} \leqslant U'_{min} \leqslant U' \leqslant U'_{max}$, of the secondary diffraction pattern is

$$P_{s.m.} = \frac{cP_iN}{\pi \nu_e d \cos\theta'} \int_{NU'_{min}}^{NU'_{max}} \frac{\sin^2 NU'}{(NU')^2} d(NU') \qquad (72)$$

2. Constraints on the order number and free range of the grating system.

We require that the free range of the grating system

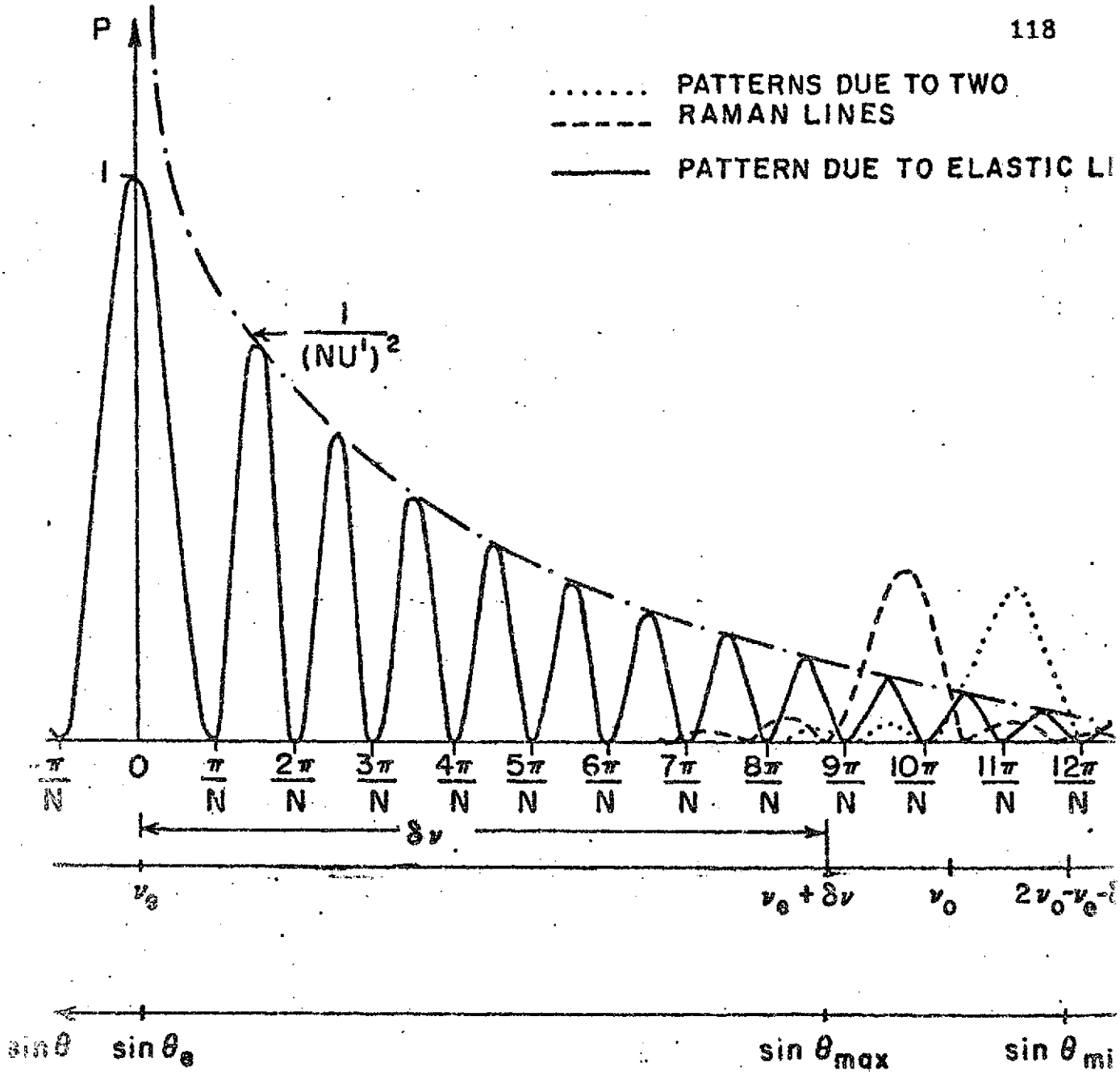

Figure 23. Patterns due to elastic line and two Raman lines as generated by a diffraction grating (not to scale).

be some minimum value, ν_f, so as to insure that the patterns due to adjacent orders do not overlap to an extent that would interfere with observations. Consider an observation made at an angle θ_o. Using (68), we see that the principal maximum of frequency ν_e diffracted in order K will be observed at this angle if

$$\sin \theta_e - \sin \theta_o = \frac{cK}{d\,\nu_e} \tag{73}$$

Similarly, the principal maximum of frequency $\nu_e + \nu_f$, diffracted in order K+1 will be observed at this same angle if

$$\sin \theta_e - \sin \theta_o = \frac{c\,(K+1)}{d\,(\nu_e + \nu_f)} \tag{74}$$

Combining (73) and (74), we see that the criterion for both frequencies to be observed at the same angular location is that

$$K = \frac{\nu_e}{\nu_f} \tag{75}$$

This constitutes the maximum usable order number if frequency ν_e is not to interfere with $\nu_e + \nu_f$. The magnitude of ν_f is determined by the character of the received signal and by the additional filtering in the system. For

instance, if we were certain that the received signal, including background, extended no farther than 1000 cm^{-1} to either side of ν_e, taken as 14,400 cm^{-1} (6943 Å), then the maximum order number would be 14,400/1000 = 14. Thus, a system of this sort must operate in the range

$$1 \ll K \ll 14$$

approximately.

3. Interference of diffraction due to elastic scattering with that due to Raman scattering.

Suppose that we are interested in observing the principal maxima due to a group of Raman lines lying in the interval $(\nu_e + \delta\nu) \ll \nu \ll (2\nu_o - \nu_e - \delta\nu)$ (see Figure 23). Then, applying the grating equation at these frequencies, we obtain

$$\sin\theta_{min} - \sin\theta_o = \frac{cK}{d\,(\nu_e + \delta\nu)} \qquad (76)$$

and

$$\sin\theta_{max} - \sin\theta_o = \frac{cK}{d\,(2\nu_o - \nu_e - \delta\nu)} \qquad (77)$$

Therefore, using (67), we find

$$U'_{min} = K\pi\left(\frac{\delta\nu}{\nu_e + \delta\nu}\right) \qquad (78)$$

and

$$U'_{max} = K\pi \left(\frac{2\nu_o - 2\nu_e - \delta\nu}{2\nu_o - \nu_e - \delta\nu} \right) \qquad (79)$$

If the Raman energy received is presumed to vary with $\nu_e + \delta\nu$ through E(h), as given in Figure 18, then the ratio of primary Raman scattering to secondary elastic scattering in the interval is

$$\frac{P_{e}^{s.m.}}{P_{r}^{p.m.}} = \frac{1}{2} \frac{P_e}{P_r E(h)} \frac{\int_{\pi KN\left(\frac{\delta\nu}{\nu_e + \delta\nu}\right)}^{\pi KN\left(\frac{2\nu_o - 2\nu_e - \delta\nu}{2\nu_o - \nu_e - \delta\nu}\right)} \frac{\sin^2 NU'}{(NU')^2} d(NU')}{\int_{\pi}^{0} \frac{\sin^2 NU'}{(NU')^2} d(NU')} \qquad (80)$$

The value of the integral in the denominator is a constant, approximately equal to $\pi/2$.

To estimate the values taken on by the integral in the numerator for a given set of limits, we let

$$\sin^2 NU' = \overline{\sin^2 NU'} = \sqrt{2}/2$$

and integrate:

$$\frac{\sqrt{2}}{2}\int_{\pi KN\left(\frac{\delta\nu}{\nu_e+\delta\nu}\right)}^{\pi KN\left(\frac{2\nu_o-2\nu_e-\delta\nu}{2\nu_o-\nu_e-\delta\nu}\right)}\frac{d(NU')}{(NU')^2} = \frac{\sqrt{2}}{\pi KN}\,\frac{\nu_e}{\delta\nu}\left[\frac{(\nu_o-\nu_e)-\delta\nu}{2(\nu_o-\nu_e)-\delta\nu}\right] \quad (81)$$

Thus, the ratio becomes, approximately,

$$\frac{P_{s_e m.}}{P_{\substack{p.m.\\ r}}} = \frac{P_e}{P_r E(h)}\,\frac{\nu_e}{KN}\,\frac{\sqrt{2}}{\pi^2\delta\nu}\left[\frac{(\nu_o-\nu_e)-\delta\nu}{2(\nu_o-\nu_e)-\delta\nu}\right] \quad (82)$$

Where the wavenumber resolution is equal to the quotient, ν_e/KN (Born and Wolf, 1959). The term

$$\frac{\sqrt{2}}{\pi^2\delta\nu}\left[\frac{(\nu_o-\nu_e)-\delta\nu}{2(\nu_o-\nu_e)-\delta\nu}\right]$$

is determined by our previously described requirements, is independent of our choice for ν_e, and takes on a value of approximately 10^{-2}. The magnitude of the factor $P_e/P_r E(h)$ is determined by the ratio of the elastic and Raman backscatter cross sections and the fraction of the total Raman energy utilized, is also relatively independent of the system parameters and is approximately equal to 1.7×10^2. The ratio, $P_{s_e m.}/P_{p_r m.}$, is determined by the level of ac-

curacy that we wish to achieve in our observation and, for one percent accuracy, is equal to 10^{-2}. Thus determined, the required resolution of the grating is found to be approximately 0.006 cm^{-1}, a value essentially independent of the system parameters. Such a grating, particularly one of good quality, is exceedingly expensive. It should be remembered that, even though a grating is used to separate the components, filters are still necessary to produce the desired weighting function.

The required parameters for the grating may be relaxed somewhat by using a combination of grating and filter to produce the rejection. For instance, if a filter were employed which had a transmission of $10^{-1}T_c$ at ν_e, then the resolution of the grating system could be reduced by a factor of ten.

4. Interference due to grating "ghosts".

The use of a grating presents another problem, one whose magnitude is not as readily determined. That is the problem of grating "ghosts" or anomalous diffraction properties which appear due to errors in ruling the grating. These patterns also tend to appear in the region where the Raman lines are observed, and vary in location and inten-

sity from one grating to another.

5. Collimation requirements.

In order that we may focus the received rays closely enough to allow them to pass through the monochrometer entrance slit, we must impose a constraint upon the blur radius produced by the optical system.

The maximum allowable size of the entrance slit (and thus, that of the blur radius) is determined by the spectral resolution that we wish to achieve in the monochrometer exit plane, as well as by the optics comprising the instrument.

Fundamentally, we require that the monochrometer be capable of separating the primary diffraction due to elastic scattering from that due to Raman scattering. That is, the dispersion of the instrument must be such that, in the exit plane, the distance, ΔL, of the Raman-scattered energy from the elastically scattered energy must be at least as great as the half-width of the entrance slit. The expression for the linear dispersion of a monochrometer may be written as

$$\frac{\Delta L}{\Delta \nu} = \frac{KN f \rho}{\nu_e^2 \cos \theta} \tag{83}$$

If we parameterize this expression in terms of the blur radius of the optical system, $\mathcal{F}$, and solve for the ratio $\mathcal{F}/\mathcal{N}$ discussed in Chapter IV.C.2., we find that

$$\frac{\mathcal{F}}{\mathcal{N}} = \frac{\mathcal{F}}{\Delta L} \frac{KN}{\nu_e} \frac{\Delta\nu}{\nu_e \cos\theta} \tag{84}$$

For an estimate of $\mathcal{F}/\mathcal{N}$, we suppose first that the distance, in the exit plane, between the Raman-scattered and elastically scattered energy, ΔL, is equal to the radius of the focal region, $\mathcal{F}$. That is, that $\mathcal{F}/\Delta L \sim 1$. Further, we assume that the resolution, ν_e/KN, is 0.008 cm^{-1}, compatible with the computations of the previous section. The frequency difference between the elastic and Raman lines, $\Delta\nu$, is about 25 cm^{-1} and cos θ is not much different from one. If ν_e = 14400 cm^{-1}, the ruby laser frequency, we find that

$$\frac{\mathcal{F}}{\mathcal{N}} = 0.22 \text{ cm}$$

This figure is comparable to those obtained when one examines the constraints on interference filters (see Figure 19). That is, the constraints on the optical system utilizing a diffraction grating are of the same magnitude as those on

the system employing an interference filter.

F. Filtering through use of a Fabry-Perot interferometer.

1. General.

According to Jenkins and White (1957), the reflectance of a Fabry-Perot interferometer varies with wavelength in the manner shown in Figure 24. Regardless of the magnitude of R, the reflectance of the individual interferometer element, the reflectance of the interferometer always reaches zero at points spaced periodically in wavelength space. This is not true in practice, since the reflectance minimum is limited by random scattering from the interferometer surfaces. The magnitude of this scattering is of the order of one percent.

2. Constraints on the design of the interferometer.

We wish to design an interferometer which has reflection characteristics such that the region of near-zero reflection is wide enough to accomodate a laser line with a spectral width of about 1 $\mathring{A}$, yet sufficiently narrow so that the reflectance in the region about 10 $\mathring{A}$ - 70 $\mathring{A}$ away from the line is fairly large.

These requirements lead to selection of $\Delta\lambda = 80\ \mathring{A}$, and mirror reflectances of about 25 percent. The theore-

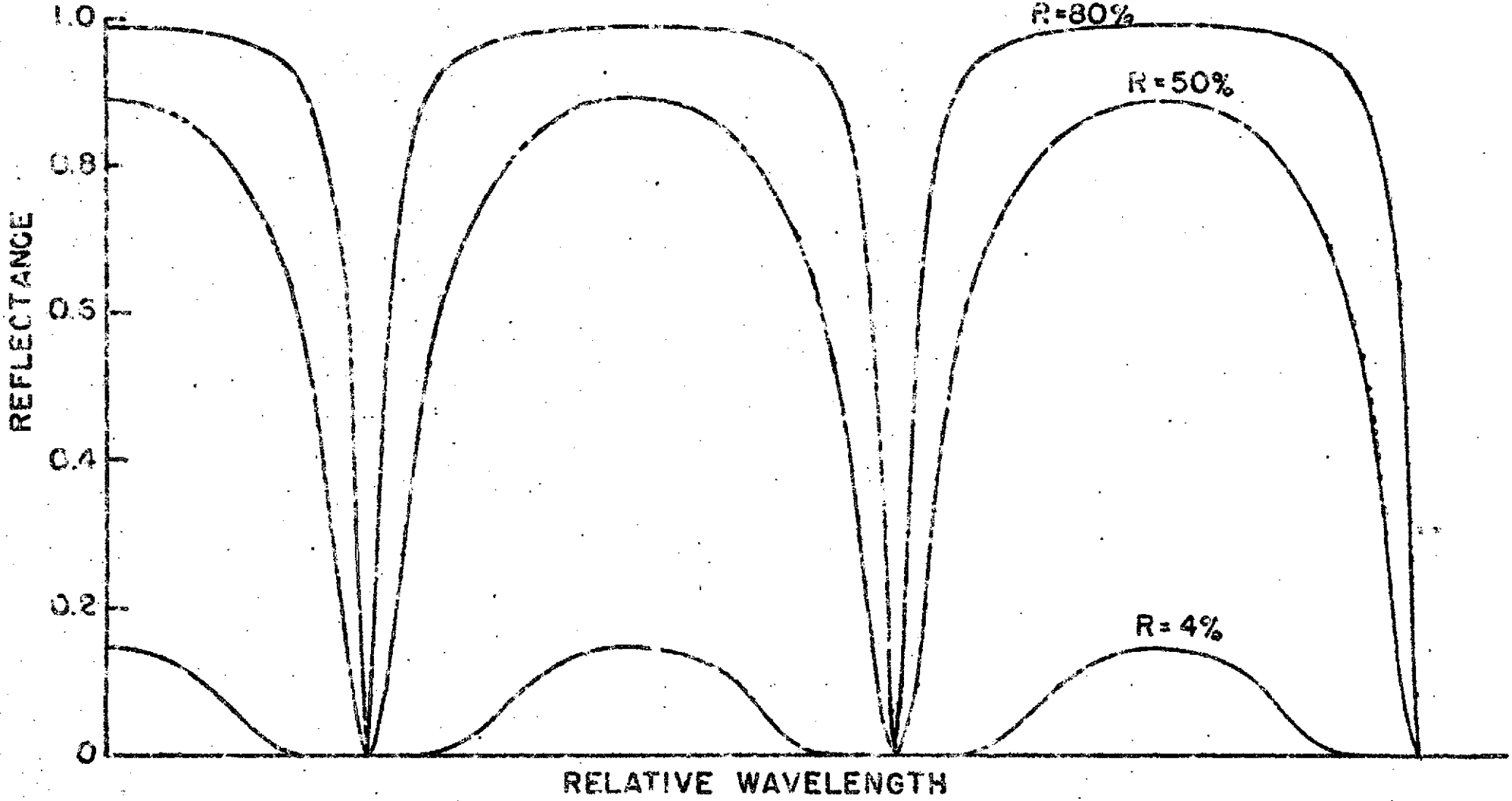

Figure 24. Reflectance pattern of a Fabry-Perot interferometer.

tical reflectance curve for such an interferometer, superimposed on the rotational Raman spectrum of air, is shown in Figure 25.

Since the free range is large, an interferometer of this design is not as sensitive to the angle of incident light as is a sharp transmission filter. Suppose that the mean incidence angle is five degrees (The angle must be as small as possible, in order to minimize polarization effects). Then, a one degree deviation in this angle will produce a wavelength shift of 12 Å in the interferometer pattern. This is much too large, of course. The sensitivity of an interferometer to angular deviation of the incident light decreases as the angle of the incident light decreases. The limit is reached when the mean incidence angle is zero degrees. Suppose that this is the case, and that the beam has a one degree deviation to either side. In that case,

$$\frac{\lambda_1}{\lambda_2} = \frac{\cos \theta_1}{\cos \theta_2} \tag{85}$$

$$\frac{\lambda_1}{6943 \text{ Å}} = \frac{\cos 1^\circ}{\cos 0^\circ} = 0.99985$$

Therefore, $\lambda_1 = 6941.95$ Å or $\lambda_2 - \lambda_1 = 1.05$ Å

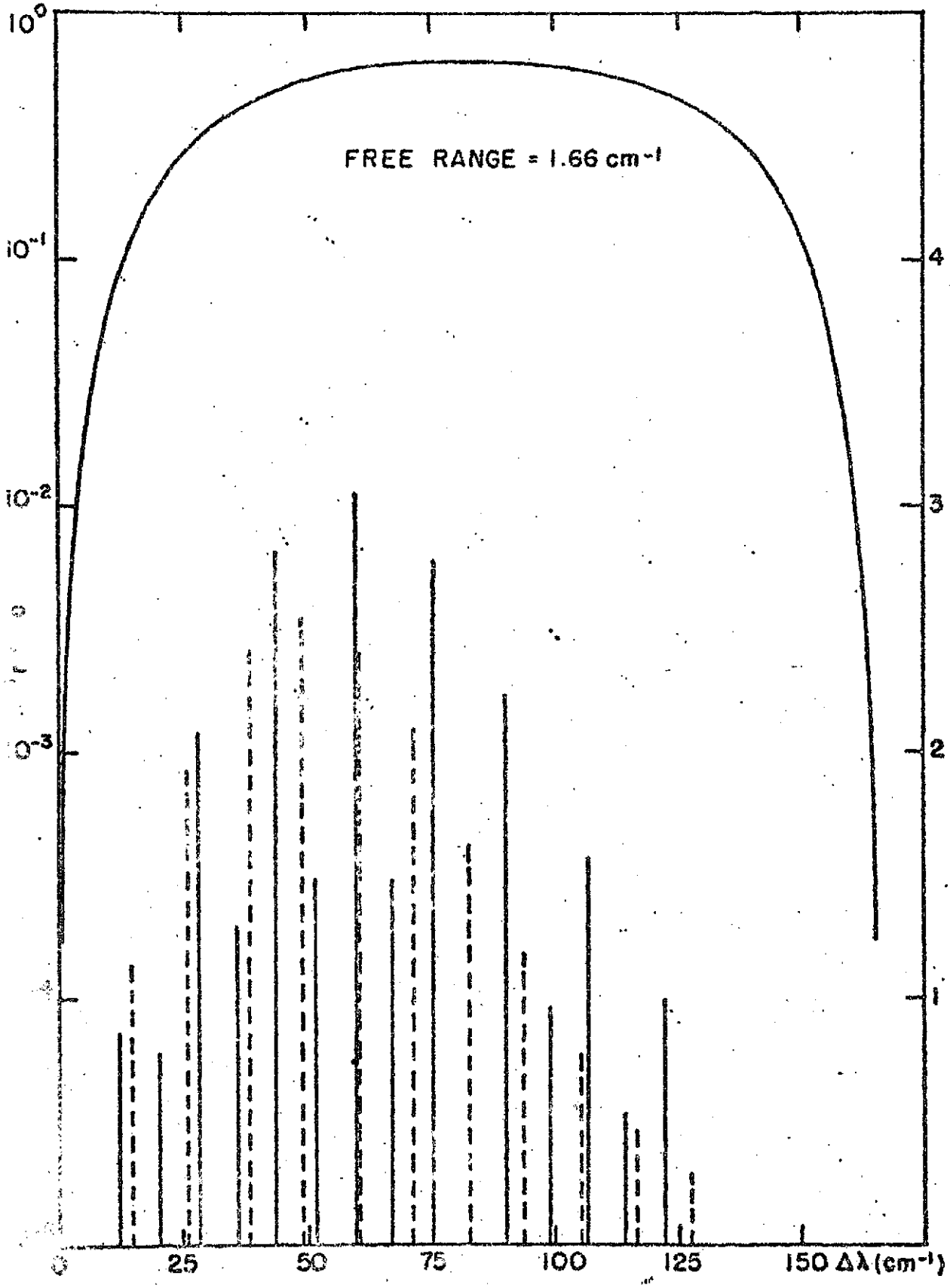

Figure 25. Reflectance pattern of a Fabry-Perot interferometer with R=25%, $\Delta\lambda$=80Å, superimposed on the rotational Raman spectrum of air.

Since this is about the maximum spectral deviation that we can tolerate, it is obvious that our system must operate at reflection angles very close to zero degrees. Suppose that the beam is centered at one degree to the normal. Then,

$$\frac{\lambda_1}{6943\ \text{Å}} = \frac{\cos\ \frac{1}{2}^{o}}{\cos\ 1\frac{1}{2}^{o}}$$

$$\lambda_1 = 6945.08\ \text{Å} \quad \text{or} \quad \lambda_2 - \lambda_1 = 2.08\ \text{Å}$$

This is about the minimum deviation that we can realistically expect from a beam divergence of one degree. If we decrease the divergence to 0.5^{o}, then

$$\frac{\lambda_1}{6943\ \text{Å}} = \frac{\cos\ \frac{1}{2}^{o}}{\cos\ 1^{o}}$$

$$\lambda_1 = 6943.76\ \text{Å} \quad \text{or} \quad \lambda_2 - \lambda_1 = 0.76\ \text{Å}$$

So, if the beam divergence of the incoming light is 10^{-4} radians, then the maximum ratio between the diameter of the collecting mirror and the Fabry-Perot interferometer is

$$\frac{0.5^{\hat{0}}\ /\ 57.3}{10^{-4}} = 87.3$$

For an effective interferometer spot 1 cm wide, the maximum collector diameter is 87.3 cm (34.4"). For a beam width of 10^{-3} radians, this diameter is only 8.73 cm (3.44").

Suppose that we wish to improve the rejection characteristics of our system by allowing the beam of light to pass $\hat{n}$ times through the interferometer. The geometric aspects of such a system are shown in Figure 26.

The effect of passing the beam through the interferometer $\hat{n}$ times is to produce a new overall transmission function that is determined by raising the original function to the $\hat{n}$th power. This produces a curve whose rejection characteristics are greatly enhanced, but whose transmission qualities are mediocre. For example, an interferometer whose null reflectance is 10^{-2} and whose "band pass" reflectance is 0.6, when used in a 3-pass configuration, will theoretically yield a null reflectance of 10^{-6} and a "band pass" reflectance of 0.22.

Referring to the figure, we see that, in order to just separate the incoming and reflected beams, the distance between the interferometer and the reflecting mirror must be

$$D = \frac{H}{2(\Phi - \theta)} \tag{86}$$

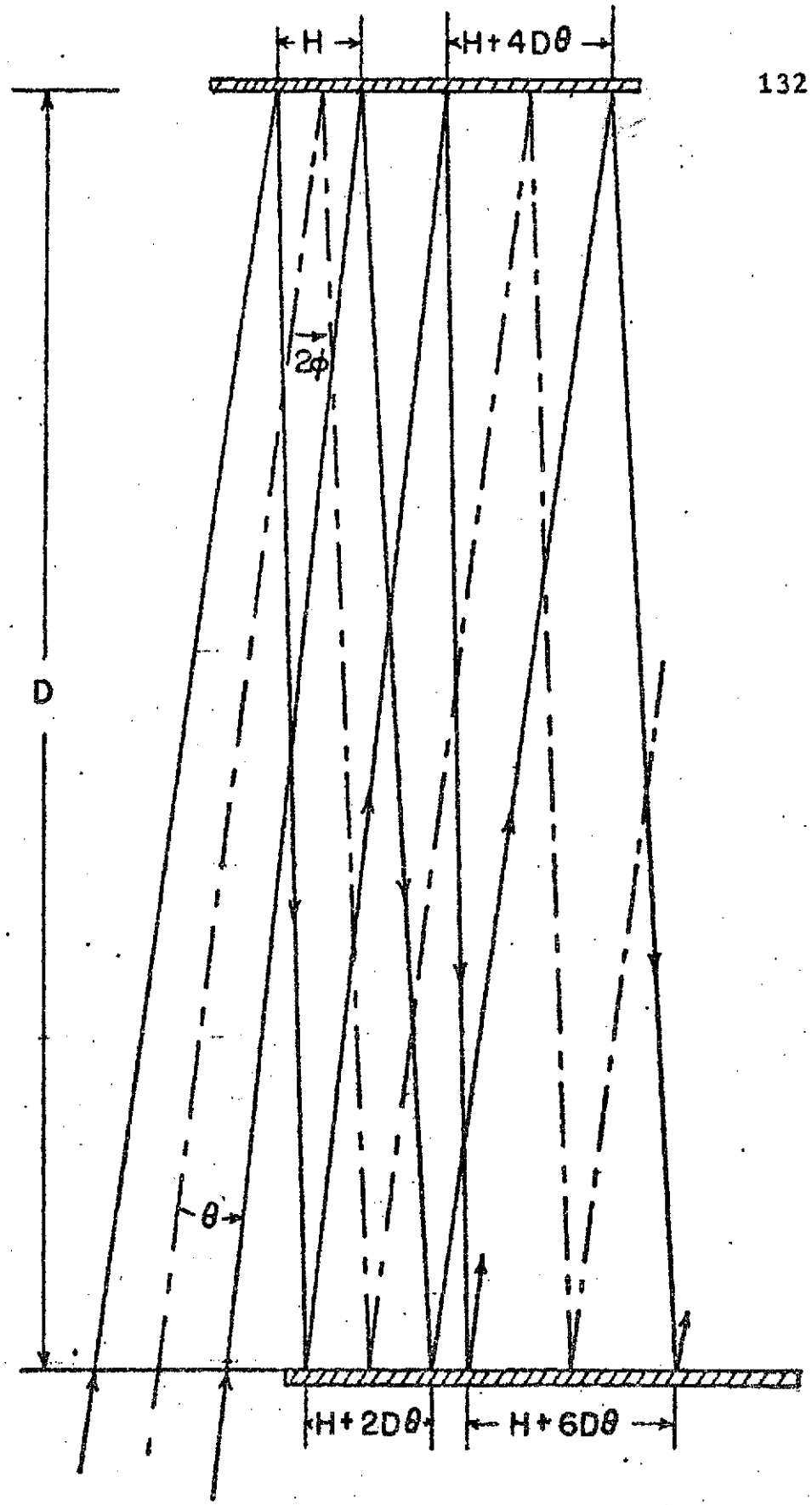

Figure 26. Geometry of a multipass Fabry-Perot interferometer

where H is the size of the individual spot on the interferometer, and that the minimum width of the interferometer must be

$$w = \left[1 + (\hat{n} - 1)\frac{1 + \frac{\theta}{\mathcal{Q}}}{1 - \frac{\theta}{\mathcal{Q}}} \right] \qquad (87)$$

If $\theta = \frac{1}{4}^{\circ}$, $\mathcal{Q} = 3/4^{\circ}$ and H = 0.29 cm, then

$$\therefore D = 17 \text{ cm.}$$

If $\hat{n} = 3$, then

$$w = 1.45 \text{ cm.}$$

3. Collimation requirements.

The value of $\mathcal{F}/\mathcal{N}$ associated with an interferometer of this sort is about 0.004 cm, a value much smaller than those computed for the interference filters or diffraction grating. This is attributable to the fact that, in a multipass arrangement, it is necessary to keep the spot size very small in order that the total size of the interferometer be kept reasonable, and because the individual spots may not overlap. The interference filters discussed earlier are really nothing more than a large number of Fabry-Perot interferometers in a series or cascade arrange-

ment. The sharp pattern is not produced by multipassing, and thus a much larger spot size may be used to obtain a given interferometer pattern for a given interferometer size.

It is to be concluded that use of a multipass Fabry-Perot interferometer results in severe restrictions on the optical quality of the total system, and that from this point of view, the other devices discussed earlier are highly preferable.

G. Filter system utilizing selective absorption of elastically scattered light.

1. General.

In view of the high optical quality required in systems which attempt to separate, interferometrically, the strong elastically scattered light from the much weaker Raman scattering, an investigation was made of the possibility of selecting a laser wavelength which corresponds to an isolated absorption line in some substance. A measured amount of that substance could then be introduced along the light path in the receiver, thereby absorbing the bulk of the elastically scattered light, and reducing its intensity to a low enough level that rejection would no longer be a problem.

2. Choice of an absorbing substance.

In choosing an absorbing substance, the following factors were considered:

(1) The absorption line should be isolated, with the nearest significant line more than about 150 cm^{-1} away.

(2) The absorption line must be so narrow that it does not cause significant absorption at the Raman frequencies.

(3) The absorption line must be strong enough that transmission at its center can be reduced to $< 10^{-4}$ times that in the wings, using a manageable amount of absorbing material.

(4) The transmission properties of the absorbing material must be such that defocussing of light at the Raman frequencies (e.g., due to spatial fluctuations in refractive index) be minimized.

(5) The chemical properties of the substance must be such that it is not unduly dangerous or awkward to handle in the laboratory or in the field.

(6) The wavelength of the absorption line must lie in the region bounded approximately by 0.4 and 0.7 microns.

(7) The absorbing substance must not be present in the atmosphere in sufficient quantity to appreciably affect the return signal.

(8) The (half) half width of the line must be at least of the order of 1 Å in order that it include the entire spectral extent of the laser line.

Liquids and solids, by virtue of their large intermolecular forces, have absorption lines which are too broad for our purposes. Requirements (2) and (3) thus dictate the use of a gaseous absorber. The absorption lines of polyatomic molecules are always accompanied by a fine structure; that is, by nearby secondary lines. Except in the case of H_2, a molecule with extremely low mass, these nearby lines fall within 150 cm^{-1} of the primary line, and thus render polyatomic gases undesirable due to requirement (1). We thus limit our search to monatomic gases. Because of the strong absorbing properties that we require, we limit our search to the resonance absorption lines of these gases. The only elements which produce stable monatomic gases at reasonable temperatures, and whose resonance absorption lines lie within the wavelength region given in requirement (7) are the Group I (alkali) elements. Of these, the one that is to be preferred is sodium (The others are either too reactive, too rare, or both).

3. Characteristics of the resonance absorption lines of sodium.

The Handbook of Chemistry and Physics indicates that sodium has two very strong resonance absorption lines at 5890 Å and 5896 Å. Walsh (1961) gives Doppler (half) half widths of the 5890 Å line as observed in flames at one atmosphere pressure and flame temperatures of 1000°K, 2000°K and 3000°K. Penner (1968) shows that the Doppler (half) half width, b_D, is given by

$$b_D = C_1 T^{\frac{1}{2}} \tag{88}$$

and is independent of pressure. Figure 27 shows a curve of this form fitted to the data given by Walsh. Walsh also states that, in a sodium flame, where p = 1 atm and T = 2200°K (broadening gas assumed to be N_2), the pressure broadening is approximately one half the Doppler broadening. From Figure 27, then, we determine that at 2200°K, $b_D = 0.116\ cm^{-1}$. Thus, $b_p = 0.058\ cm^{-1}$ at that temperature.

Pressure broadening, according to Penner (1968), varies according to

$$b_p = C_2 \frac{p}{T^{\frac{1}{2}}} \tag{89}$$

The pressure broadening (half) half width, b_p, deduced from

Doppler (Half) Half Width of Sodium Line at 5890 Å, b_D (cm^{-1})
.5
.1
.01
100
1000
10,000
$b_D = .00251\ T^{1/2}$
(cm^{-1})

Walsh's data, is plotted as a function of pressure in Figure 28 for a temperature of 673°K, the anticipated temperature of the sodium cell.

Füchtbauer and Dinkelacker (1923) studied the shape of the mercury resonance line as a function of the broadening gas and density. It is to be expected that, since the resonance in mercury is not as intense as that in sodium, the mercury line is more readily pressure broadened, and thus b_p for mercury is greater than that for sodium at any given temperature and pressure. Thus, the results of Füchtbauer and Dinkelacker for mercury vapor, taken at 300°K, provide a means of checking the consistency of the results for sodium. Their figures, reduced to 673°K, are shown for comparison in Figure 28. The two sets of figures are indeed compatible, with the values of b_p for mercury greater than those for sodium by a factor of about 2.0. For a sodium line width of 1 Å, these results indicate that a pressure of about 28 atm of N_2 is required. If argon is used as the broadening gas, the results of Füchtbauer and Dinkelacker for mercury indicate that the results would be about the same. It should be noted here that, at T = 673°K and p = 28 atm, about 94 percent of the total line width is produced by pressure broadening.

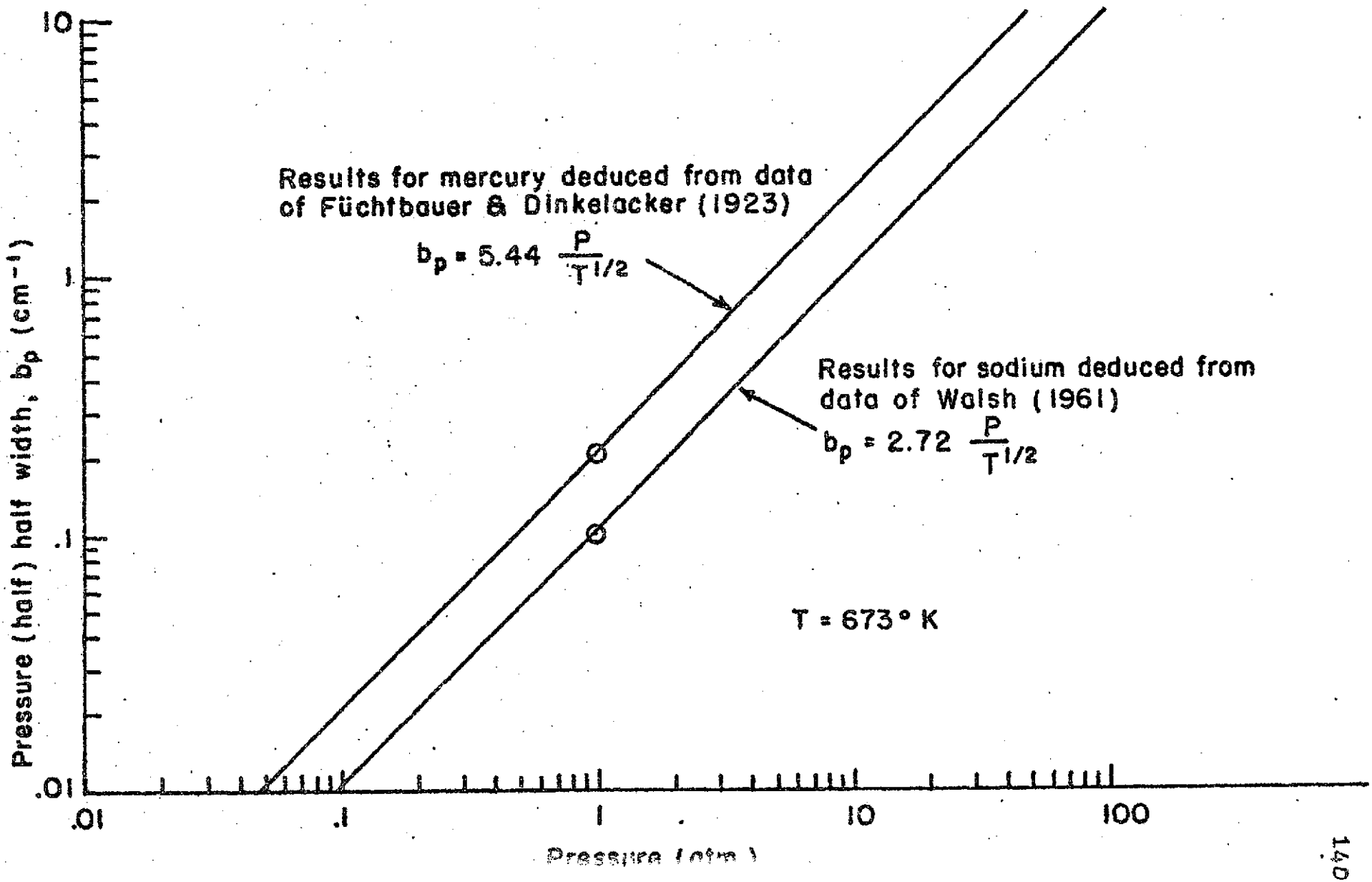
Results for mercury deduced from data of Füchtbauer & Dinkelacker (1923)
$b_p = 5.44 \frac{P}{T^{1/2}}$
Results for sodium deduced from data of Walsh (1961)
$b_p = 2.72 \frac{P}{T^{1/2}}$
T = 673° K
Pressure (half) half width, b_p (cm^{-1})
10
1
.1
.01
.01
.1
1
10
100
Pressure (atm.)

4. Resonance absorption cross section of the sodium molecule.

The resonance absorption cross section of sodium was measured in the laboratory, using a Cary* Model 14 Spectrophotometer. A sample cell was constructed which gave an optical path length of about 2.5 cm (see Figure 29). A small quantity of metallic sodium was introduced into the cell, and the cell was evacuated and sealed. By means of a heating coil wound around the cell, the sample temperature was increased. The temperature of the cell was measured by means of an iron-constantan thermocouple with which it was in contact.

The Handbook of Chemistry and Physics gives the vapor pressure of sodium corresponding to several temperatures above 712°K. If we assume that the equilibrium between metallic sodium and its vapor obeys the Clausius-Clapeyron equation (Hess, 1959), that the vapor is an ideal gas and that the latent heat of vaporization varies linearly with temperature, then

$$\ln \frac{e(Na)}{e_o(Na)} = \frac{LM(Na)}{R^*} \left[\frac{1}{T} - \frac{1}{T_o} \right] + \frac{M(Na)}{R^*} \frac{dL}{dT} \ln \frac{T}{T_o} \qquad (90)$$

*Cary Instruments, 2724 South Peck Road, Monrovia, CA 91016.

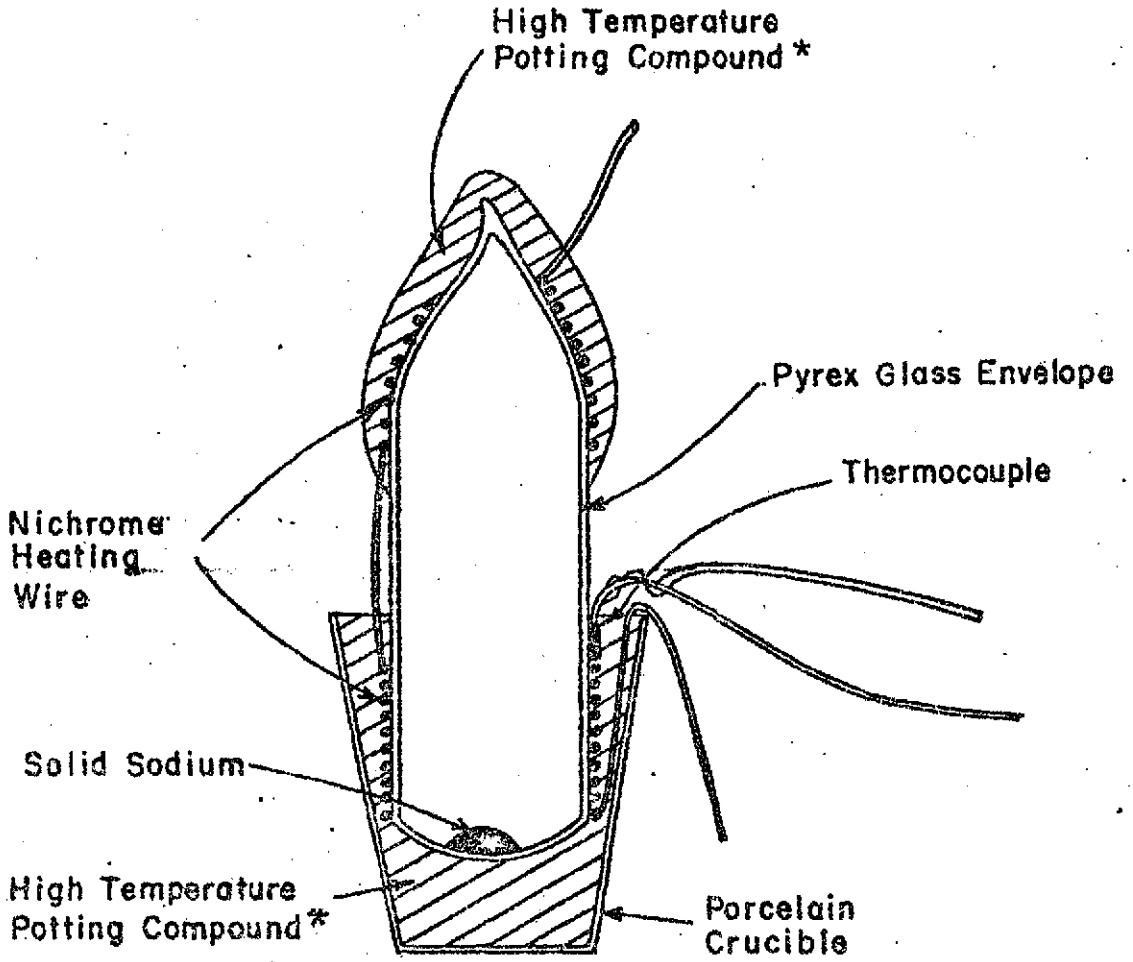

* Sauereisen Insa-Lute Cement, No. 1.

Figure 29. Construction details of temperature controlled sodium vapor absorption cell.

Using this equation and the data given in the Handbook, we find that

$$L = 4.281 \times 10^{11} \text{ erg-gm}^{-1}$$

$$\frac{dL}{dT} = 1.94 \times 10^{7} \text{ erg-gm}^{-1}\text{-}^{o}\text{K}^{-1}$$

Through use of these values, we may now obtain e(Na) for any temperature from (90). We obtain the number density of sodium molecules in gaseous form at each temperature from

$$n(Na) = \frac{e(Na)}{KT} \tag{91}$$

Graphs of e(Na) versus T and n(Na) versus T are given in Figures 30 and 31.

The absorption of light passing through the sample cell at $\lambda_1 = 5890$ Å and at $\lambda_2 = 5896$ Å, as well as adjacent wavelengths, was measured for various cell temperatures through use of the spectrophotometer. Spectral slit width was set at 0.5 Å, corresponding to an anticipated laser bandwidth of that order of magnitude. Results of these measurements are shown in Figure 32. The transmission through the cell at the center of each line is given by

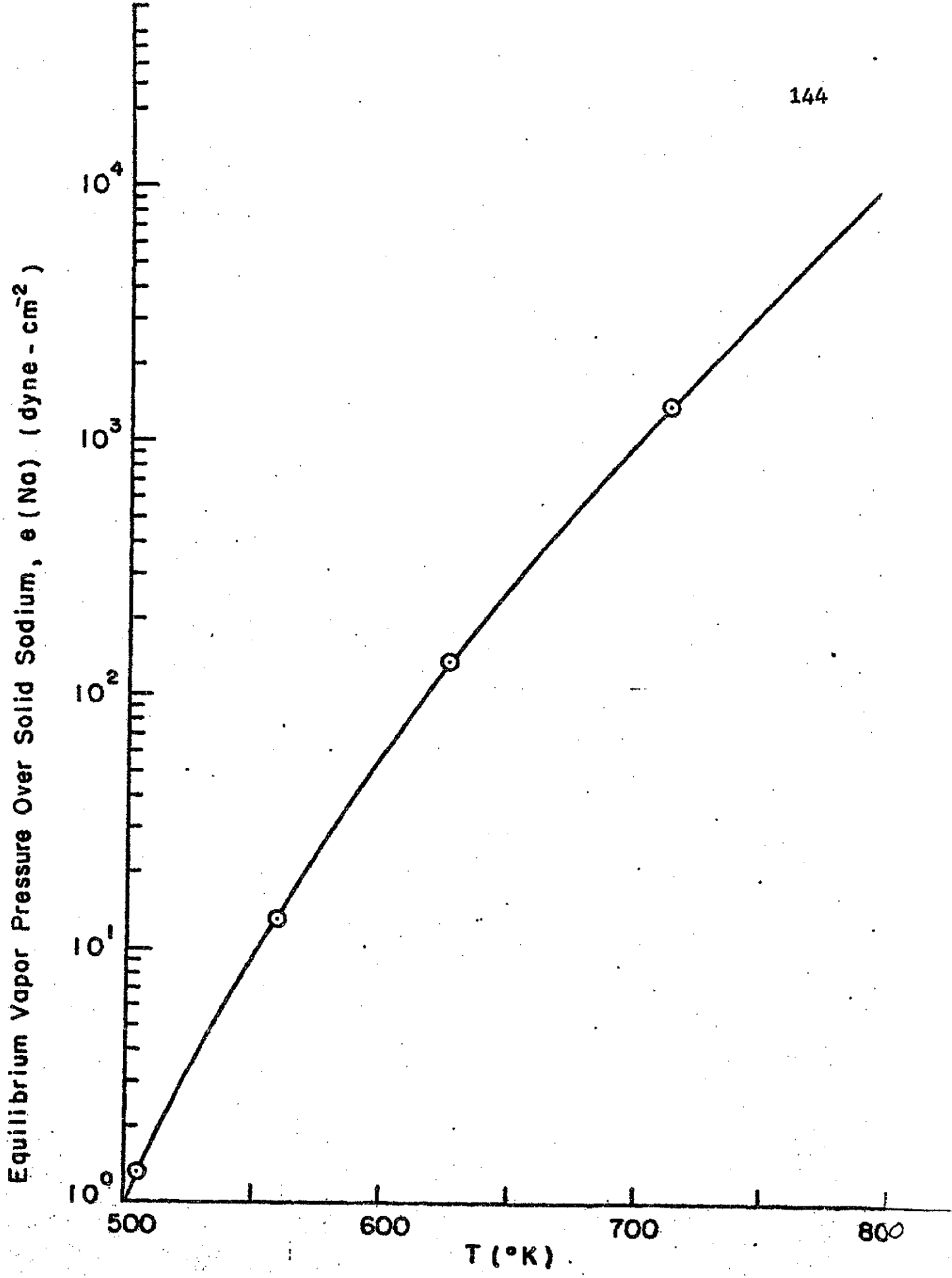

Figure 30. Equilibrium vapor pressure over solid sodium, e(Na), as computed using data given in the Handbook of Chemistry & Phys.

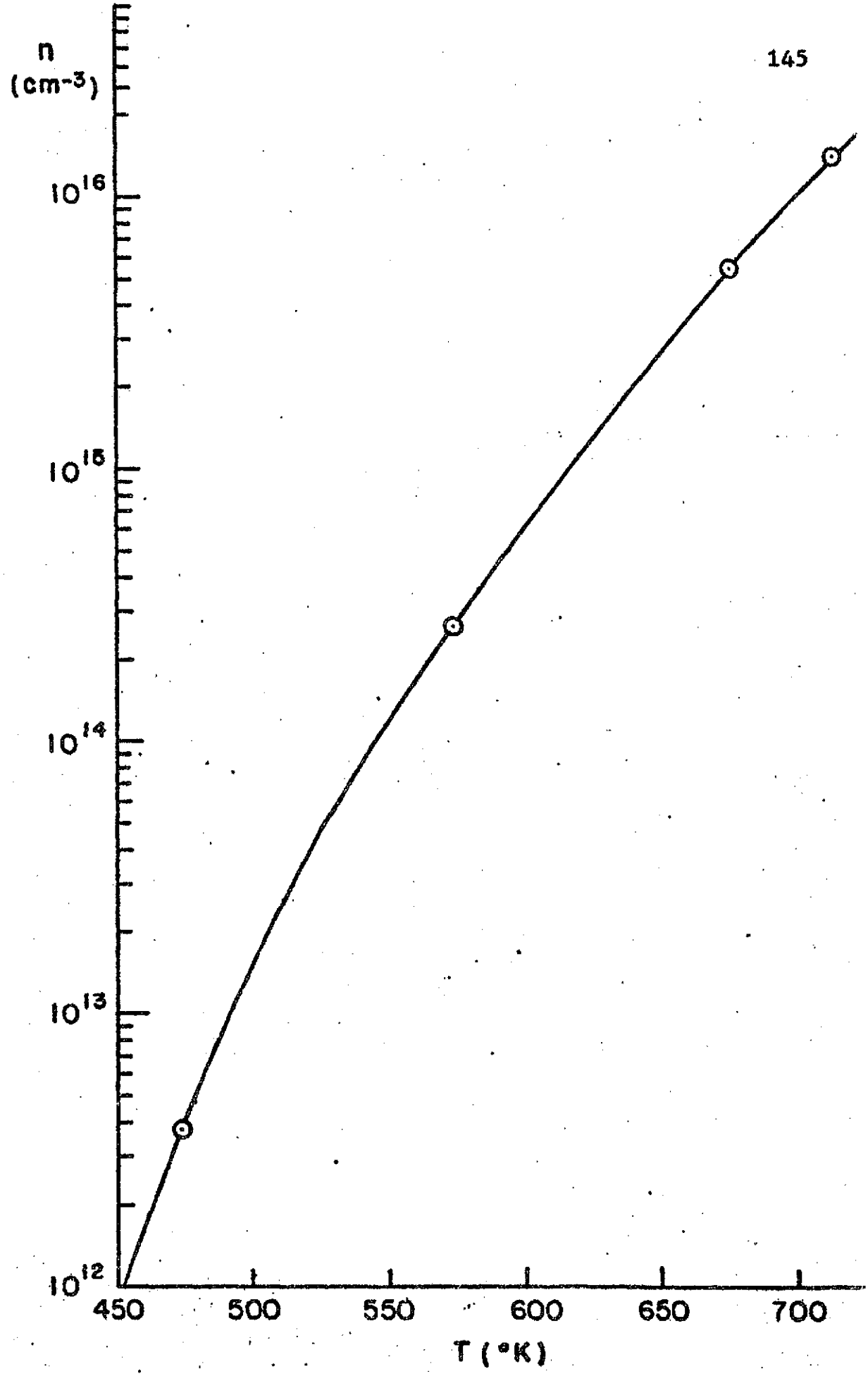

Figure 31. Number density of sodium vapor in equilibrium with solid sodium.

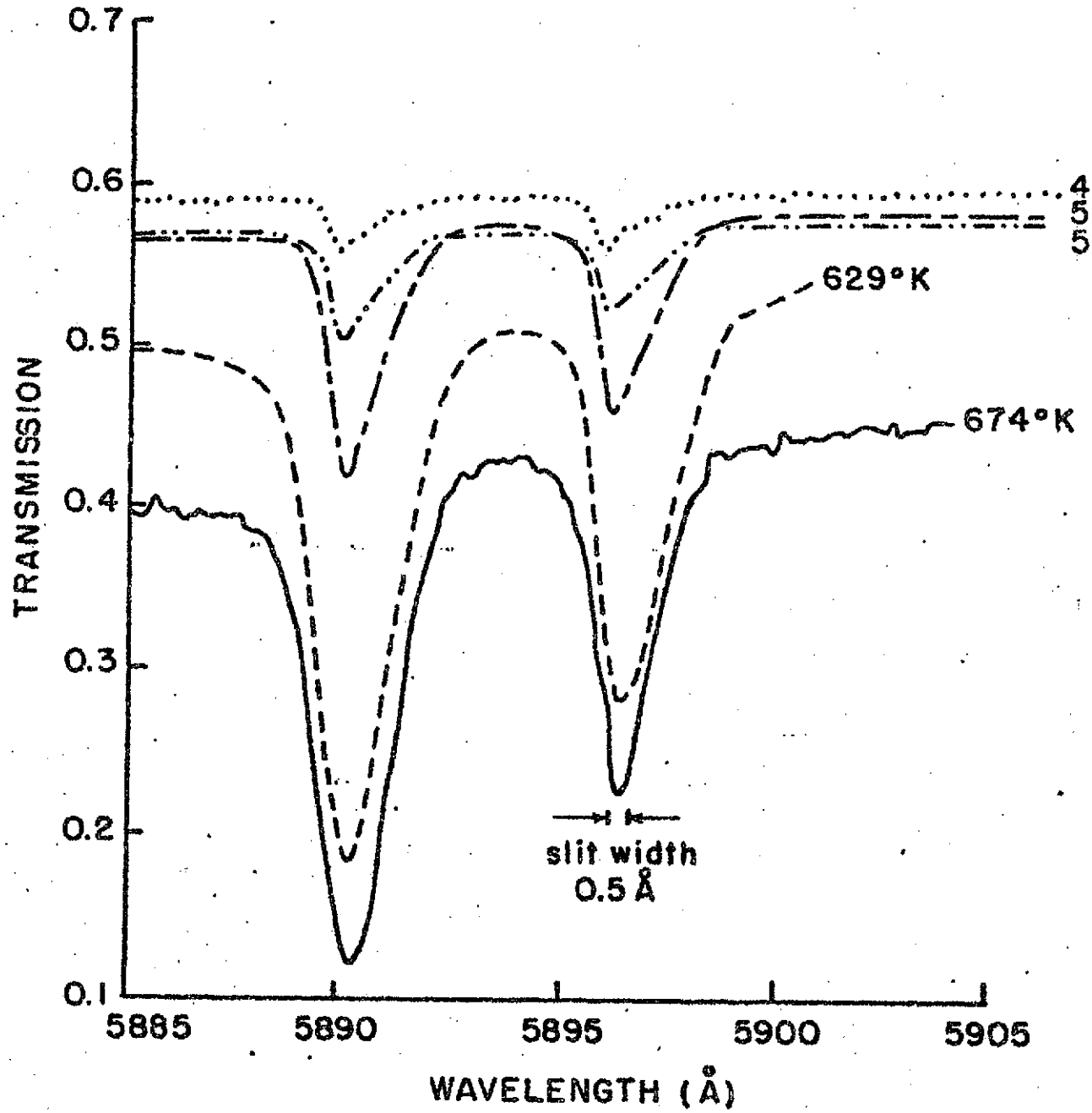

Figure 32. Observed transmission at various temperatures through absorption cell containing sodium vapor in equilibrium with solid sodium.

$$T_{\lambda_1} = e^{-\sigma_{\lambda_1} n x_c - \tau_c} \tag{92}$$

$$T_{\lambda_2} = e^{-\sigma_{\lambda_2} n x_c - \tau_c} \tag{93}$$

The transmission at some wavelength, λ_3, away from the influence of the two lines is given by

$$T_{\lambda_3} = e^{-\tau_c} \tag{94}$$

Through use of the third of these equations, we may eliminate the unknown quantity τ_c from the other two, with the result:

$$\sigma_{\lambda_1} = \frac{1}{n x_c} \ln \frac{T_{\lambda_3}}{T_{\lambda_1}} \tag{95}$$

$$\sigma_{\lambda_2} = \frac{1}{n x_c} \ln \frac{T_{\lambda_3}}{T_{\lambda_2}} \tag{96}$$

Results of the computations, shown in Table 11 and in Figures 33 and 34, indicate that the absorption cross sections vary somewhat with temperature (pressure). This is attributable to resonance effects as described by Fabelinskii (1968) for mercury vapor and other gases at

Table 11. Parameters of the absorption lines of sodium vapor at 5890 Å and 5896 Å, and factors used in their computation.

T(°K)	e(Na) from Eqn (90) ($dyne\text{-}cm^{-2}$)	n from Eqn (91) (cm^{-3})	T_{λ_1}	T_{λ_3}	T_{λ_2}	T_{λ_3}*	(full) half width $\Delta\lambda_1$(Å)	(full) half width $\Delta\lambda_2$(Å)	Computed σ_{λ_1} (cm^2)	Computed σ_{λ_2} (cm^2)
479	4.8×10^{-1}	7.3×10^{12}	0.557	0.590	0.565	0.590	1.05	0.975	3.1×10^{-15}	2.5×10^{-15}
542	6.7×10^{0}	9.0×10^{13}	0.503	0.568	0.523	0.571	1.13	1.09	5.4×10^{-16}	3.7×10^{-16}
582	2.8×10^{1}	3.5×10^{14}	0.415	0.572	0.458	0.574	1.24	1.24	3.7×10^{-16}	2.6×10^{-16}
629	1.5×10^{2}	1.7×10^{15}	0.181	0.517	0.279	0.533	1.58	1.65	2.5×10^{-16}	1.6×10^{-16}
674	5.2×10^{2}	5.6×10^{15}	0.119	0.436	0.225	0.450	1.28	1.58	9.3×10^{-17}	5.0×10^{-17}

* Transmission outside of the absorption lines appeared to have a slight tendency to increase with increasing wavelength (see Figure 32). To compensate for this, separate off-line transmission values were extracted for each line.

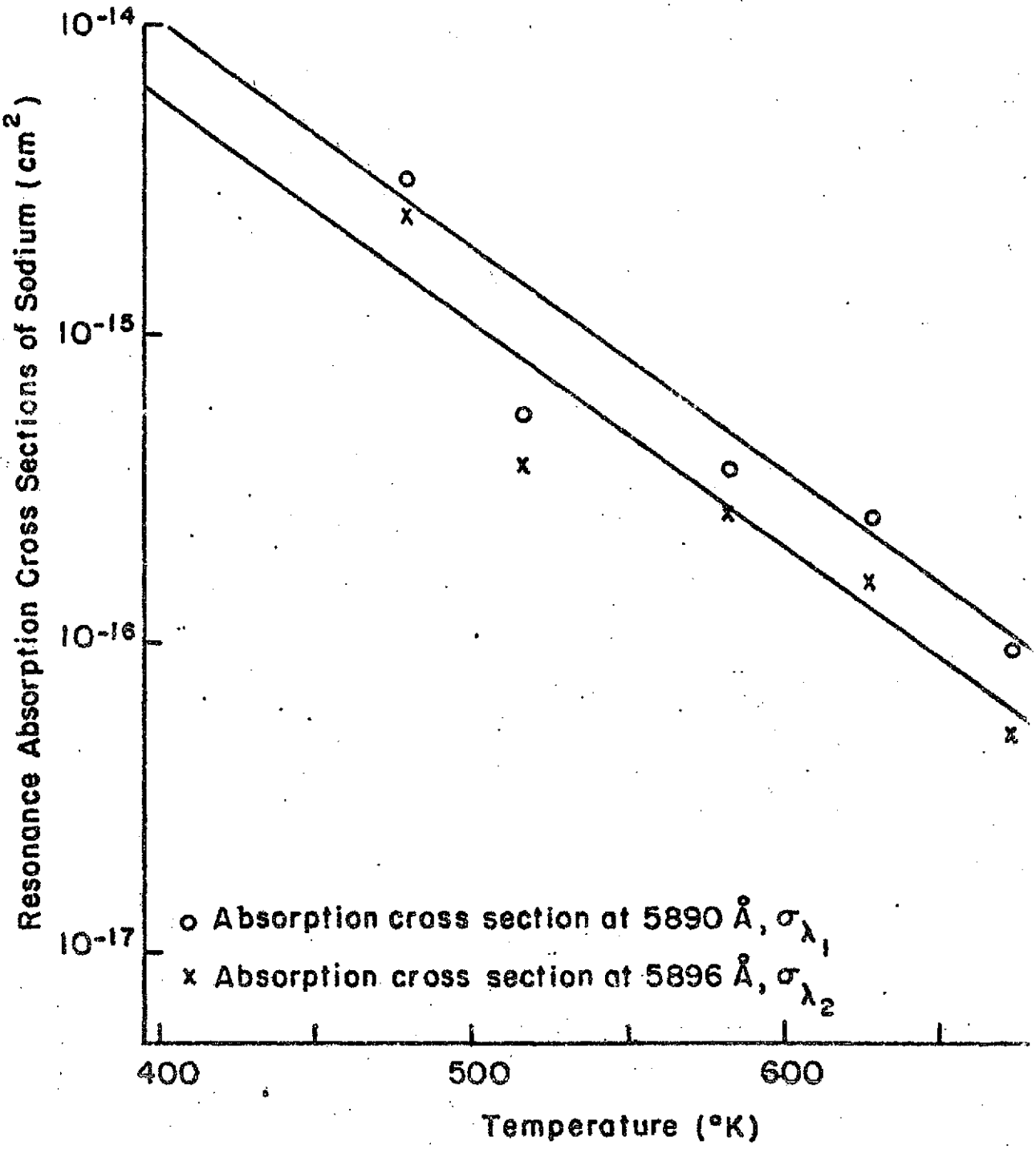

Figure 33. Computed absorption cross sections for the two resonance absorption lines of sodium vapor.

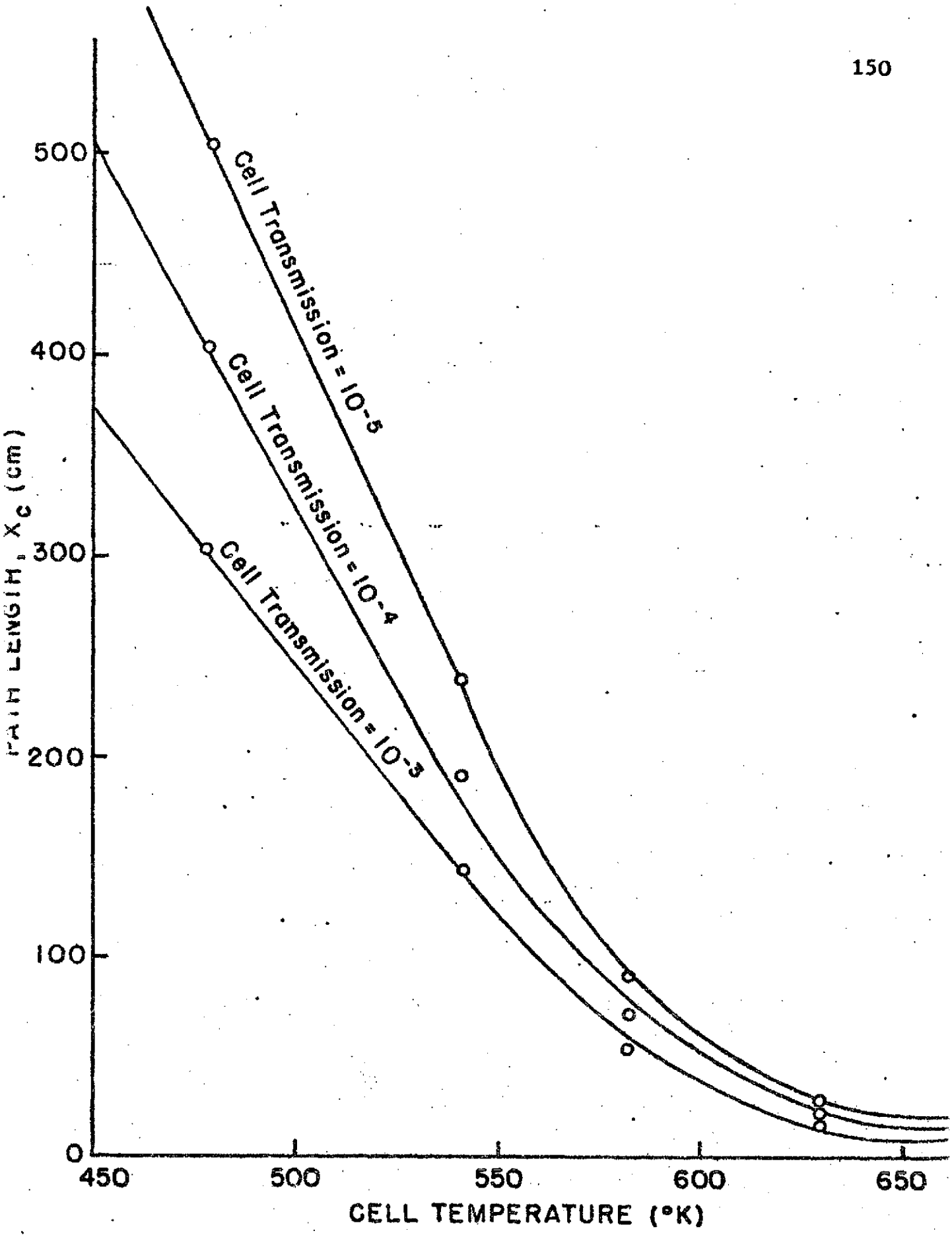

Figure 34. Required absorption cell lengths for transmission values of 10^{-3}, 10^{-4}, and 10^{-5} at the center of the 5890 Å sodium line.

low pressures.

For large optical thicknesses, we may neglect τ_c and write, for the center of the stronger absorption line:

$$x_c = -\frac{1}{\sigma_{\lambda_1} n} \ln T_{\lambda_1} \qquad (97)$$

Figure 34 shows the required path lengths for various combinations of center transmission and cell temperature, as obtained through use of this equation and the values of σ_{λ_1} and n that were determined experimentally. The required path length reaches a minimum near 650°K, since it depends on the quantity, $1/\sigma_{\lambda_1} n$, which is a minimum at that temperature.

Aside from the advantage of a relatively small cell size, we would prefer to operate our cell near this temperature because in this region, cell absorption is relatively insensitive to small fluctuations in cell temperature. Suppose that we decide to operate the cell at 650°K, with a minimum transmission value of 10^{-5}. The required path length is 20 cm.

5. Materials for construction of the cell.

Having determined the size of the absorption cell and

the regions of temperature and pressure in which it is to operate, a search was conducted for materials that could possibly be used in its construction.

Three samples of special alkali-resistant glass (Types 1720, 1723 and 1915) were obtained from the Corning Glass Works* and were baked for about 70 hours at 650^{o}K in a sealed chamber containing sodium. In all cases, a brown coloration, as well as severe etching of the surfaces was observed, rendering the glass totally unsatisfactory from an optical standpoint.

The Westinghouse Electric Corporation**, a manufacturer of sodium vapor street lamps, was consulted. They stated that, while the glass used in street lamps is translucent, it cannot be made transparent. They suggested, however, that perhaps sapphire might fulfill our requirements. Sapphire is a hard, inert substance that is transparent to yellow light.

Tyco Laboratories***, a manufacturer of industrial sapphire material was contacted. It was determined that they do not, at this time, manufacture optical quality

---

* Mr. Robert Tichane, Corning Glass Works, Corning, NY 14830.

** Mr. R.D. Hutchinson, Westinghouse Electric Lamp Division, Bloomfield, NJ.

***Tyco Saphikon Division, 16 Hickory Drive, Waltham, Mass 021

sapphire in pieces large enough for the desired purpose.

6. Conclusions.

It has been concluded that, while the use of a sodium absorption cell to selectively attenuate light at the transmitted frequency has merit, it is not feasible to implement such a system at this time, due to the temperatures and pressures involved, as well as the high chemical activity of sodium. Perhaps with the development of tunable lasers which operate efficiently with a narrower spectral output, it will not be necessary to broaden the sodium line as much, thereby increasing the practicability of a system of this sort.

Use of an absorption type filter is particularly appealing in that it all but does away with the stringent optical collimation requirements inherent in all interferometric devices.

Chapter V.

SIGNAL TO NOISE RATIOS

List of Symbols

A_r Effective collection area of receiver (cm^2).

c Speed of light ($cm\text{-}sec^{-1}$).

$E(h)$ Fraction of available Raman energy used by filter with (half) half width, h.

h Filter (half) half width (cm^{-1}).

i_b Relative background current received in Raman channel.

i_s Relative signal current received in Raman channel.

k_r System constant.

N Number of laser pulses per observation.

n Number density of air (N_2 and O_2) molecules (cm^{-3}).

q Electronic charge (coul).

R Responsivity of photomultiplier tube ($mA\text{-}W^{-1}$).

Background radiance $\left[W\text{-}cm^{-2}\text{-}(cm^{-1})^{-1}\text{-}ster^{-1} \right]$.

T_c Transmission of filter at center of its transmission curve.

$T_\nu(h,\nu_c)$ Transmission at frequency ν of filter centered at ν_c, with (half) half width, h.

$\tilde{\mathcal{T}}_m$ Atmospheric transmission - molecular component.

$\tilde{\mathcal{T}}_p$ Atmospheric transmission - particulate component.

W_t Transmitted energy (J).

z Height (cm).

Δf Bandwidth of signal processing apparatus (sec^{-1}).

λ Wavelength (μ).

ν Frequency (cm^{-1}).

ν_c Frequency at which filter transmission curve is centered (cm^{-1}).

ρ Signal to noise ratio.

σ_r Effective Raman backscatter cross section of air (cm^2-$ster^{-1}$).

Ω Receiver acceptance angle (ster).

A. Absolute signal to noise ratios at 0.7μ.

In Equations (2) through (4), it was shown that the signal current received in the Raman channel of a monostatic pulsed lidar system may be written as

$$i_s(h,z) = k_r \sigma_r n (\tilde{\mathcal{J}}_m \tilde{\mathcal{J}}_p)^2 \tag{98}$$

The system constant k_r is given by

$$k_r = \frac{W_t A_r R c E(h) T_c}{2z^2} \tag{99}$$

In the following discussion, T_c will be assumed to be independent of the type of filter employed. This is approximately true for relatively broad filters. For very narrow filters, the attainable center transmission can be expected to decrease somewhat with decreasing width.

The current received due to background radiance is

$$i_b(h) = \mathcal{R} R A_r \Omega T_c \int_{-\infty}^{\infty} T_\nu(h,\nu_c) d(\nu - \nu_c) \tag{100}$$

For a Gaussian filter function,

$$T(h,\nu_c) = e^{-(\ln 2)\left(\frac{\nu - \nu_c}{h}\right)^2} \tag{101}$$

and

$$\int_{-\infty}^{\infty} T_{\nu}(h,\nu_c)\,d(\nu-\nu_c) = \int_{-\infty}^{\infty} e^{-(\ln 2)\left(\frac{\nu-\nu_c}{h}\right)^2} = h\left[\frac{\pi}{\ln 2}\right]^{\frac{1}{2}} \qquad (102)$$

Thus,

$$i_b(h) = \mathcal{R}RA_r\Omega T_c h\left[\frac{\pi}{\ln 2}\right]^{\frac{1}{2}} \qquad (103)$$

If both the signal and background levels were of constant intensity, the observation would be noise-free, in that the constant background could be precisely determined by monitoring the current received with the laser not in operation, and subtracted out during the computations. In reality, both the signal and background levels are subject to random statistical fluctuations about their mean values, even though the means themselves may be constant. If we treat the arrivals of photons as rare events, then we may apply Poisson statistics and assume that the RMS fluctuation in the number of photons received by a receiver with bandwidth Δf is equal to the square root of the mean number received. It is this random fluctuation about the mean which constitutes the noise. Thus, the signal to noise ratio is given by

$$\rho(h,z) = \frac{i_s(h,z)}{\sqrt{2q\,\Delta f\left[i_s(h,z) + i_b(h)\right]}} \qquad (104)$$

We can evaluate $\rho(h,z)$ approximately by considering a model atmosphere and a typical laser radar system. We choose number densities given in the U. S. Standard Atmosphere, 1962, and the following system parameters:

$\lambda = 0.6943\,\mu$

$W_t = 0.2$ J

$A_r = 1.3 \times 10^3$ cm^2 (16" diameter)

$(\tilde{J}_m \tilde{J}_p)^2 = 0.6$

$\sigma_{\substack{\text{Ram} \\ \pi+\perp}} = 2.06 \times 10^{-30}$ cm^2-ster^{-1}

$\sigma_{\substack{\text{Ram} \\ \pi+\perp}} = 2.85 \times 10^{-30}$ cm^2-ster^{-1}

$\Delta z = 2 \times 10^4$ cm (0.2 km)

$\Delta f = 1.5 \times 10^6$ sec^{-1}

$T_c = 0.4$

$R = 35$ mA-W^{-1}

$\mathcal{R}_{\text{Night}} = 9.66 \times 10^{-15}$ W-cm^{-2}-(cm^{-1})$^{-1}$-ster^{-1}

$\mathcal{R}_{\text{Day}} = 9.66 \times 10^{-8}$ W-cm^{-2}-(cm^{-1})$^{-1}$-ster^{-1}

$\Omega = 10^{-6}$ ster

In the above discussion we have assumed that, in collecting the signal and background photons, the laser is fired only once. Signal to noise ratios may be improved somewhat by averaging over a number of laser pulses, if the pulses are sequenced in such a way that

1) consecutive pulses are sufficiently far apart that the fluctuations about the means are independent for each

pulse, and

2) the total time period involved in taking the observation is short enough for the mean value to be considered as stationary.

When the above requirements are met, the signal to noise ratio increases as $N^{\frac{1}{2}}$. Clearly, the times involved in 1) and 2) above depend upon the temporal, spatial and spectral scales of the observation

For the sake of simplicity, and due to the fact that one hundred pulses are required to produce a factor of ten increase in the signal to noise ratio, we shall pursue our analysis with the assumption of a single pulse observation.

Results of the computations, shown in Figures 35 and 36, indicate that, for nighttime work, the signal to noise ratio is shot-noise limited; that is,

$$i_b \ll i_s$$

and thus, the signal to noise ratios are proportional to $\sqrt{E(h)}$. Since

$$\lim_{h \to \infty} E(h) = 1$$

this dependence results in a slow increase in ρ at moderate half widths, reaching an asymptotic value for large widths.

For daytime work, i_s and i_b are of the same order of magnitude at low altitudes, with i_b predominating over i_s

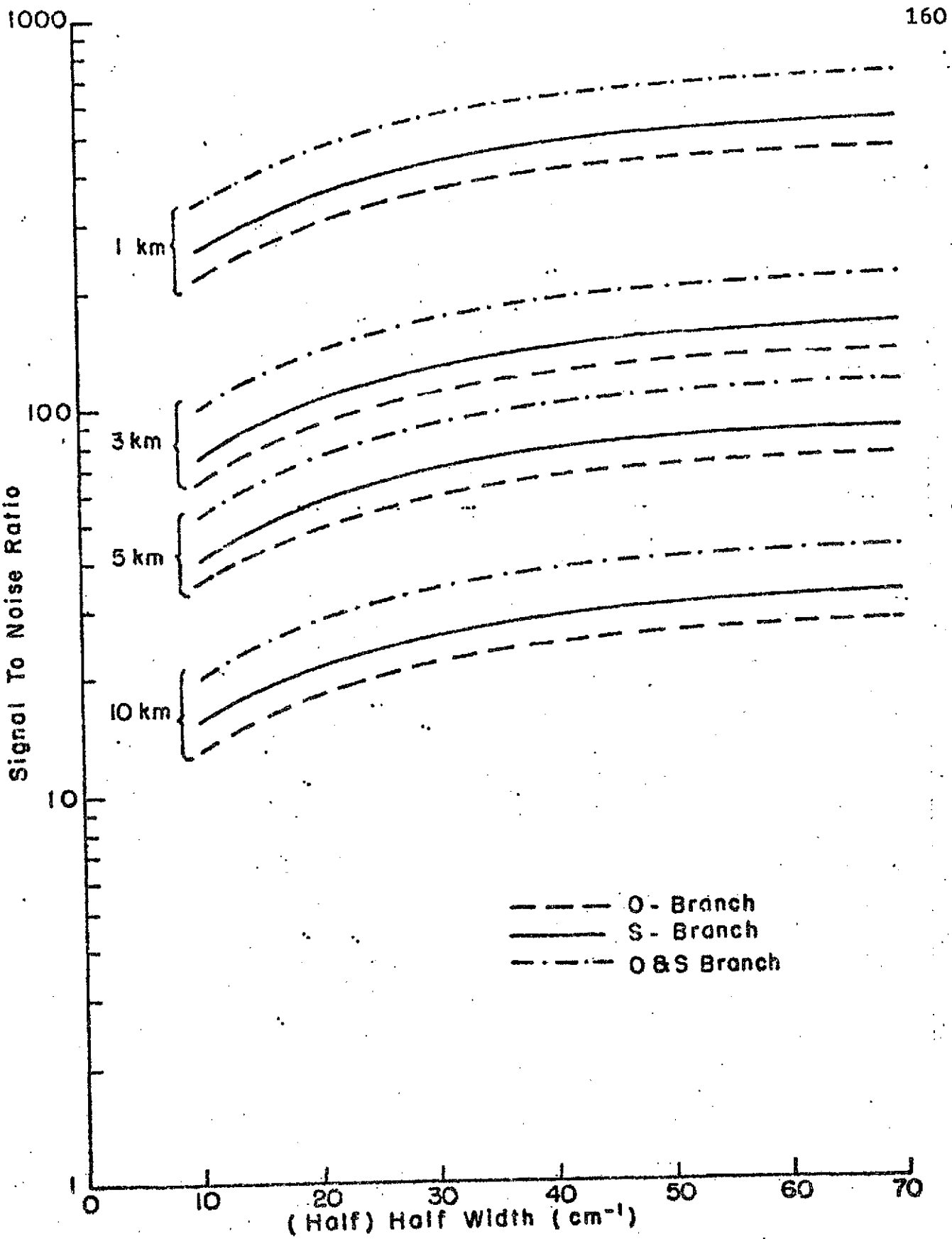

Figure 35. Nighttime signal to noise ratios for a typical laser radar system, showing the effect of filter half width.

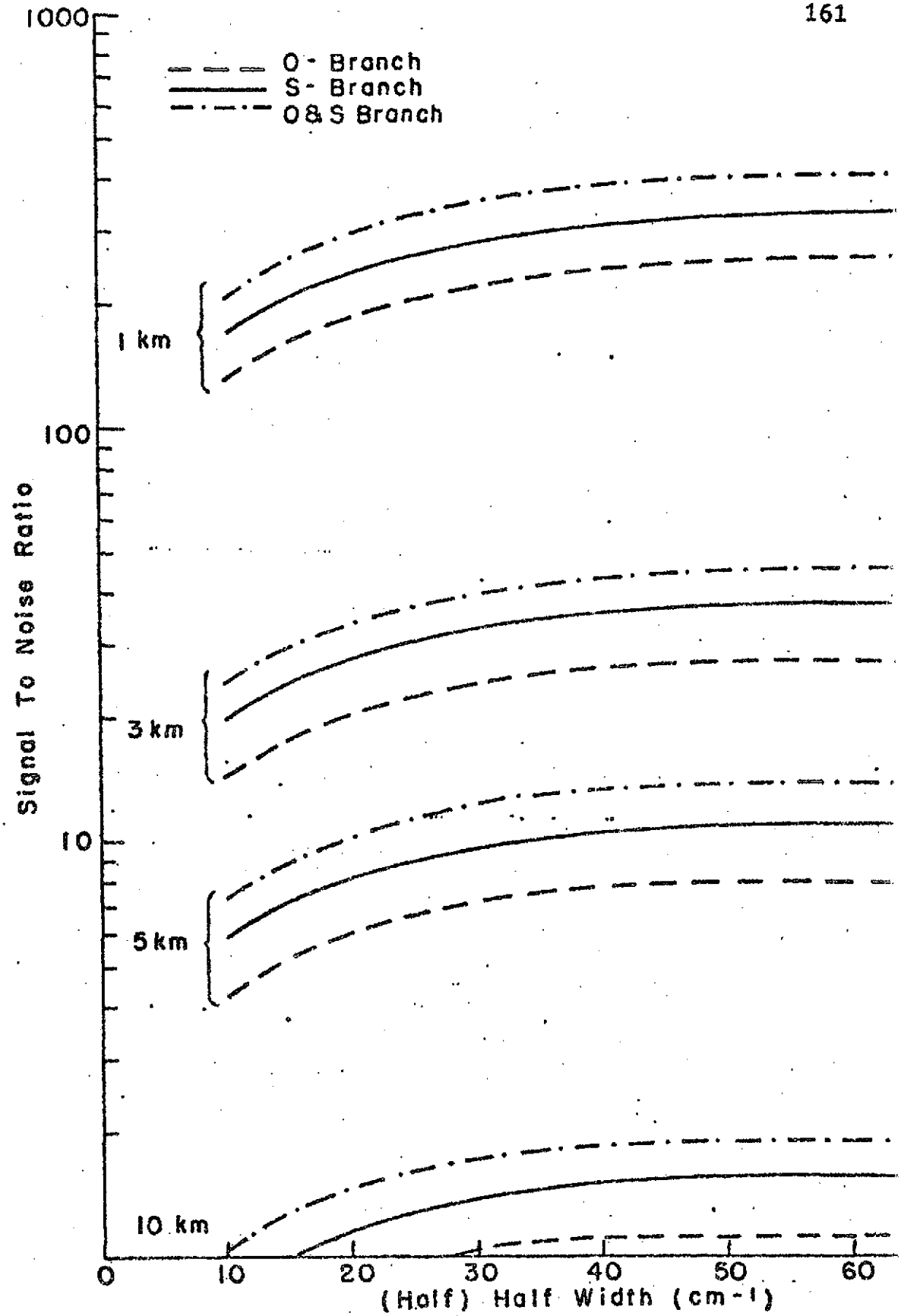

Figure 36. Daytime signal to noise ratios for a typical lase radar system, showing the effect of filter half width.

at greater heights. In the background-limited case, when

$$i_b \gg i_s$$

the signal to noise ratios are proportional to $E(h)/\sqrt{h}$. Here, if E(h) increases more rapidly with h than does $\sqrt{h}$, the signal to noise ratio increases with increasing h. If E(h) increases less rapidly with h than does $\sqrt{h}$, then the signal to noise ratio decreases with increasing h. For purposes of analysis, we wish to locate the point which gives the optimum signal to noise ratio for a background-limited signal; that is, the point where

$$\frac{d}{dh}\left[\frac{E(h)}{\sqrt{h}}\right] = 0 \tag{105}$$

or

$$\frac{d}{dh}E(h) = \tfrac{1}{2}\frac{E(h)}{h} \tag{106}$$

For both the O- and S-branches, this point lies near $h = 50\ cm^{-1}$. For signal to noise ratios falling between the background-limited and shot-noise limited values, the optimum half widths are shifted toward larger values.

For the system parameters assumed here, the optimum half width falls at some value greater than $70\ cm^{-1}$, but the signal to noise ratio does not deteriorate significantly as long as h is greater than about $30\ cm^{-1}$.

B. Determination of wavelength of optimum signal to noise ratio.

A computation was made of signal to noise ratio as a function of wavelength (daytime operation), with a view toward finding the optimum wavelength region in which to operate, and to determine the penalty paid for operating away from that wavelength.

Table 12 shows the magnitude of each of the wavelength-dependent variables affecting the signal levels, relative to their magnitudes at 0.7μ, in the range $0.3\mu \leqslant \lambda \leqslant 0.7\mu$, and Table 13 shows the variation of background level, i_b, with wavelength. The signal level, i_s, is also a function of $1/z^2$, so the optimum wavelength may also be expected to be a function of height.

Relative signal to noise ratios derived using these data, together with the computations of the previous chapters, are shown in Figure 37. The ratios are shown to be optimally large near about 0.45μ, but the ratios are shown to vary by less than a factor of three between 0.35μ and 0.7μ.

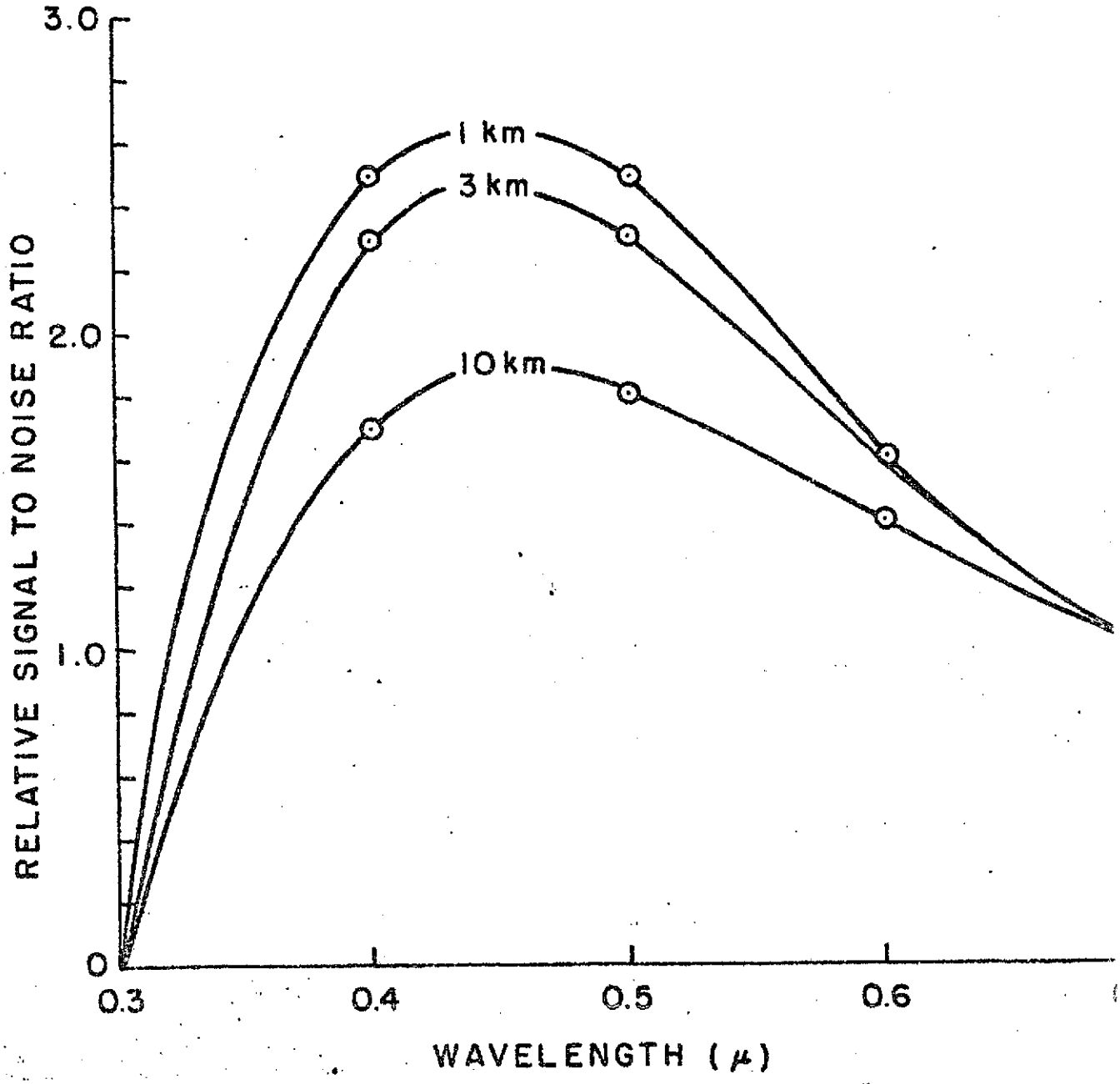

Figure 37. Relative signal to noise ratios for various heigh showing the effect of varying the laser wavelength.

Table 12. Magnitude (relative to that at 0.7μ) of each of the wavelength-dependent variables affecting the signal level, i_s.

$\lambda(\mu)$	$\frac{1}{\lambda^4}$	$\sigma^2_{J_{0-\infty}}$ After Elterman (1968)	R After RCA Corp. (1970)	W_t	i_s (product of preceding four columns)
0.3	29.	7.6×10^{-5}	1.09	0.10	2.5×10^{-4}
0.4	9.4	0.43	1.78	0.25	1.8
0.5	3.8	0.72	1.55	0.50	2.1
0.6	1.9	0.83	1.36	0.75	1.6
0.7	1.0	1.0	1.00	1.0	1.0

Table 13. Magnitude (relative to that at 0.7μ) of each of the wavelength-dependent variables affecting the background level, i_b.

$\lambda(\mu)$	$\mathcal{R}$	R After RCA Corp. (1970)	i_b (Product of preceding two columns)
0.3	0.14	1.09	0.15
0.4	0.28	1.78	0.50
0.5	0.46	1.55	0.71
0.6	0.69	1.36	0.94
0.7	1.0	1.00	1.0

Chapter VI.

CONCLUSIONS

The conclusions to be drawn from this research may be divided into two parts: those pertaining to the theoretical aspects of the technique and those pertaining to its practical application.

It has been shown that the rotational Raman spectrum of light scattered from air contains regions in which the effects of both temperature and particulate content are negligible. This fact is of importance not only for the present study, where it is desired to extract turbidity data from the elastic scattering, but may also be helpful to investigators such as Salzman, et.al. (1971), who are attempting to utilize the temperature-sensitive portions of the rotational Raman spectrum of air to obtain remote temperature soundings.

It has been established here that particulate effects are negligible at 4880 $\mathring{A}$, the operational wavelength of the Raman spectrophotometer. It is quite possible, however, that off-frequency scattering from particulates could become significantly large at shorter wavelengths, where resonance scattering and flourescence become important. It

is well known that resonance scattering and fluorescence cross sections may be orders of magnitude greater than those discussed here. In any case, it was shown in this study that wavelengths below about 4500 Å are not desirable for turbidity measurements because of the large rate of change of atmospheric transmission with wavelength. However, this caveat should be borne in mind by any investigator contemplating the extension of these results into the blue or ultraviolet portion of the spectrum.

With the attainability in recent years of high resolution, low noise rotational Raman spectra, the rotational Raman spectrum has been routinely observed and, indeed, is even used in the alignment of Raman spectrophotometers. By utilizing some of these observations, an attempt was made in this study to check for consistency the polarizability anisotropies for N_2 and O_2 obtained by earlier investigators. While there is still some doubt as to the absolute values of the anisotropies, it can at least be said that the values for N_2 and O_2 obtained by Bridge and Buckingham (1966) are correct relative to each other.

Investigation of the practical applicability of this remote sensing system reduced primarily to the development of a technique for spectrally and spatially separating the

Raman scattering from the much stronger elastic scattering. This phase of the study gave the author considerable insight into the problems involved in optical signal processing. Most importantly, the computations revealed (to the author, at least) the basic unity of all interferometric systems: the problem of focussing rays of light through a slit on to the face of a diffraction grating is transformed to a problem of similar difficulty if one decides instead to collimate the rays and use an interference filter.

It was ascertained that the rigid requirements for an interferometric system could be relaxed somewhat if an absorption cell could be used to preattenuate the elastically-scattered light. Such a cell, if it were to be effective, however, would present construction problems distinct from, but perhaps more difficult than those encountered in an interferometric system.

All told, it appears that, although a suitable filter system is within the realm of possibility today, the present state of the art makes such a system expensive and/or inefficient. Despite these inefficiencies, it is found that a typical laser radar system can produce daytime signal to noise ratios of the order of 10 db to heights of at least

5 km. For nighttime work, 10 db signal to noise ratios are achievable to heights of at least 15 km.

REFERENCES

Abe, K. and T. Shimanouchi, 1969: Rotational Raman spectrum of oxygen. Bull. Chem. Soc. Japan, 42: 3047.

Barrett, E. W. and O. Ben-Dov, 1967: Application of lidar to air pollution measurements. J. Appl. Meteor., 6: 500-515.

Born, M. and E. Wolf, 1959: Principles of Optics. Pergamon Press, New York, pp. 86, 187, 405.

Bridge, N. J. and A. D. Buckingham, 1966: The polarization of laser light scattered by gases. Proc. Roy. Soc. (London), 295A: 334-349.

Chandrasekhar, S., 1960: Radiative Transfer. Dover Publications, Inc., New York. pp. 6, 36, 49.

Clemesha, B. R., G. S. Kent and R. W. H. Wright, 1966: Laser probing the lower atmosphere. Nature, 209: 184-185.

Collis, R. T. H. and M. G. H. Ligda, 1966: Note on lidar observations of particulate matter in the stratosphere. J. Atmos. Sci., 23: 255-257.

Cross, P. C., J. Burnham and P. A. Leighton, 1937: The Raman spectrum and structure of water. J. Amer. Chem. Soc., 59: 1134-1147.

DeBary, E., B. Braun and K. Bullrich, 1965: Tables Related to Light Scattering in a Turbid Atmosphere. Report AFCRL-65-710, AFCRL, Bedford, Mass. p. 3.

Deirmendjian, D., 1969: Electromagnetic Scattering on Spherical Polydispersions. Elsevier, New York. 290 pp.

Ditchburn, R. W., 1963: Light. Vol. 1. Blackie and Son, Ltd., London. p. 181.

Dorsey, N. E., 1940: Properties of Ordinary Water Substance. Reinhold Publishing Corp., New York. pp. 50, 53.

Edlen, B., 1953: The dispersion of standard air. J. Opt. Soc. Am., 43: 339-344.

Eisenberg, D. and W. Kauzmann, 1969: The Structure and Properties of Water. Oxford University Press, London. p. 1

Elterman, L., 1966: An Atlas of Attenuation and Extinction Profiles for the Troposphere and Stratosphere. Report AFCRL-66-828, AFCRL, Bedford, Mass. 128 pp.

_____, 1968: UV, Visible and IR Attenuation for Altitudes to 50 km, 1968. Report AFCRL-68-0153, AFCRL, Bedford, Mass. 49 pp.

Fabelinskii, I. L., 1968: Molecular Scattering of Light. Plenum Press, New York. p. 556.

Fiocco, G. and L. D. Smullen, 1963: Detection of scattering layers in the upper atmosphere (60 - 140 km) by optical radar. Nature., 199: 1275-1276.

_____, and G. Grams, 1964: Observations of the aerosol layer at 20 km by optical radar. J. Atmos. Sci., 21: 323-324.

Fuchtbauer, C., G. Joos and O. Dinkelacker, 1923: Über Intensität, Verbreiterung und Drucksverschiebung vor Spektrallinien, inbesondere der Absorptionslinie 2537 des Quecksilbers. Ann. d. Phys., 71: 204-227.

Goody, R. M., 1964: Atmospheric Radiation, I. Theoretical Basis. Oxford University Press, London. pp. 10, 293.

Haber, H., 1972: Cary Instruments, Applications Section, 2724 S. Peck Rd., Monrovia, Cal. 91016. Personal Communication.

Herzberg, G., 1939: Molecular Spectra and Molecular Structure, I. Diatomic Molecules. Prentice Hall, Inc., New York. 592 pp.

_____, 1945: Molecular Spectra and Molecular Structure, II. Infrared and Raman Spectra of Polyatomic Molecules. D. Van Nostrand Co., Inc., New York. pp. 38, 41, 53, 60,

Hess, S. L., 1959: Introduction to Theoretical Meteorology. Henry Holt and Company, New York. p. 42.

Jenkins, F. A. and H. E. White, 1957: Fundamentals of Optics. McGraw-Hill Book Co., Inc., New York. pp. 142, 274, 345.

Junge, C. E., 1963: Air Chemistry and Radioactivity. Academic Press, New York. pp. 116, 178, 186.

Kent, G. S., B. R. Clemesha and R. W. Wright, 1967: High altitude atmospheric scattering of light from a laser beam. J. Atm. and Ter. Phys., 29: 169-181.

_____, P. Sandland and R. W. H. Wright, 1971: A second-generation laser radar. J. Appl. Meteor., 10: 443-452.

Kolker, H. J. and M. Karplus, 1963: Electric polarizability of some diatomic molecules. J. Chem. Phys., 39: 2011-2016

Middleton, W. E. K., 1951: Visibility in meteorology. In Compendium of Meteorology (T. F. Malone, Ed.). American Meteorological Society, Boston. pp. 91-97.

Miller, R. E., 1970: Personal communication.

_____, K. L. Treuil, R. R. Getty and G. E. Leroi, 1968: Redesign and Construction of a Laser Raman Spectrophotometer. Technical Report No. 4(29), Contract N00014-68-A-0109-0003, NR 014-203. University of Michigan, Ann Arbor. AD669797. 45 pp.

Mitra, S. S., 1969: Infrared and Raman spectra due to lattice vibrations. In Optical Properties of Solids. (S. Nudelman and S.S. Mitra, Eds.) Plenum Press, New York. pp. 333-451.

Nagel, M. R., 1960: Background Measurements During the Infrared Measuring Program 1956 (IRMP 56). GRD Research Notes No. 46. AFCRL, Bedford, Mass. 315 pp.

Narayanaswamy, P. K., 1948: The Raman spectrum of water, heavy water and ice. Proc. Indian Acad. Sci., 27A: 311-315.

Nee, P. F., 1964: Hourly variability of density at radiosonde heights. J. Appl. Meteor., 3: 175-178.

Oriel Optics Corporation, 1971: Narrow Band Interference Filters. Publication No. 684, Oriel Optics Corp., Stamford, Conn. 2 pp.

Ory, H. A. and H. T. Yura, 1965: Rayleigh and Raman Scattering in Molecular Nitrogen. Memorandum RM-4664-ARPA, The Rand Corporation, Santa Monica, Cal. 23 pp.

Placzek, G. and E. Teller, 1933: Die Rotationsstruktur der Ramanbanden mehratomiger Moleküle. Z. Phys., 81: 209-258.

Salzman, J. A., W. J. Masica and T. A. Coney, 1971: Determination of Gas Temperatures from Laser Raman Scattering. Report No. NASA TN D-6336, NASA, Washington, D. C. 20546. 34 pp.

Schotland, R. M., 1969: Some aspects of remote atmospheric sensing by laser radar. In Atmospheric Exploration by Remote Probes, Vol. 2. National Academy of Sciences, Washington, D. C. pp. 179-200.

Schuster, B. G., 1970: Detection of tropospheric and stratospheric aerosol layers by optical radar (lidar). J. Geophys. Res., 75: 3123-3132.

Senior, W. A. and W. K. Thompson, 1965: Assignment of the infra-red and Raman bands of liquid water. Nature, 205: 170.

Smith, J. W., 1964: Density variation and isopycnic layers. J. Appl. Meteor., 3: 290-298.

Stansbury, E. J., M. F. Crawford and H. L. Welsh, 1953: Determination of rates of change of polarizability from Raman and Rayleigh intensities. Can. J. Phys., 31: 954-96[illegible]

Stoicheff, B. P., 1959: High resolution Raman spectroscopy. In Advances in Spectroscopy, Vol. I, (H. W. Thompson, Ed.) Interscience Publishers, Inc., New York. pp 91-174.

Stuart, H. A., 1934: Molekulstruktur. Julius Springer, Berlin. pp. 173, 179-180.

Wacker, P. F., M. Mizushima, J. D. Peterson and J. R. Ballard, 1964: Microwave Spectral Tables: Diatomic Molecules. NBS Monograph 70, Vol. I., U. S. Govt. Printing Office, Washington, D. C. p. 56.

Walrafen, G. E., 1964: Raman spectral studies of water structure. J. Chem. Phys., 40: 3249-3256.

_____, 1967: Raman spectral studies of the effects of temperature on water structure. J. Chem. Phys., 47: 114-12

Walsh, A., 1961: Application of atomic absorption spectra to chemical analysis. In Advances in Spectroscopy, Vol. II (H. W. Thompson, Ed.) Interscience Publishers, Inc., New York. pp. 1-22.

Weber, A., S. P. S. Porto, L. E. Cheesman and J. J. Barrett, 1967: High resolution Raman spectroscopy of gases with cw-laser excitation. J. Opt. Soc. Am., 57: 19-28.

Wilkinson, P. G., 1957: High resolution absorption spectra of nitrogen in the vacuum ultraviolet. Astrophys. J., 126: 1-9.

Handbook of Chemistry and Physics, 25th Ed., 1953. Chemical Rubber Publishing Co., Cleveland.

Handbook of Physics and Space Environment. AFCRL, Bedford, Mass. pp. 3-23 - 3-27.

International Critical Tables of Numerical Data - Physics, Chemistry and Technology, 1930. Vol. VII., p. 7. Natl. Research Council. McGraw Hill, New York.

Landolt-Bornstein Zahlenwerte und Funktionen aus Physik, Chemie, Astronomie, Geophysik und Technik., 6. Auflage, I. Band, 3. Teil, 1951. Springer Verlag, Berlin. p. 510.

RCA Typical Photocathode Response Characteristics, 1970. RCA Electronic Components, Harrison, N. J. (A Wall Chart)

U. S. Standard Atmosphere, 1962. U. S. Govt. Printing Office, Washington, D. C. pp. 9, 80.

Appendix

1. COMPUTATION OF THE RATIO $\gamma^2(N_2)/\gamma^2(O_2)$ FROM OBSERVED DATA.

The intensities of individual nitrogen and oxygen rotational Raman lines, relative to a common datum level, are given by

$$I_\nu(N_2) = \left[\frac{I_\nu(N_2)}{I_{Tot}(N_2)}\right] I_{Tot}(N_2) + Z \qquad (107)$$

$$I_\nu(O_2) = \left[\frac{I_\nu(O_2)}{I_{Tot}(O_2)}\right] I_{Tot}(O_2) + Z \qquad (108)$$

where Z is the zero displacement of the scale. If we recognize that intensities are proportional to $n\gamma^2$, then we may write

$$I_\nu(N_2) = \left[\frac{I_\nu(N_2)}{I_{Tot}(N_2)}\right] Kn(N_2)\gamma^2(N_2) + Z \qquad (109)$$

$$I_\nu(O_2) = \left[\frac{I_\nu(N_2)}{I_{Tot}(N_2)}\right] Kn(O_2)\gamma^2(O_2) + Z \qquad (110)$$

Thus, if we plot a graph of $I_\nu(N_2)$, the intensities extracted from the results of Miller, et.al. (1968), versus $\left[I_\nu(N_2)/I_{Tot}(N_2)\right]$, the resulting curve should be a straight

line, with slope proportional to

$$Kn(N_2)\gamma^2(N_2)$$

The analogous graph for O_2 has a slope proportional to

$$Kn(O_2)\gamma^2(O_2)$$

The constant of proportionality, K, is of course, the same for both curves, as is the intercept point with the coordinate axis (the zero displacement of the scale). The two curves plotted in this manner are shown in Figure 38, together with the best fit straight lines through the points.

It should be noted that I_ν / I_{Tot} is a function of temperature. According to Miller (1970), their experiment was conducted at, or slightly above room temperature, but no attempt was made to measure the temperature. Graphs were plotted for several temperatures, and the best straight line fits were obtained for $T = 287^oK$.

The quotient of the two slopes was found to be

$$\frac{n(N_2)\gamma^2(N_2)}{n(O_2)\gamma^2(O_2)} = 1.496$$

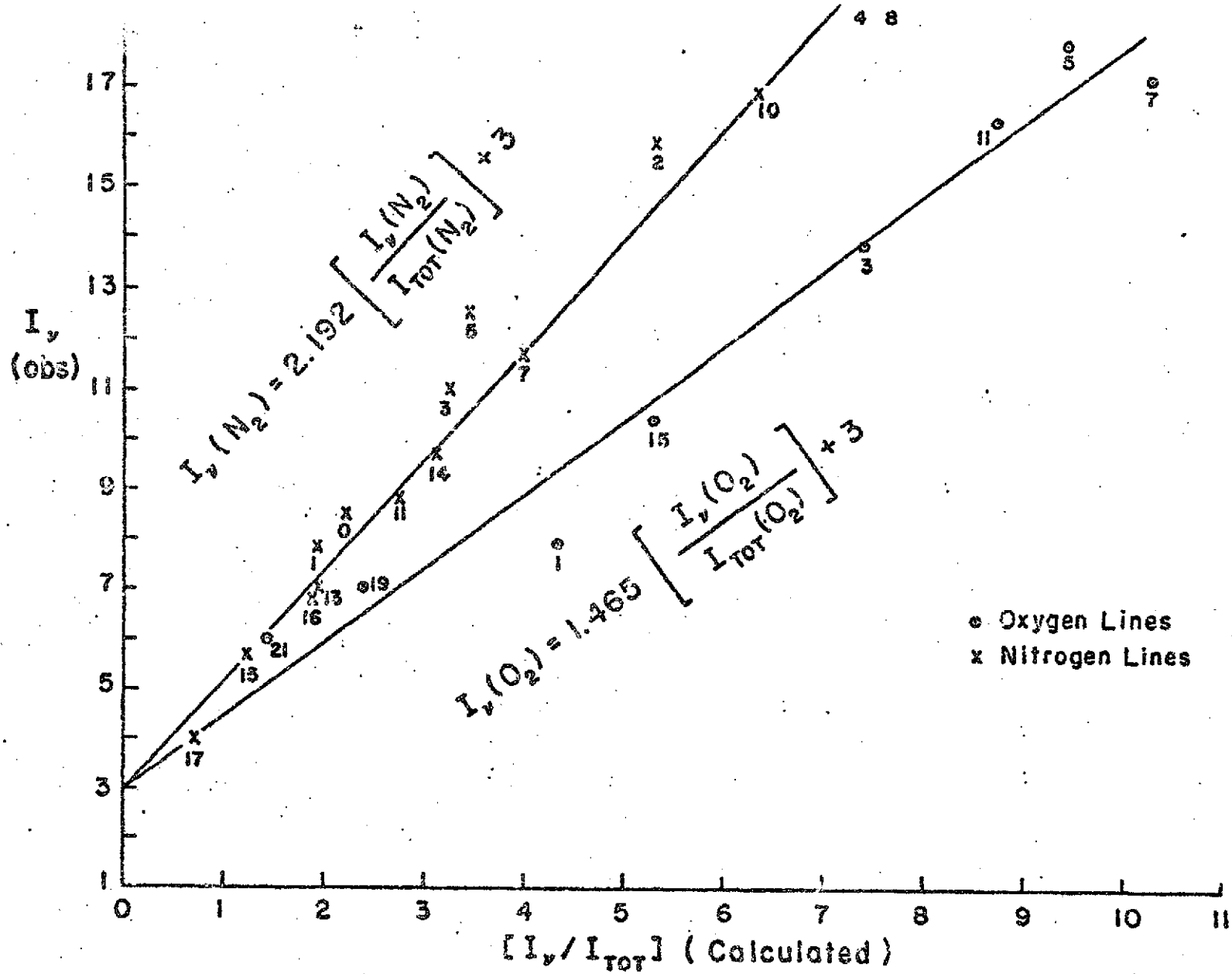

Figure 38. Intensities of lines in the rotational Raman spectra of N_2 and O_2 in air, as observed by Miller, et.al. (1968), versus intensities computed in Chapter III.

2. TESTING OF THE INTERFERENCE FILTER.

It is desired to determine whether the interference filter for the Raman channel has a transmission of 10^{-4} to 10^{-5} as specified by the manufacturer. Furthermore, it is desired to examine the sensitivity of this transmission value to the angle of the incident light.

An optical system was constructed to determine the filter parameters at 6943 Å for a range of incidence angles near zero degrees. A schematic diagram of the device is shown in Figure 39. The mirror M, actually an unsilvered piece of glass, has a low reflectance, and is used to direct a small percentage of the laser output into the test apparatus. The lens combination L_1 and L_2 was chosen to produce:

1. A collimated beam of light with a diameter about equal to that of the interference filter (one inch).

2. A sensitivity of the degree of collimation to the location of L_2. That is, it was desired to vary the beam width of the light striking the filter from about one degree of convergence through about one degree of divergence.

3. A spot of light nearly constant in size at the location of F, the interference filter, regardless of the

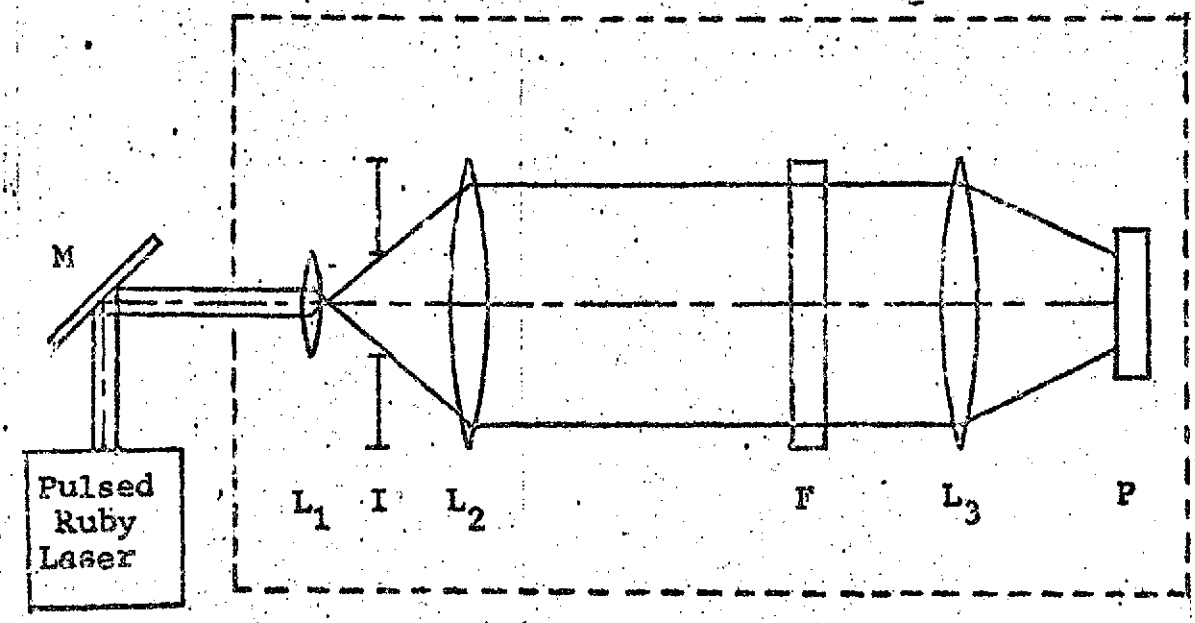

Figure 39. Schematic diagram of device constructed to test transmission characteristics of interference filter.

location of L_2.

L_3 is used to concentrate the light transmitted through the interference filter on to a cadmium sulfide photocell, P. The iris diaphragm, I, is used to adjust the size of the spot.

The lens L_2 is located on a vernier mount which allows its position along the optical axis to be adjusted over about ± 2.5 cm from its mean position. The interference filter, F, is mounted in such a way that it can be tilted up and down and from side to side.

The entire apparatus is enclosed in a lightproof box, which is painted on the inside with flat black paint to minimize diffuse reflection.

The device is designed so that the interference filter, F, can readily be removed and replaced by broad band absorption type filters whose transmissions are known, and which lie in the same range as that of the interference filter.

Calibration of the system and testing for photocell linearity was accomplished by measuring the photocell output with filter combinations as shown in Table 14 and in Figure 40.

Calibration of the vernier mount supporting the filter consisted of replacing the filter, F, with a plane mirror,

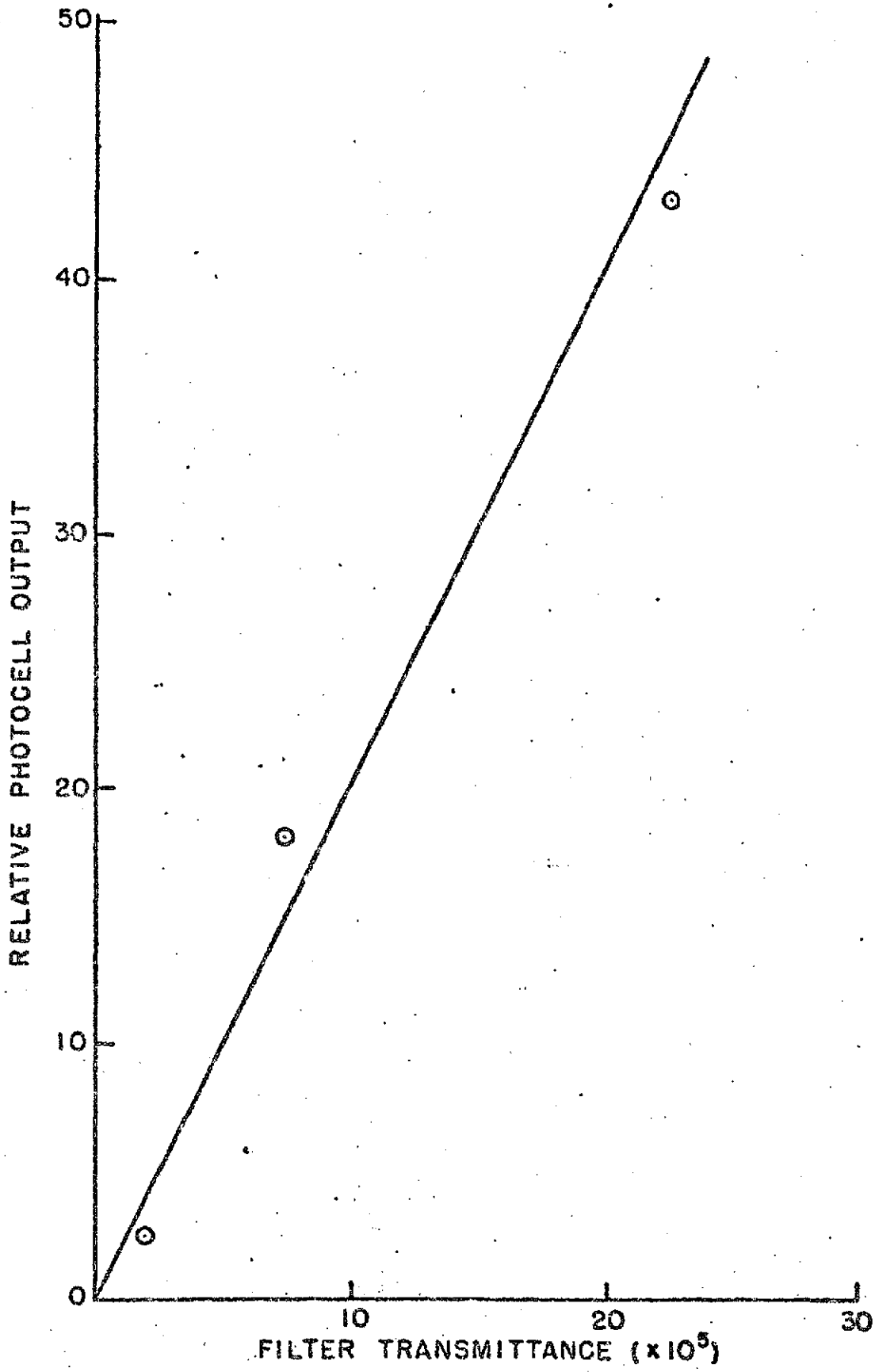

Figure 40. Results of test for linearity of photocell output when operating in the configuration shown in Figure 39.

and applying trigonometry to the location of the reflected light to obtain the mirror angle. Results of these measurements are shown in Figures 41 and 42.

Figure 43 shows resulting transmitted intensities obtained when the interference filter was mounted at various vernier settings. Transmitted intensity through a neutral density filter with a transmittance of 2×10^{-5} is shown for comparison. Several pulses of the laser are recorded for each setting in order that a suitable average reading could be obtained. The variability from pulse to pulse is attributable to the laser, the output of which fluctuates considerably.

Figure 44 shows the average intensity values plotted against the vernier (angular) setting. When the filter is optimally tilted (at some angle very close to zero degrees), transmittances as low as about 5×10^{-5} are attainable. For off-angle radiation, the transmittance rapidly increases, reaching nearly 2×10^{-4} for incidence angles of less than one degree.

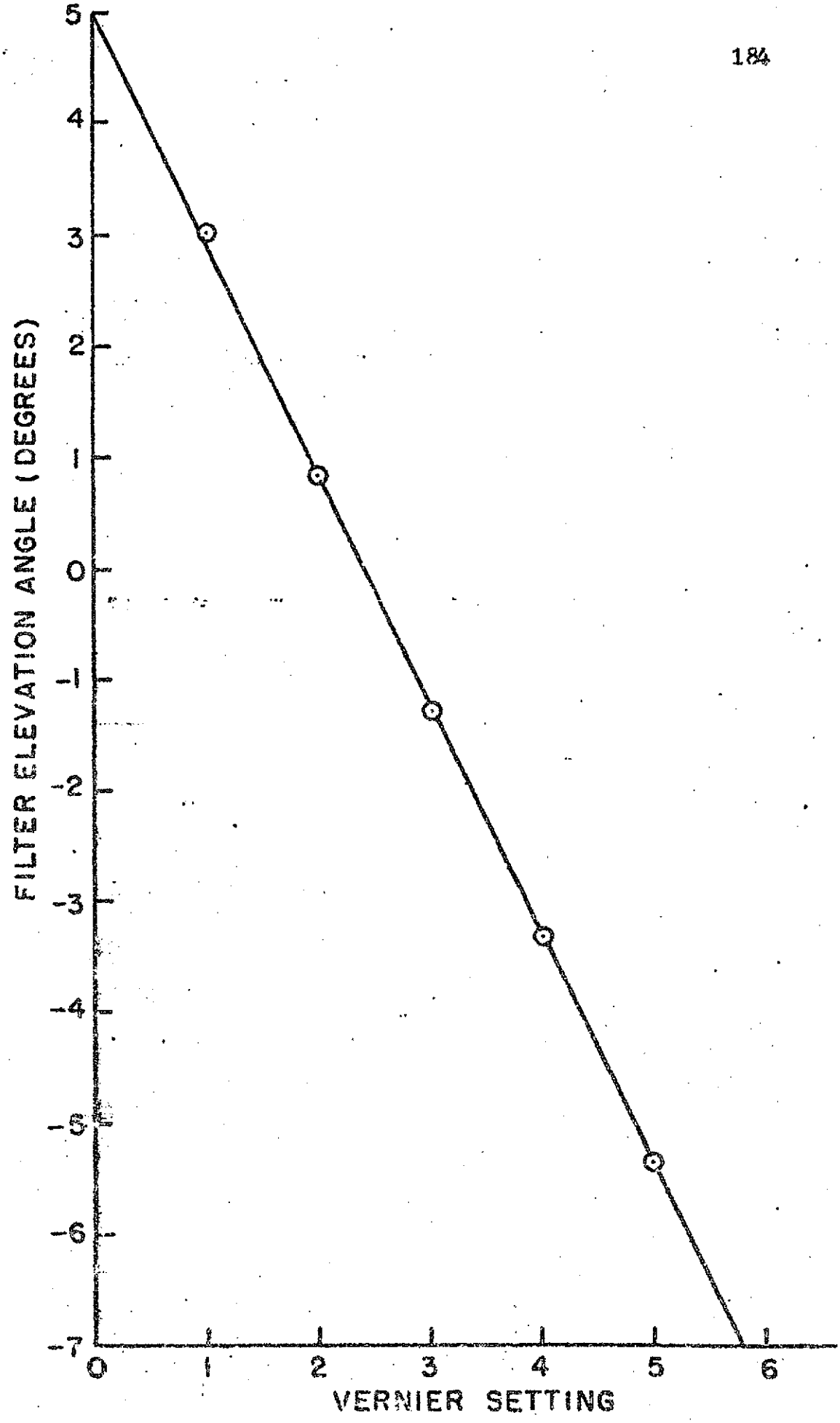

Figure 41. Calibration curve for vernier controlling the ele
angle of the interference filter mounting assembly.

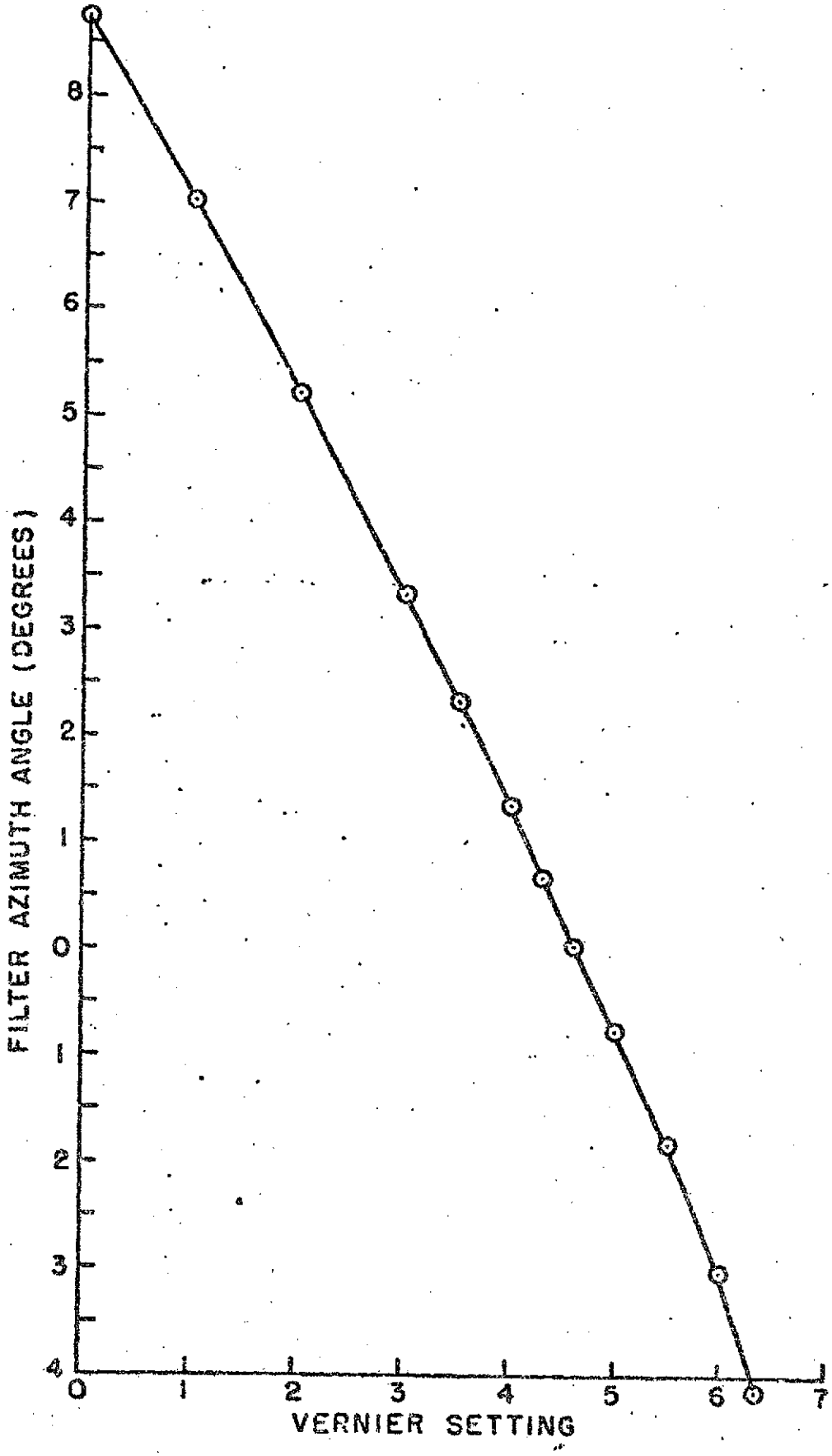

Figure 42. Calibration curve for vernier controlling the azimuth angle of the interference filter mounting assembly.

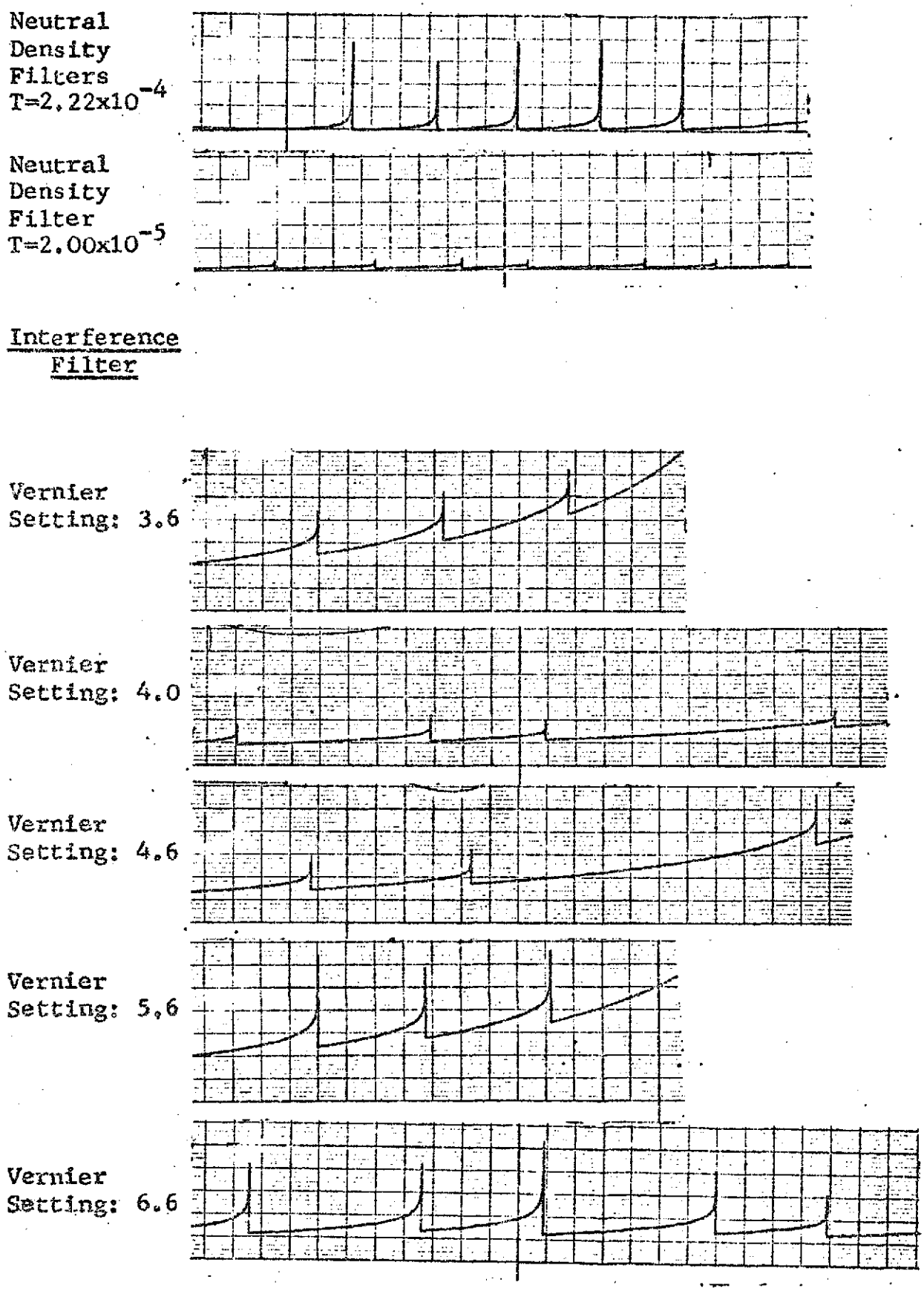

Figure 43. Observed photocell output values for light passing through neutral density filters of known transmission and thro the interference filter at various azimuth angles.

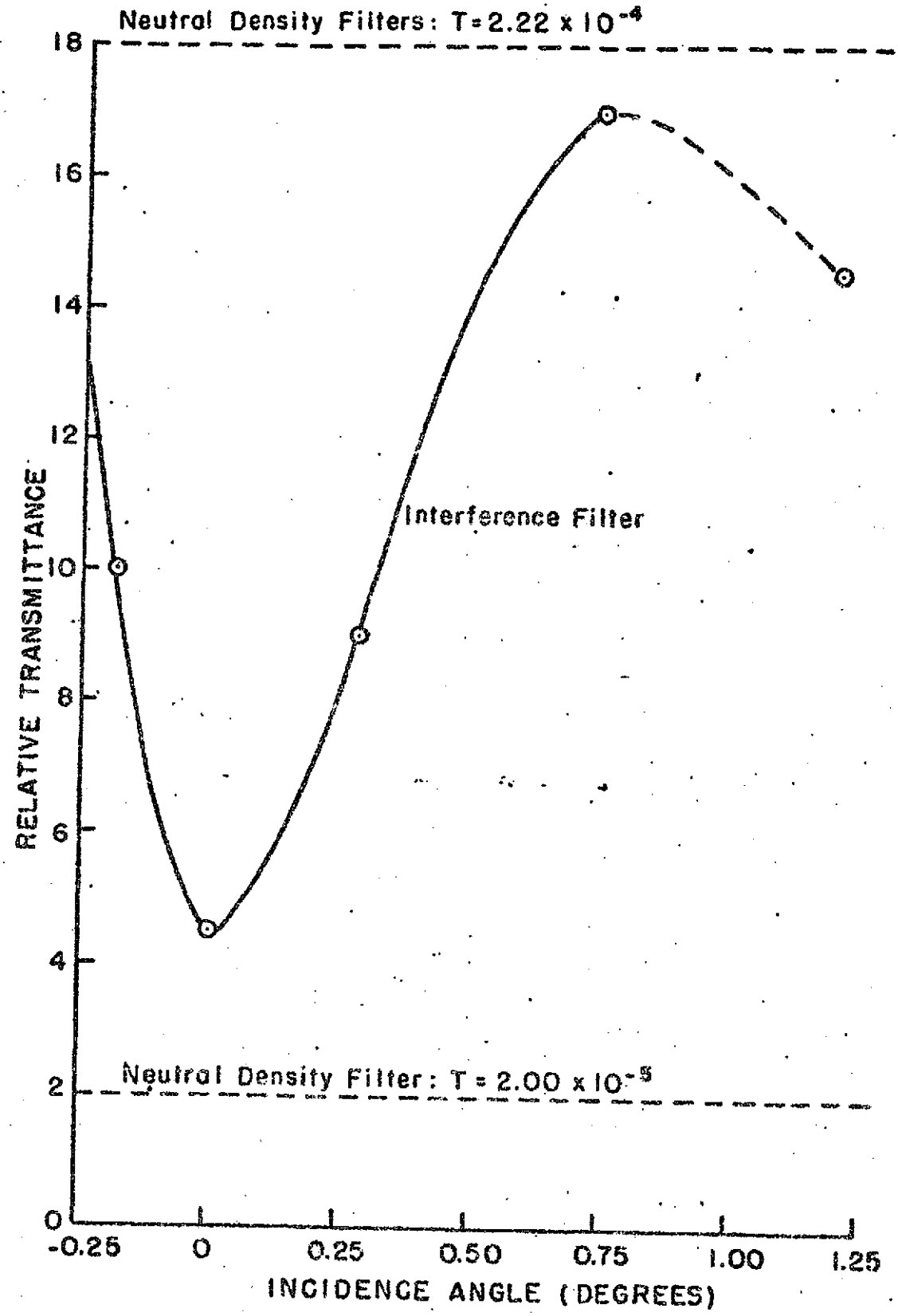

Figure 44. Intensity values of Figure 43. plotted against incid angle deduced from vernier setting. Relative transmittance of the neutral density filters is shown for comparison.